

# Contract Research

GDOT Research Project No. 2041

## Evaluation of a Highway Bridge Constructed Using High Strength Lightweight Concrete Bridge Girders

### Final Report

Prepared for

Office of Materials and Research  
Georgia Department of Transportation

By

R. Brett Holland, Jennifer Dunbeck, Jong-Han Lee,  
Lawrence F. Kahn, and Kimberly E. Kurtis

April 2011

The contents of this report reflect the views of the authors who are responsible for the facts and the accuracy of the data presented herein. The contents do not necessarily reflect the official views or policies of the Georgia Department of Transportation. This report does not constitute a standard, specification or regulation.

## Executive Summary

The use of high performance concretes to provide longer bridge spans has been limited due to the capacity of existing infrastructure to handle the load of the girders during transportation. The use of High Strength Lightweight Concrete (HSLW) can provide the same spans at a 20% reduction in weight. This paper presents the findings from an ongoing performance evaluation of HSLW concrete bridge girders used for the I-85 Ramp “B” Bridge crossing SR-34 in Coweta County, Georgia,. The girders are AASHTO BT-54 cross-sections with a 107 feet 11½ inch (32.9 m) length cast with a 10,000 psi (68.9 MPa) design strength HSLW mix and an actual average unit weight of 120 lb/ft<sup>3</sup> (1922 kg/m<sup>3</sup>). The prestressing losses measured experimentally by embedded vibrating wire strain gauges have been compared to the AASHTO LRFD loss equations, as well as the proposed methods by Tadros (2003) and Shams (2000). The investigation also included camber measurements and the effect of temperature changes. A load test was performed on the girders at 56-days of age and on the bridge after completion of construction to determine a stiffness estimator for use with the girders and to determine their performance as a completed system. The girders are the first use of HSLW girders in the state of Georgia, and they have proven to perform well for use in highway bridges.

## Acknowledgements

The research reported herein was sponsored by the Georgia Department of Transportation through Research Project 2041, Task Order Number 02-06. Mr. Paul Liles, Assistant Pre-construction Engineer; Mr. Myron Banks, Concrete Engineer; Ms. Lyn Clements, Bridge Engineer; and Ms. Supriya Kamatkar, Research Engineer, of GDOT provided many valuable suggestions throughout the study.

The opinions and conclusions expressed herein are those of the authors and do not represent the opinions, conclusions, policies, standards or specifications of the Georgia Department of Transportation or of other cooperating organizations.

Standard Concrete Products personnel, especially Mr. Steve Snowe, Mr. Brett Martin, and Mr. Miles McGuire, assisted in all aspects of the field study. Michael Gantt, of Archer Western Contractors, provided valuable assistance and advice in the completion of the study during construction of the bridge. The following Georgia Tech graduate research assistants aided in the concrete specimen construction and testing: Robert Moser, Jonathan Hurff, Victor Garas, and Kennan Crane. Additionally, the following undergraduate research assistants aided in the completion of this project: Gabriel Vega, Robert Heusel, and Mitchell McKay. Dr. Reid Castrodale of Carolina Stalite Company provided many valuable comments and suggestions. The assistance and support from these individuals and organizations is gratefully acknowledged.

# Table of Contents

Executive Summary	iii
Acknowledgments	iv
Table of Contents	v
Chapter	
1. Introduction	1-1
2. HSLW Material Property Characterization	2-1
3. Deck Concrete Material Properties	3-1
4. Load Test of Bridge Structure	4-1
5. Prestress Losses	5-1
6. Camber in HSLW Girders	6-1
7. Conclusions and Recommendations	7-1
References	R-1
Appendix A: Bridge Load Test Data	A-1
Appendix B: Prestress Loss Calculations	B-1
Appendix C: Camber Data	C-1
Appendix D: Development Length	D-1

# 1. Introduction

The purpose of this research was to characterize the performance of High Strength Lightweight Concrete (HSLW) in precast, prestressed bridge girders and to evaluate their performance in a highway bridge. The mechanical properties and long-term time-dependent behavior of HSLW girders made using expanded slate lightweight aggregate were examined by monitoring their internal strain and deflection performance from initial construction through one-year of bridge operation.

## 1.1 Research Motivation

The development of high performance concretes (HPC) allowed for construction of longer spans on bridge structures. However, the weight of the girders during transport began limiting the constructible span lengths due to load capacities of existing infrastructure, as well as the need for super-load permits. HSLW has been shown capable of providing the longer spans associated with HPC, while decreasing the weight of the girders by up to 20% (Meyer and Kahn, 2002).

Buchberg (2002) developed HSLW mix designs capable of providing 8,000 psi (55.2 MPa), 10,000 psi (68.9 MPa), and 12,000 psi (82.7 MPa) ultimate strengths using expanded slate lightweight coarse aggregate. Investigations into the mechanical properties of the mix designs demonstrated that current code equations were unable to accurately predict the elastic modulus (Meyer, 2002). Additionally, through full scale testing of AASHTO Type II girders constructed with 8,000 psi (55.2 MPa) and 10,000 psi (68.9 MPa) HSLW, it was concluded that the flexural and shear behavior of the girders was satisfactory for safe implementation of HSLW into bridge structures. Previous research by Lopez (2005) studied the long-term properties of HSLW and

demonstrated that existing prestress loss estimation techniques overestimated the losses observed and that HSLW experienced significantly less creep and shrinkage than typical structural lightweight concretes (LWC). Research by Ozyildirim (2009) agreed with results found by Lopez (2005), that HSLW has similar creep behavior to normal weight concrete (NWC), but a reduced modulus of elasticity that must be properly estimated for design. For efficient use of HSLW for bridge structures, the field behavior and performance must be evaluated and compared with current design methods to determine their applicability.

## **1.2 Research Objectives**

The primary goal of this research was to characterize the field performance of HSLW precast, prestressed bridge girders. This was accomplished by completing six objectives that encompassed both the short-term and long-term behavior of the girders and the composite bridge structure:

1. Determine the mechanical properties of field cast HSLW and its maturation behavior and determine most accurate estimation method of the elastic modulus
2. Characterize the time-dependent creep and shrinkage properties of HSLW
3. Quantify the loss of prestressing force and determine the most accurate method of predicting the observed losses
4. Evaluate the performance of the composite bridge system under test loading and compare with finite element analysis models (FEA)
5. Determine the effect of prestress losses and seasonal temperature variations on camber of HSLW girders

6. Provide design recommendations for future use of HSLW concrete for precast, prestressed bridge girders

### 1.3 Research Bridge Description

The I-85 Ramp “B” Bridge over SR-34, Bullsboro Drive, in Coweta County, Georgia was selected by the Georgia Department of Transportation (GDOT) to be constructed using HSLW girders for the center two spans. Figure 1-1 shows a plan view of the bridge girders, with Figure 1-2 presenting a magnified view of Span 2 which was instrumented as part of this study. Span 2 consists of five AASHTO BT-54 cross-section girders with a 107 feet 11½ inch (32.9 m) length. The bridge girders were placed with a 90 in. (228 cm) spacing and a skew angle of 50°-08'-08". Figure 1-3 shows the typical cross-section of the girders and deck. The deck had a thickness of 7.75 in. (19.7 cm) above the top of the 3 in. (7.6 cm) corrugated metal decking. Additionally, a haunch existed between the bottom of the deck and the top of the beams. The height of the haunch varied by girder, as well as along the length of each girder.

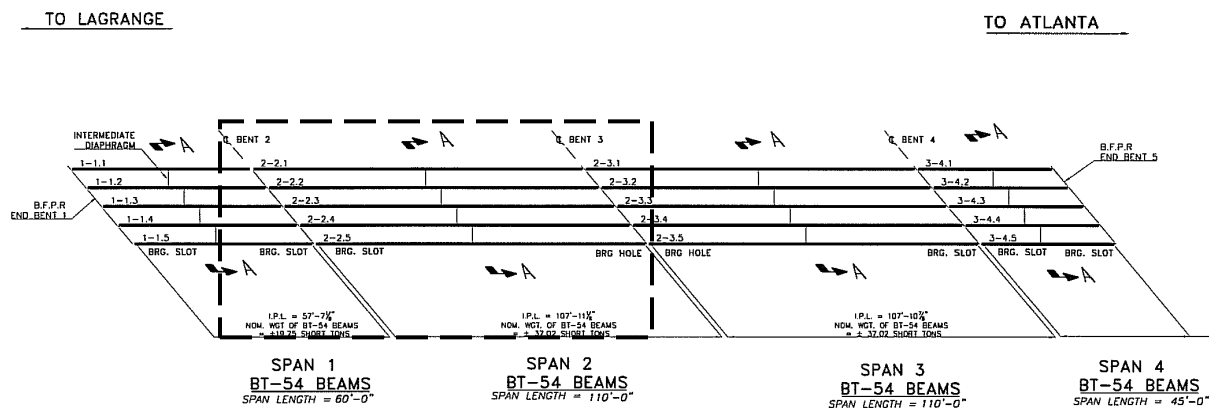


Figure 1-1: I-85 Ramp “B” Bridge over SR-34, Bullsboro Drive  
(Standard Concrete Products, 2006)

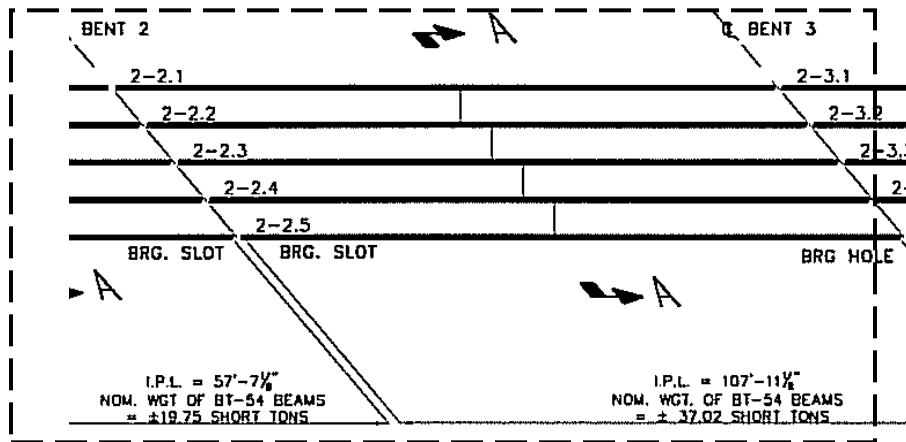


Figure 1-2: Magnified view of Figure 1 detailing Span 2.

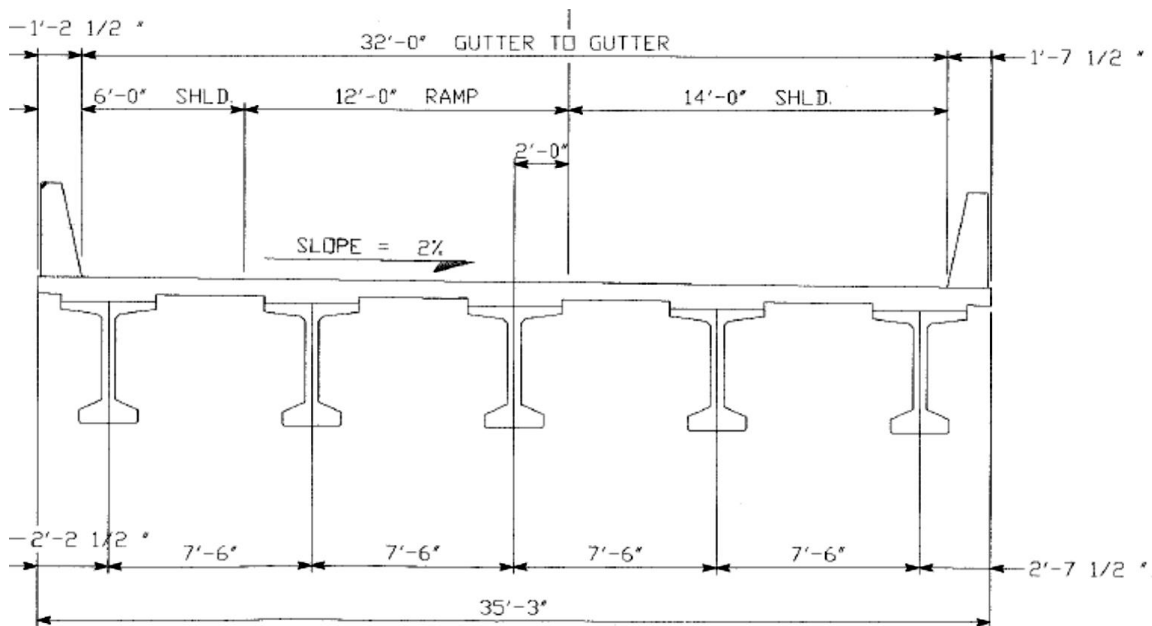


Figure 1-3. Bridge cross section showing all 5 girders.

The girders were instrumented with vibrating wire strain gages (VWSG) at mid-span which were placed prior to casting. Additionally, VWSG's were placed in the deck at the top and bottom mats of reinforcement at mid-span above each girder, and thermocouples (TC) were placed near the surface of the deck and at the interface between the deck and girder above

girder 3. Figure 1-4 shows a diagram of embedded vibrating wire strain gages (VWSG) at mid-span of each beam.

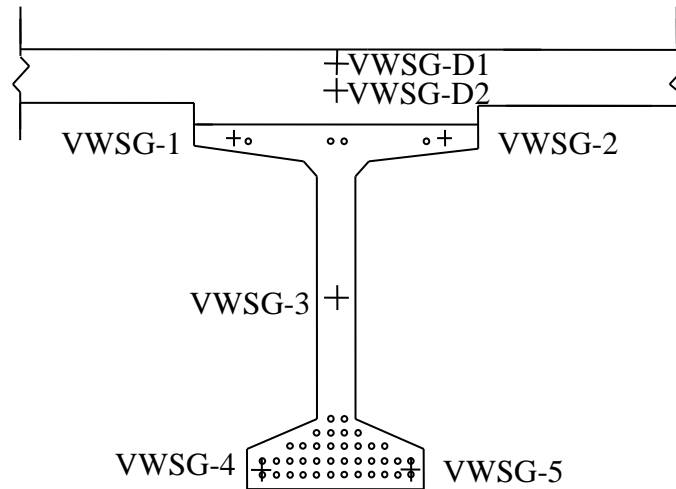


Figure 1-4: Instrumentation of girder and bridge deck

The girders were cast with a 10,000 psi (68.9MPa) design strength HSLW mix and a unit weight of 120 lb/ft<sup>3</sup> (1922 kg/m<sup>3</sup>). The HSLW mix design used is given in Table 1-1. This mix design was based off of the 12,000 psi (82.7 MPa) mix developed by Buchberg (2002). The deck was constructed using a Class AA, 3,500 psi (24.1 MPa) design strength normal weight concrete. The deck concrete mix design is given in Table 1-2.

Table 1-1: HSLW concrete mix design

<b>Material</b>	<b>Units</b>	<b>Quantity</b>
Type III cement	lb/yd <sup>3</sup> (kg/m <sup>3</sup> )	740 (439)
Type F fly ash	lb/yd <sup>3</sup> (kg/m <sup>3</sup> )	150 (89)
Silica fume	lb/yd <sup>3</sup> (kg/m <sup>3</sup> )	100 (59.3)
Normal weight fine aggregate	lb/yd <sup>3</sup> (kg/m <sup>3</sup> )	931.6 (552.7)
Expanded slate lightweight aggregate	lb/yd <sup>3</sup> (kg/m <sup>3</sup> )	980 (581.4)
Water	gal (L)	32 (121.3)
Water reducer	oz/yd <sup>3</sup> (L/m <sup>3</sup> )	29.7 (1.15)
Superplasticizer	oz/yd <sup>3</sup> (L/m <sup>3</sup> )	59.4 (2.3)
Air entrainer	oz/yd <sup>3</sup> (L/m <sup>3</sup> )	2 (0.08)
Set accelerator	oz/yd <sup>3</sup> (L/m <sup>3</sup> )	148.5 (5.74)
Wet unit weight	lb/ft <sup>3</sup> (kg/m <sup>3</sup> )	121 (1,938)
Dry unit weight	lb/ft <sup>3</sup> (kg/m <sup>3</sup> )	118 (1,890)

Table 1-2: Class AA Deck Concrete Mix Design

<b>Material</b>	<b>Units</b>	<b>Quantity</b>
Type I cement	lb/yd <sup>3</sup> (kg/m <sup>3</sup> )	635 (376.7)
Normal weight fine aggregate	lb/yd <sup>3</sup> (kg/m <sup>3</sup> )	1,102 (653.9)
Normal weight coarse aggregate	lb/yd <sup>3</sup> (kg/m <sup>3</sup> )	1,872 (1,111)
Water	gal (L)	33 (124.9)
Set Retarder	oz/yd <sup>3</sup> (L/m <sup>3</sup> )	4.0 (0.155)

#### 1.4 Report Organization

The properties of field cast HSLW are presented in Chapter 2. Chapter 3 presents the material properties of the deck concrete. Chapter 4 discusses a comparison of observed bridge behavior under a test loading with FEA models. Chapter 5 investigates the observed loss of prestressing and compares it with current estimation methods. Chapter 6 examines camber variations in the girders and compares with estimation techniques. Chapter 7 presents the conclusions and recommendation drawn from this study.

## 2. HSLW Material Property Characterization

The properties of prestressing plant-cast HSLW were determined by casting 6 in. x 12 in. (15.2 cm x 30.5 cm) and 4 in. x 8 in. (10.1 cm x 20.2 cm) cylinder specimens from all batches made in the production of the girders. Girders 1, 2, and 3 were cast on August 6<sup>th</sup>, 2008 and girders 4 and 5 on August 8<sup>th</sup>, 2008. The transfer of prestressing force occurred at 5 days of age for girders 1, 2, and 3, and at 3 days of age for girders 4 and 5. There were approximately six 3 cubic yard (2.29 m<sup>3</sup>) batches per beam. The strength gain characteristics (Section 2.1), elastic modulus (Section 2.2), coefficient of thermal expansion (Section 2.3), and creep and shrinkage properties (Section 2.4) of HSLW were investigated.

### 2.1 Compressive Strength

The compressive strength of the cylinders was measured in accordance with ASTM C 39 (2005). The tests were conducted at various ages after casting. Three 4 in. x 8 in. (10.1 cm x 20.2 cm) cylinders were taken from every batch for compressive strength testing at 56 days. The batches corresponding to mid-span in each beam were sampled extensively for testing at various ages with three cylinders being used to determine the mean of each batch; over 240 cylinders were tested. An ANOVA statistical analysis was run on the 56 day data, and it was shown that all batches in each girder, as well as all of the girders, could be considered statistically equivalent within a 95% confidence interval.

Table 2-1 shows the compressive strengths of each girder at various ages. Figure 2-1 shows the average strength gain curve for the girders along with +/- one standard deviation. All girders met the required design strength by 56 days of age.

Table 2-1: Compressive strength data

Girder	Compressive Strength, psi (MPa)				
	Release	7 days	28 days	56 days	180 days
1	7,760 (53.5)	8,190 (56.5)	9,300 (64.2)	10,020 (69.1)	10,540 (72.6)
2	8,620 (59.4)	8,530 (58.8)	9,690 (66.8)	10,220 (70.5)	10,430 (71.9)
3	8,610 (59.3)	8,890 (61.3)	9,800 (67.6)	10,170 (70.1)	11,470 (79.1)
4	7,180 (49.5)	7,170 (49.4)	9,280 (64.0)	10,470 (72.2)	10,750 (74.1)
5	7,090 (48.9)	8,110 (55.9)	10,300 (71.0)	10,310 (71.1)	11,540 (79.6)
Average	7,850 (54.1)	8,180 (56.4)	9,680 (66.7)	10,240 (70.6)	10,950 (75.5)

The measured compressive strength of 10,240 psi (70.6 MPa) at 56 days is 11.3% lower than the 11,550 psi (79.6 MPa) value measured by Meyer (2002) for the same mix design. Meyer's tests were conducted on both laboratory and plant-batched samples. It was concluded that for the girders being constructed, the lightweight aggregate was not fully saturated which led to a lower compressive strength.

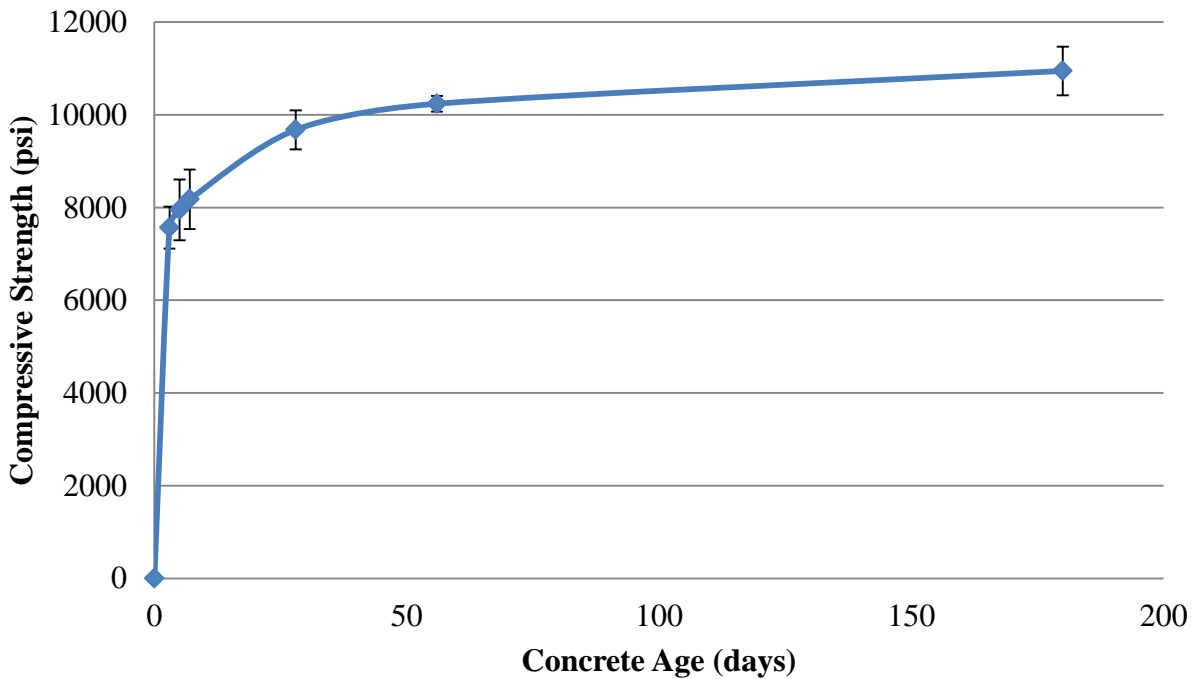


Figure 2-1: HSLW compressive strength gain curve, (1 psi = 6.89 kPa)

## 2.2 Elastic Modulus

Although HSLW concrete is able to gain high strengths, the modulus of elasticity is significantly lower than that of normal weight concretes which leads to a more flexible bridge girder. The design of the bridge deck profile requires an accurate estimate of the girder stiffness. The ability to predict the camber and deflections allows for a satisfactory road profile resulting in a smooth ride. A key component to both camber and girder stiffness is the elastic modulus. The elastic modulus of HSLW was determined using 6 in. x 12 in. (15.2 cm x 30.5 cm) cylinder tests, load testing of the girders, and through measuring deflections during deck placement. The experimental elastic modulus values were compared with estimation equations.

### 2.1.1 Cylinder Measurements

Samples for elastic modulus testing were cast from every batch of HSLW. At 56 days, all batches had one modulus test performed, and at all other dates only one cylinder from the batches corresponding to mid-span of each girder was tested and used for the mean modulus calculation. Modulus of elasticity tests were conducted according to ASTM C 469 (2002). The values were calculated using a chord modulus through  $0.4\bar{f}_c$ , where  $\bar{f}_c$  is the average compressive strength of the concrete at time of testing. The average elastic modulus is given in Table 2-2 for ages tested.

Table 2-2: Cylinder elastic modulus data

Girder	Elastic Modulus, ksi (GPa)		
	Strand Release	56 day	180days
1	3,660 (25.2)	3,850 (26.6)	3,760 (25.9)
2	3,720 (25.6)	3,700 (25.5)	3,820 (26.3)
3	3,680 (25.4)	3,500 (24.1)	3,890 (26.8)
4	3,380 (23.3)	3,790 (26.1)	3,330 (23.0)
5	3,220 (22.2)	3,790 (26.1)	3,890 (26.8)
Average	3,530 (24.3)	3,730 (25.7)	3,740 (25.8)
Std. Dev.	220 (1.52)	254 (1.75)	235 (1.62)

### 2.2.2 Elastic Modulus Estimation Methods

The modulus of elasticity is often unknown during the design process, therefore estimator equations are used. Previous research suggested that the elastic modulus of lightweight concretes is dependent on both the type of aggregate used and whether it was fully saturated prior to batching (Lopez, 2005).

AASHTO LRFD (2007) uses Eq. 2-1 to calculate the modulus of elasticity in section 8.4.2.4 of the code. This equation is identical to the one used by ACI 318 (2008) for normal strength concretes.

$$E_c = w_c^{1.5} 33 \sqrt{f_c'} \quad (\text{Eq. 2-1})$$

Where,

$E_c$  = Modulus of elasticity, psi

$w_c$  = weight of concrete, lb/ft<sup>3</sup>

$f_c'$  = compressive strength of concrete, psi

ACI 363 (1997) suggests the use of Eq. 2-2 when prediction modulus of elasticity for high strength concrete.

$$E_c = \left(40,000\sqrt{f'_c} + 1.0 \times 10^6\right) \left(\frac{w_c}{145}\right)^{1.5} \quad (\text{Eq. 2-2})$$

Meyer (2002) developed a new equation specifically for High Strength Lightweight concrete, shown in Eq. 2-3.

$$E_c = 44,000 \sqrt{f'_c \frac{w_c}{145}} \quad (\text{Eq. 2-3})$$

Cook and Meyer (2006) developed Eq. 2-4 for concrete using lightweight aggregates. The equation is based off of several mix designs utilizing various types of lightweight aggregates.

$$E_c = w_c^{2.687} f_c^{0.24} \quad (\text{Eq. 2-4})$$

The National Cooperative Highway Research Program (2007) utilizes Eq. 2-5, which was developed by Rizkalla, to estimate the elastic modulus of high performance concrete.

$$E_c = 310,000 K_1 w_c^{2.5} f_c^{0.33} \quad (\text{Eq. 2-5})$$

Where,

- $E_c$  = Modulus of elasticity, ksi
- $w_c$  = weight of concrete, kip/ft<sup>3</sup>
- $f'_c$  = compressive strength of concrete, ksi
- $K_1$  = Correction factor for aggregate source, taken as 1.0 unless tested

### 2.2.3 Field Load Testing of Girders

A load test was performed at 56 days of age on each bridge girders to determine their stiffness for profiling of the bridge deck. The tests were performed by loading each girder at

mid-span with a concrete block weighing 17.9 kip (8,120 kg) applied at the harp point on the bottom of the beam. Deflection was measured using a taut wire system. Figure 2-2 shows the load test set-up at the precast plant.



Figure 2-2: Load test set-up

Table 2-3 presents the measured deflections, except for girder 5 which was recorded incorrectly. An average deflection of 0.64 in (1.63 cm) was observed during the tests.

Table 2-3: Load test deflections

Girder	1	2	3	4
Deflection in. (cm)	0.69 (1.75)	0.65 (1.65)	0.63 (1.59)	0.61 (1.55)

The stiffness,  $EI$ , of each girder was computed using Equation 2-6 with the measured deflections, loading, and boundary conditions. Table 2-4 presents the measured stiffness values,

which were, on average, 21% larger than predicted using the measured elastic modulus from cylinder data and standard gross cross-section of a BT-54 girder.

$$\Delta = \frac{P*L^3}{48*E_c*I} \quad (\text{Eq. 2-6})$$

Where,

- $\Delta$  = Deflection, in.
- P = Applied load at mid-span, kips
- L = Span Length, in.
- $E_c$  = Elastic modulus of concrete, ksi
- I = Moment of inertia, in.<sup>4</sup>

Table 2-4: Experimental and theoretical stiffness of girders

<b>Girder</b>	<b>Measured EI, kip ft<sup>2</sup> (kN m<sup>2</sup>)</b>	<b>Theoretical EI, kip ft<sup>2</sup> (kN m<sup>2</sup>)</b>	<b><u>EI Measured</u> <u>EI Theory</u></b>
1	7.883 x 10 <sup>6</sup> (3.255 x 10 <sup>6</sup> )	6.942 x 10 <sup>6</sup> (2.867 x 10 <sup>6</sup> )	1.14
2	8.258 x 10 <sup>6</sup> (3.410 x 10 <sup>6</sup> )	6.942 x 10 <sup>6</sup> (2.867 x 10 <sup>6</sup> )	1.19
3	8.671 x 10 <sup>6</sup> (3.581 x 10 <sup>6</sup> )	6.942 x 10 <sup>6</sup> (2.867 x 10 <sup>6</sup> )	1.25
4	8.899 x 10 <sup>6</sup> (3.675 x 10 <sup>6</sup> )	6.942 x 10 <sup>6</sup> (2.867 x 10 <sup>6</sup> )	1.28
<b>Average</b>	8.428 x 10 <sup>6</sup> (3.481 x 10 <sup>6</sup> )	6.942 x 10 <sup>6</sup> (2.867 x 10 <sup>6</sup> )	1.21

The actual cross-section dimensions of each girder were measured; the calculated moment of inertia was 5.3% larger than the standard tabulated value. The values for the measured gross moment of inertia and transformed section, including steel reinforcement, moment of inertia are given in Table 2-5.

Table 2-5: Measured gross and transformed moments of inertia of girders

<b>Girder</b>	<b>Measured I, in<sup>4</sup> (cm<sup>4</sup>)</b>	<b>Transformed Measured I, in<sup>4</sup> (cm<sup>4</sup>)</b>	<b><u>I Measured</u> I Standard</b>
1	281,001 (11.696 x 10 <sup>6</sup> )	287,821 (11.980 x 10 <sup>6</sup> )	1.048
2	280,597 (11.679 x 10 <sup>6</sup> )	287,719 (11.976 x 10 <sup>6</sup> )	1.047
3	283,731 (11.810 x 10 <sup>6</sup> )	291,046 (12.114 x 10 <sup>6</sup> )	1.058
4	282,799 (11.771 x 10 <sup>6</sup> )	291,208 (12.121 x 10 <sup>6</sup> )	1.055
5	283,444 (11.798 x 10 <sup>6</sup> )	291,439 (12.131 x 10 <sup>6</sup> )	1.057
<b>Average</b>	282,314 (11.7501 x 10 <sup>6</sup> )	289,858 (12.065 x 10 <sup>6</sup> )	1.053

Utilizing Eq. 2-6 with the measured transformed moment of inertia the mean elastic modulus of the beams was computed. The apparent elastic modulus in the girders was determined to be 4,190 ksi (28.9 GPa), which is 12.5% larger than the elastic modulus determined by testing of cylinders per ASTM C 469 (2002) at the same age. Table 2-6 shows the apparent elastic modulus of each beam.

Table 2-6: Elastic modulus of girders during load test

<b>Girder</b>	<b>Measured E, ksi (GPa)</b>
1	3,940 (27.2)
2	4,130 (28.5)
3	4,290 (29.6)
4	4,400 (30.3)
<b>Average</b>	4,190 (28.9)

#### 2.2.4 Deck Pour Deflections

The deflections of the bridge girders due to loading during the deck pour were monitored using a surveying total station, which had a maximum accuracy of 0.03 in. (0.8 mm). The elastic modulus of each beam was determined by using the measured deflection with the measured cross-section properties (Table 2-5) and estimated loading. Table 2-7 shows a comparison of the expected and measured deflections, as well as the elastic modulus determined from the girder

deflections. The average elastic modulus is within 2.7% of that observed during the load testing of the girders. The actual elastic modulus may be higher than the measured value from the deck pour due to assumptions that were made for the as-constructed deck thickness and height of the haunch between the deck and top of the beam. The deck thickness from construction documents and average haunch height measured at mid-span were used for the theoretical estimate.

Table 2-7: Deflections and experimental modulus from deck casting

<b>Girder</b>	<b>Deflection, in. (cm)</b>		<b>Elastic Modulus, ksi (GPa)</b>
	<b>Theoretical</b>	<b>Measured</b>	
1	1.79 (4.55)	1.88 (4.78)	3980 (26.8)
2	2.09 (5.31)	2.16 (5.49)	4070 (28.0)
3	2.09 (5.31)	2.09 (5.31)	4180 (28.8)
4	2.09 (5.31)	2.11 (5.36)	4140 (28.5)
5	1.79 (4.55)	1.86 (4.72)	4030 (27.8)
Average	N/A	N/A	4080 (28.1)

### 2.2.5 Elastic Modulus Summary

Figure 2-3 shows the modulus of elasticity data from experimental measurements and the estimator equations presented, along with a trend-line from the cylinder data. The cylinder-measured modulus provided a lower modulus than what was observed in the beams. The cylinder measured data shows a wide scatter of values for similar strengths, as well as a lower dependency with respect to compressive strength than the estimator equations predict. The predictor equations developed by Meyer, ACI 363, and Cook and Meyer best match the experimental data.

The Meyer (2002) estimator equation best agreed with the measured elastic modulus of the girders as shown in Figure 2-3. The Meyer equation provided an estimate of within 3%, which was to be expected since the equation was developed for HSLW using expanded slate lightweight aggregate. All predictor equations developed for HPC or LWC besides the Meyer

equation under-predicted the modulus. The AASHTO equation overestimated the modulus by over 6%. In conclusion, the Meyer equation should be utilized for estimating the elastic modulus of HSLW during the design process.

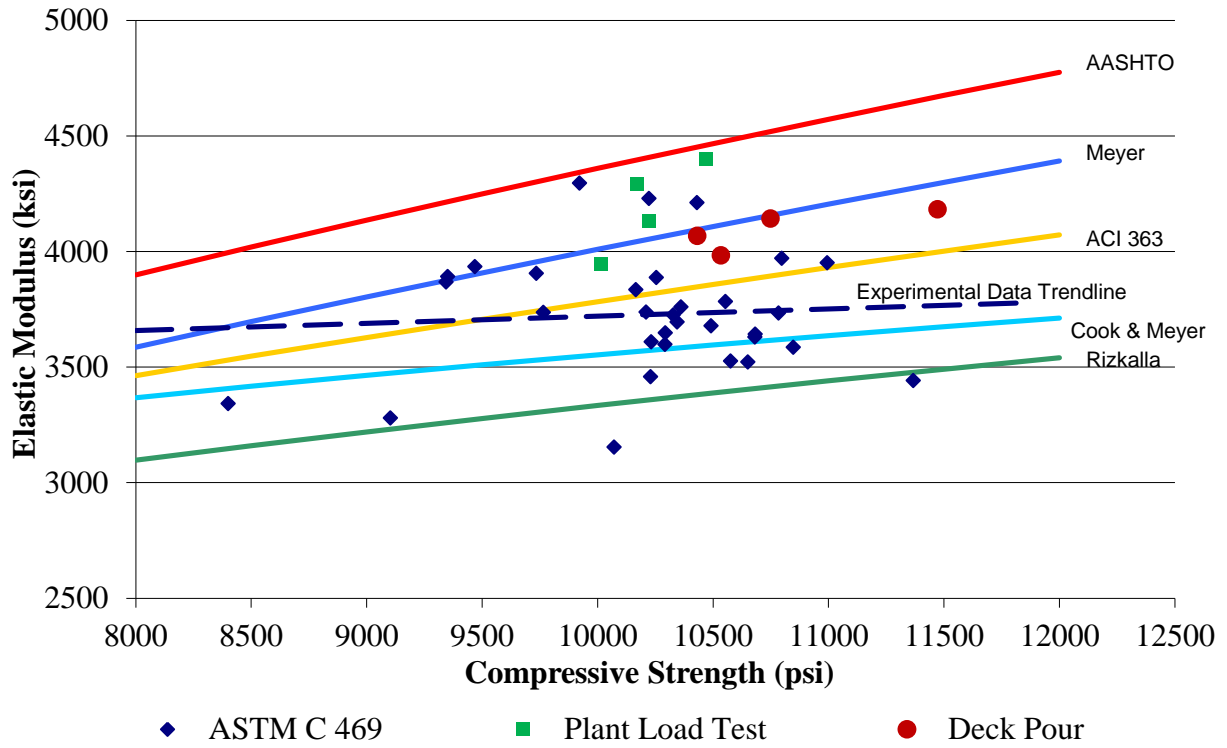


Figure 2-3: HSLW cylinder data comparison with estimator equations, (1 psi = 6.89 kPa)

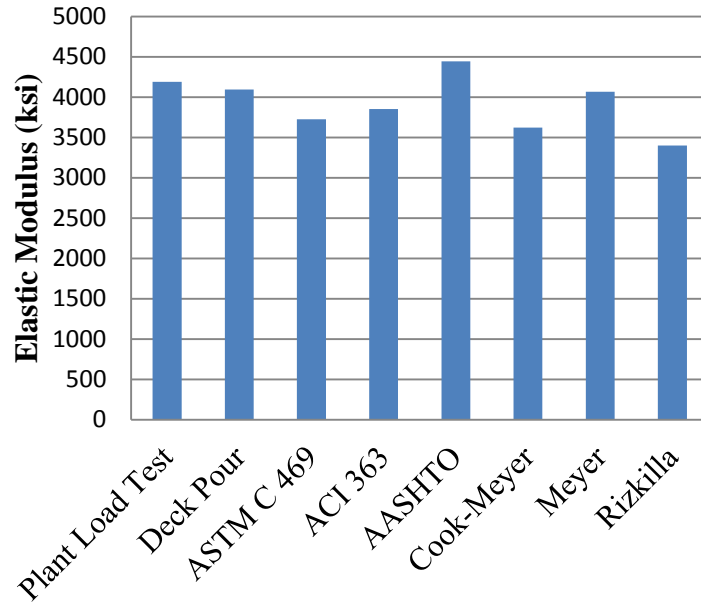


Figure 2-4: Elastic modulus comparison for HSLW with prediction methods (1ksi = 6.89MPa)

### 2.3 Coefficient of Thermal Expansion

Coefficient of thermal expansion tests were conducted in accordance with CRD-C 39 (1981). Tests were performed at 100% humidity in a Thermotron SE-1200. One cylinder from the batch corresponding to mid-span from each girder was tested at each age. Table 2-8 shows the results for the ages tested. These values were used in the determination of behavior of the bridge structure due to thermal effects. The measured values are lower than typical NWC, which is expected when using a light-weight coarse aggregate (Neville, 1997). These values were used for correcting the raw data from the VWSG's for determination of internal strains throughout the project.

Table 2-8: Coefficient of thermal expansion of HSLW

Batch	Coefficient of Thermal Expansion, $\mu\epsilon/^{\circ}\text{F}$ ( $\mu\epsilon/^{\circ}\text{C}$ )					
	14 day		56 day		180 day	
1-3	4.57	(8.23)	3.96	(7.14)	3.43	(6.18)
2-3	4.82	(8.68)	3.67	(6.61)	3.74	(6.73)
3-3	3.94	(7.09)	3.64	(6.55)	3.43	(6.18)
4-4	4.14	(7.45)	3.18	(5.73)	3.54	(6.36)
5-3	4.65	(8.36)	4.04	(7.27)	3.13	(5.64)
<b>Average</b>	4.42	(7.96)	3.70	(6.66)	3.45	(6.22)

## 2.4 Creep and Shrinkage

The creep and shrinkage characteristic of HSLW were evaluated in accordance with ASTM C 512 (2002). 6 in. x 12 in. (15.2 cm x 30.5 cm) cylinders were cast from the batch corresponding to mid-span of each beam. The study was conducted in a controlled 73° F (22.8° C) and 50% relative humidity environment after moist curing. Measurements of creep and shrinkage were started at 5 and 3 days of age for girders 1 through 3, and for 4 and 5, respectively, which coincided with release of prestressing into the girders.

The creep studies were performed at 40% of ultimate strength of the concrete at time of loading. Readings for creep and shrinkage were taken using a DEMEC gage with an accuracy of  $10^{-4}$  in ( $2.54 \times 10^{-3}$  mm) over a 10 in (25.4 cm). gage length. Only 1 cylinder from each batch was loaded, for a total of 5 cylinders. Shrinkage was measured on at least one companion specimen from each batch. Figure 2-5 shows a loaded creep frame and DEMEC gage used for measuring length changes. Measurements were performed on 4 sides of the cylinders and the observed values were averaged.



Figure 2-5: Creep frame

Figure 2-6 shows the average shrinkage from all batches of HSLW with drying starting at the same time as loading of creep cylinders and the measured values on the same mix design when measurements were started at 24 hours of age (Lopez, 2005). The observed value of  $181 \mu\epsilon$  at 750 days of age is significantly smaller than the predicted values of  $405 \mu\epsilon$  and  $603 \mu\epsilon$  predicted from the AASHTO LRFD (2007) and ACI 209 (1992) prediction methods, respectively. The values reported by Lopez (2005) are higher than the measured values due to

their decreased maturity at the start of testing. Approximately 90% of the observed shrinkage losses occurred by 110 days of age.

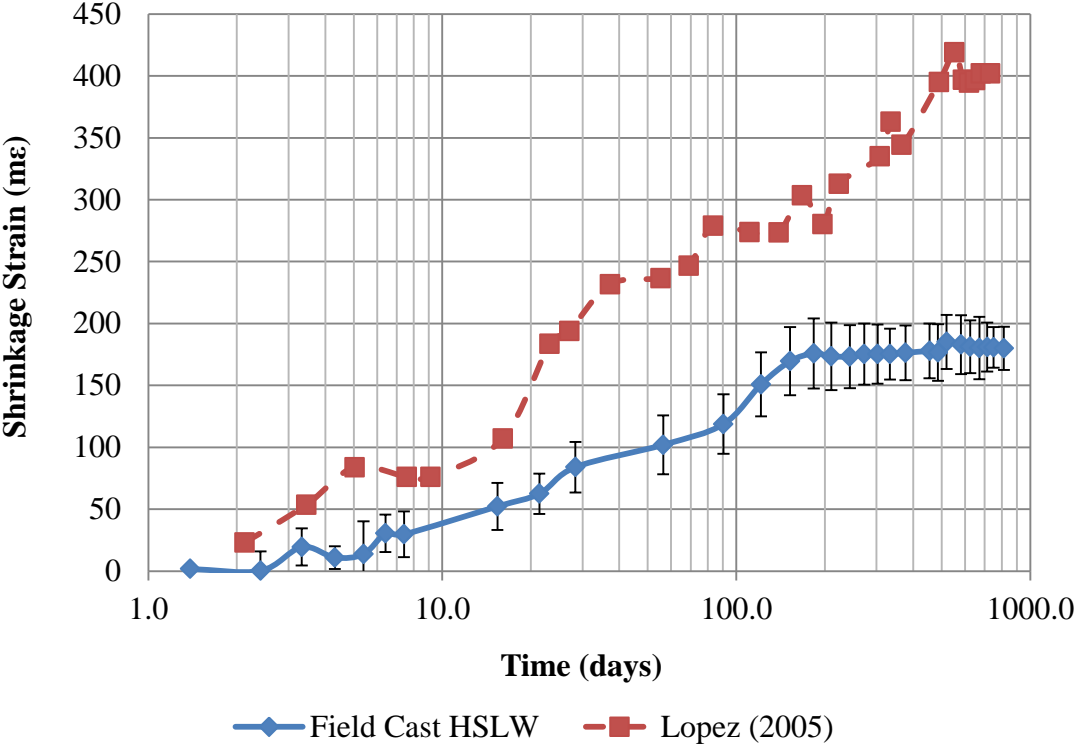


Figure 2-6: Average shrinkage of HSLW

Figure 2-7 presents the results of the creep study in the format of specific creep, which is the ratio of the creep component of measured strain to the applied stress. At 750 days, HSLW exhibited a specific creep of  $0.497\mu\epsilon/\text{psi}$  ( $72.08\mu\epsilon/\text{MPa}$ ). This is higher than the observed behavior on the same mix design under lab cast conditions by Lopez (2005), which is also shown in Figure 2-7. The difference in the creep coefficient is likely due to inadequate soaking of the lightweight aggregate prior to casting.

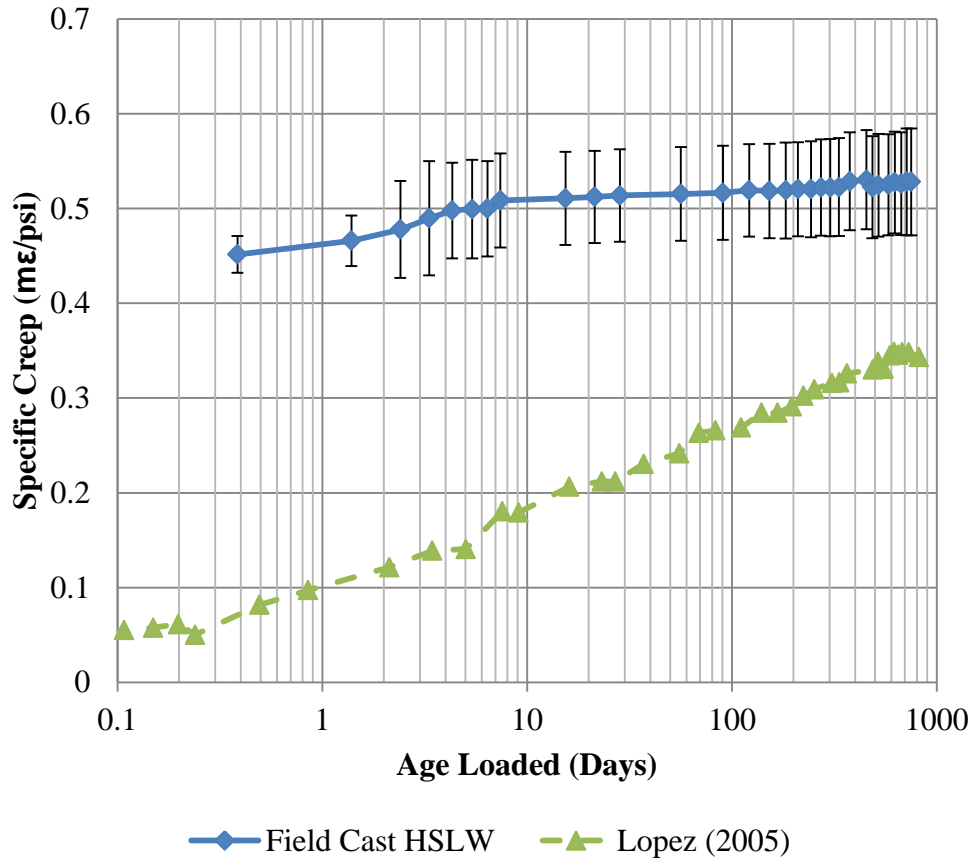


Figure 2-7: Specific creep of HSLW

Another measure of creep behavior is the creep coefficient, which is the ratio of the creep component of strain to the instantaneous elastic component. The creep coefficient is used in predicting prestress losses, as discussed in Chapter 5. The measured creep coefficient value of 0.78 at 750 days is 34% lower than the 1.18 predicted by AASHTO LRFD (2007). Both the shrinkage and creep data show that after approximately 200 days of age, no significant increases in strain occurred with HSLW.

### 3. Deck Concrete Mechanical Properties

The properties of the deck concrete were evaluated from all batches placed over the observed span on the bridge. Specimens were cast at the bridge site on October 6<sup>th</sup>, 2009. The compressive strength (Section 3.1), elastic modulus (Section 3.2), coefficient of thermal expansion (Section 3.3), and shrinkage characteristics (Section 3.4) were investigated.

#### 3.1 Compressive Strength

The compressive strength of the cylinders was measured in accordance with ASTM C 39 (2005). The tests were conducted at various ages after casting. Three 4 in. x 8 in. (10.1 cm x 20.2 cm) compressive strength cylinders were taken from every batch, 19 batches total, for testing at 56 days. The batches corresponding to approximately quarter-span (S1), mid-span (S2), and three-quarter-span (S3) in the bridge were sampled extensively for testing at various ages with three cylinders being used to determine the mean of each batch.

An ANOVA statistical analysis was run on the 56 day data, and it was shown that statistically the batches could not be considered equivalent. The wide variation in strengths may be due to the addition of water to the batch on site. All batches met the required strength requirement at 28 days of age. Table 3-1 shows the average compressive strength of the batches at various ages, and Table 3-2 shows the compressive strength of all 19 batches at the time when the bridge load test was performed (96 days of age).

Table 3-1: Compressive strength of deck concrete at various ages

Batch	Compressive Strength, psi (MPa)						
	7 days		28 days		56 days		Bridge Load Test (96 days)
S1	4,350	(30.0)	4,830	(33.3)	5,560	(38.4)	6,120 (42.2)
S2	5,310	(36.6)	6,140	(42.4)	6,580	(45.3)	6,850 (47.2)
S3	3,570	(24.6)	4,140	(28.5)	4,740	(32.7)	5,190 (35.8)
<b>Average</b>	4,410	(30.4)	5,040	(34.7)	5,630	(38.8)	6,050 (41.7)

Table 3-2: Compressive strength of deck concrete at time of bridge load test (96 days)

Batch	Strength, psi (MPa)
1	6,280 (43.3)
2	5,980 (41.2)
3	7,440 (51.3)
4	5,610 (38.7)
5 (S1)	6,120 (42.2)
6	5,510 (38.0)
7	6,810 (47.0)
8	7,100 (49.0)
9	6,210 (42.8)
10 (S2)	6,850 (47.2)
11	5,980 (41.2)
12	6,960 (48.0)
13	7,400 (51.0)
14	6,740 (46.4)
15 (S3)	5,190 (35.8)
16	6,240 (43.0)
17	7,340 (50.6)
18	6,730 (46.4)
19	6,860 (47.3)
<b>Average</b>	6,490 (44.8)

### 3.2 Elastic Modulus

Samples for elastic modulus testing were cast from every batch. Tests were performed on 6 in. x 12 in. (15.2 cm x 30.5 cm) cylinders, with one cylinder per batch tested used. At the time of load testing the composite bridge structure, all batches had a modulus test performed, and at all other dates only the batches S1, S2, and S3 were tested and used for the mean modulus calculation. Modulus of elasticity tests were conducted according to ASTM C 469 (2002). The average elastic modulus is given in Table 3-3 for various ages based on batches S1, S2, and S3. Table 3-4 presents the measured modulus and Poisson's ratio of every batch at the time of the composite bridge structure load test. The observed Poisson's ratio of 0.19 is in the range of normal values for concrete (Neville, 1997).

Table 3-3: Elastic modulus of deck concrete at various ages

Batch	Elastic Modulus, ksi (GPa)			
	7 days	28 days	56 days	Bridge Load Test
S1	3,140 (21.7)	3,520 (24.3)	3,840 (26.5)	3,910 (26.9)
S2	3,510 (24.2)	3,670 (25.3)	4,020 (27.7)	4,000 (27.6)
S3	3,120 (21.5)	3,330 (23.0)	3,580 (24.7)	3,620 (25.0)
<b>Average</b>	3,260 (22.5)	3,510 (24.2)	3,810 (26.3)	3,840 (26.5)

Table 3-4: Elastic modulus of deck concrete at time of bridge load test

<b>Batch</b>	<b>Elastic Modulus, ksi (GPa)</b>	<b>Poisson's Ratio</b>
1	4,080 (28.1)	0.171
2	4,270 (29.4)	0.195
3	4,590 (31.6)	0.216
4	3,250 (22.4)	0.138
5 (S1)	3,910 (26.9)	0.187
6	3,730 (25.7)	0.171
7	3,580 (24.7)	0.178
8	4,040 (27.9)	0.191
9	3,620 (24.9)	0.165
10 (S2)	4,000 (27.6)	0.166
11	4,630 (31.9)	0.227
12	4,120 (28.4)	0.191
13	4,070 (28.1)	0.184
14	4,300 (29.7)	0.216
15 (S3)	3,620 (25.0)	0.198
16	3,960 (27.3)	0.207
17	4,210 (29.0)	0.210
18	4,160 (28.7)	0.185
19	3,790 (26.1)	0.184
<b>Average</b>	4,000 (27.6)	0.188

### 3.3 Coefficient of Thermal Expansion

Coefficient of thermal expansion tests were conducted in accordance with CRD-C 39 (1981). Tests were performed at 100% humidity in a Thermotron SE-1200. One 6 in. x 12 in. (15.2 cm x 30.5 cm) cylinder from batches S1, S2, and S3 was tested at each age. Table 3-5 shows the results of the ages tested. These values were used to correct data from the VWSG's for thermal variations between readings. The measured values at 56 days of age were 28% larger than the measured values for HSLW at the same age.

Table 3-5: Coefficient of thermal expansion of deck concrete

Batch	Coefficient of Thermal Expansion, $\mu\epsilon/^{\circ}\text{F}$ ( $\mu\epsilon/^{\circ}\text{C}$ )			
	28 day		56 day	
S1	4.78	(8.61)	4.55	(8.18)
S2	5.00	(9.00)	4.95	(8.91)
S3	4.95	(8.91)	4.78	(8.61)
<b>Average</b>	4.91	(8.84)	4.76	(8.57)

### 3.4 Shrinkage

The shrinkage of the deck concrete was measured on samples cast from batches corresponding to quarter-span (S1), mid-span (S2), and three quarter-span (S3). A set of measurements were made on prism samples using ASTM C 157 (2006), as well as on slab specimens designed to be representative of a deck cross-section and environmental restraints.

#### 3.4.1 Prism Shrinkage

Prism shrinkage tests were performed in accordance with ASTM C 157 (2006) on 3 in. x 3 in. x 11.25 in. (7.6 cm x 7.6 cm x 28.6 cm) samples with a 10 in. gage length. Three samples were made from each batch, fog-room cured for 28 days, then monitored for changes in length due to shrinkage at 73°F and 50% relative humidity. Figure 3-1 shows the results of the monitored batches. Additionally, the prediction methods of ACI 209 (1992) and AASHTO LRFD (2007) are plotted.

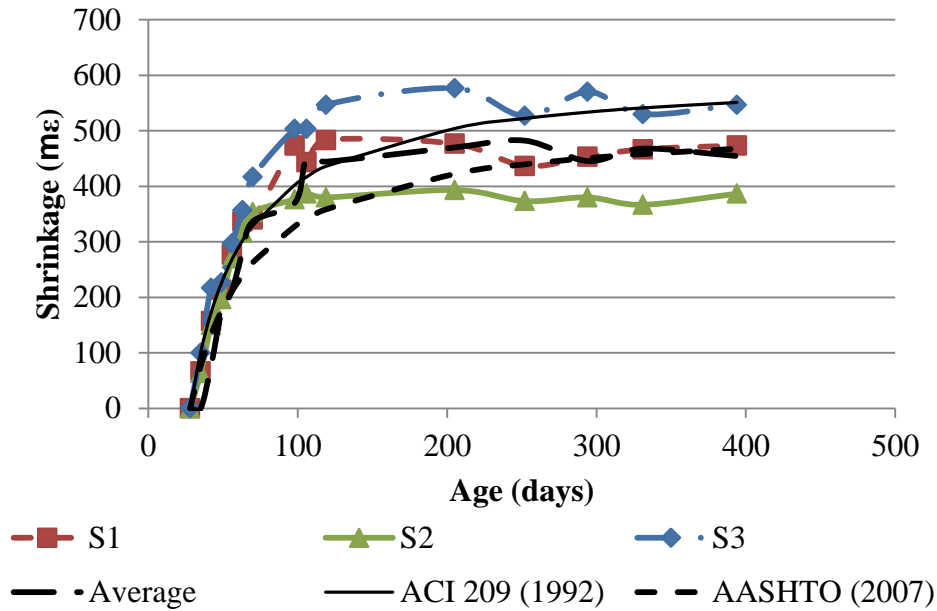


Figure 3-1: Shrinkage strains from sampled concrete batches under standard curing

Large variations in shrinkage strains occurred between batches. The ACI 209 (1992) prediction method best fits the shrinkage behavior at early ages; however, over-estimates the average shrinkage strain at 394 days. The AASHTO (2007) prediction method predicted the average shrinkage strain at 394 days to within 1%.

Additional prism specimens, 3 in. x 3 in. x 11.25 in. (7.6 cm x 7.6 cm x 28.6 cm), were cast from batch S2 (mid-span) to determine the influence of curing on the observed shrinkage behavior. The second set of specimens was moist cured for 13 days, to match the curing performed in the bridge deck. Figure 3-2 shows the effect of 13 days of moist curing versus 28 days, as required by ASTM C 157 (2006).

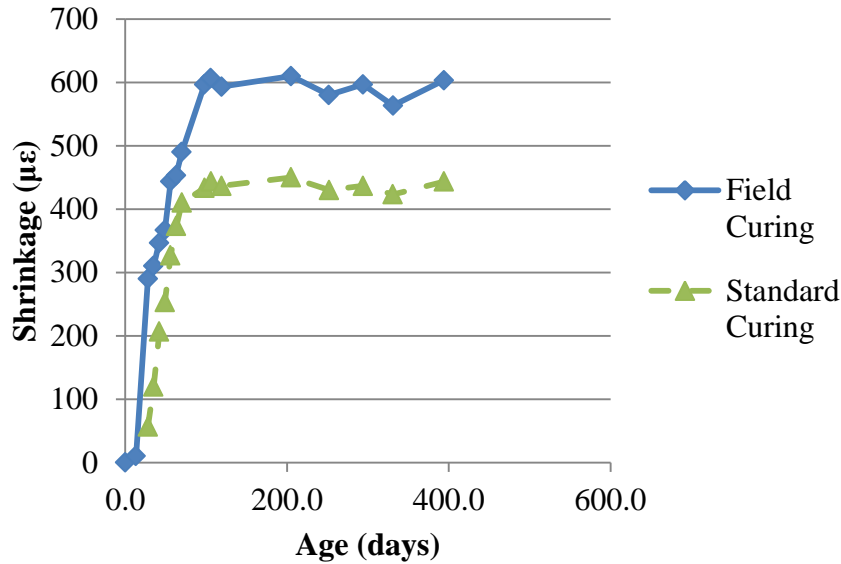


Figure 3-2: Shrinkage strains of field cured and standard cured samples

The field cured specimens showed an increased shrinkage strain of 206  $\mu\epsilon$  at 394 days of age. The ACI 209 (1992) method predicts an increase of 50  $\mu\epsilon$  due to the change in curing, and AASHTO LRFD (2007) does not explicitly incorporate the age at exposure into its calculations of predicted shrinkage strain.

### 3.4.2 Slab Shrinkage

A set of special prism specimens was cast from batch S2 (mid-span) to capture the differential shrinkage that occurs in the deck due to only one free surface for loss of moisture. These slab specimens cast were 8 in. x 8 in. x 16 in. (20.3 cm x 20.3 cm x 40.6 cm). Figure 3-3 shows the slab specimens and the gage points along the depth. Gage points were placed at 2 in. (5.08 cm) intervals along the depth of the three blocks on both sides. The sides and bottom of the slab specimens were sealed after 28 days of moist curing to prevent moisture loss from all surfaces except the top, which is the environmental condition that bridge decks are exposed to.

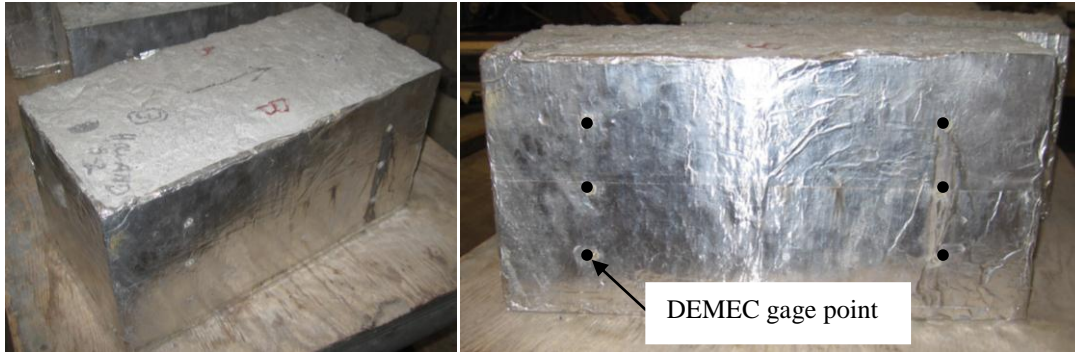


Figure 3-3: Slab shrinkage specimen and gage point locations

Figure 3-4 presents the average shrinkage for the different depths into each slab specimen. The results showed a decrease in shrinkage with increasing depth into the block. After 120 days, over 95% of the observed shrinkage had occurred, regardless of depth into section. The magnitude of shrinkage strain at the top is consistent with values measured for unrestrained shrinkage specimens (Section 3.4.1).

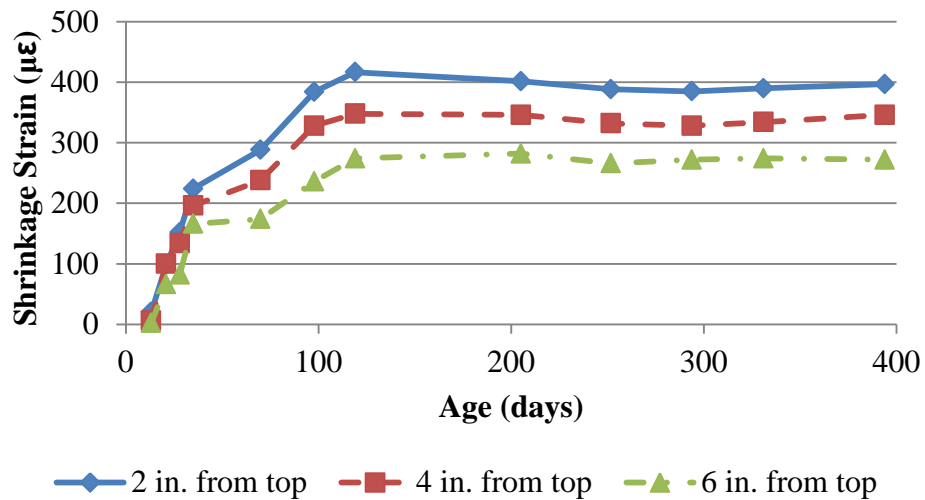


Figure 3-4: Shrinkage strains at depths into slab specimens

The pattern of decreasing shrinkage with depth causes an induced curvature in the slab specimens. The calculated curvatures from the shrinkage data are shown in Figure 3-5. The measured curvatures from the slab specimens were used in a finite element model of the bridge to predict long-term camber changes.

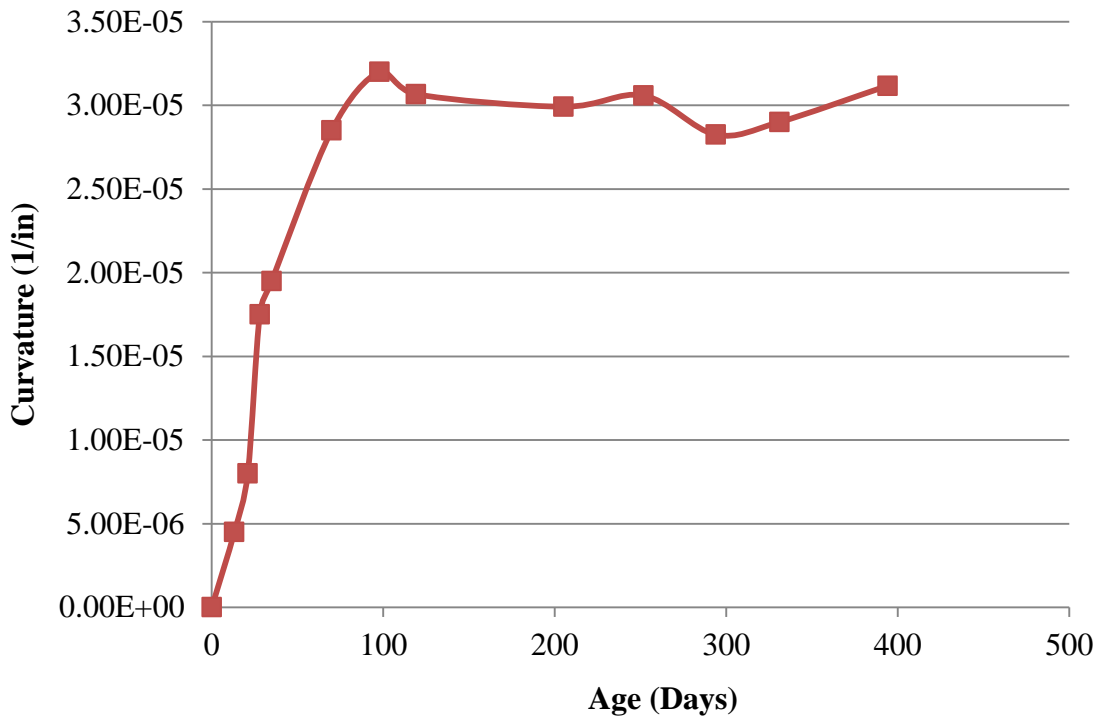


Figure 3-5: Curvature of slab specimens due to shrinkage (1 in. = 2.54 cm)

## 4. Load Test of Bridge Structure

A load test of the completed bridge structure was performed on January 14<sup>th</sup>, 2009. The objective of the load test was to characterize the composite behavior of the bridge system and to compare the observed behavior with simple and complex analyses. Mid-span deflections and internal strains of the girders and deck were measured, and each was compared with a finite element results.

### 4.1 Load Test Description

The bridge load test was performed by placing two fully loaded dump trucks at various positions along the bridge and monitoring the girder mid-span deflections and internal strains given by the VWSG's. The wheel loads and their positions are given in Figure 4-1. The weight of each wheel was measured using portable scales from the Hogansville GDOT Weight Station.

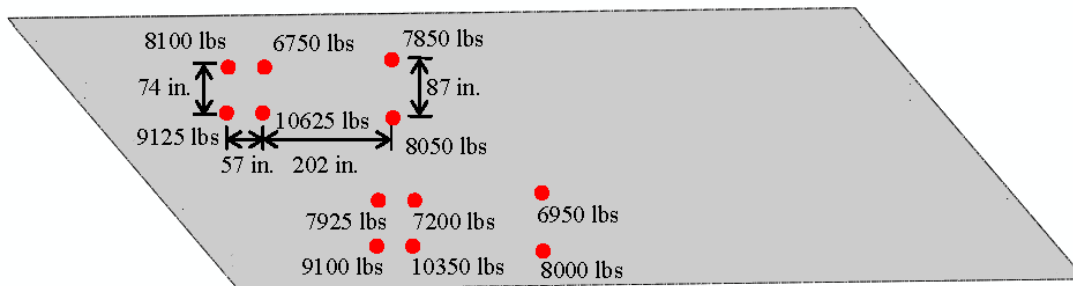


Figure 4-1: Load and arrangements of the truck wheels (1lb = 0.454kg)

Figures 4-2, 4-3, and 4-4 show the three loading positions utilized, which correspond to approximately the rear axle being centered over quarter-span (LT1), mid-span (LT2), and three quarter-span (LT3) of the bridge.

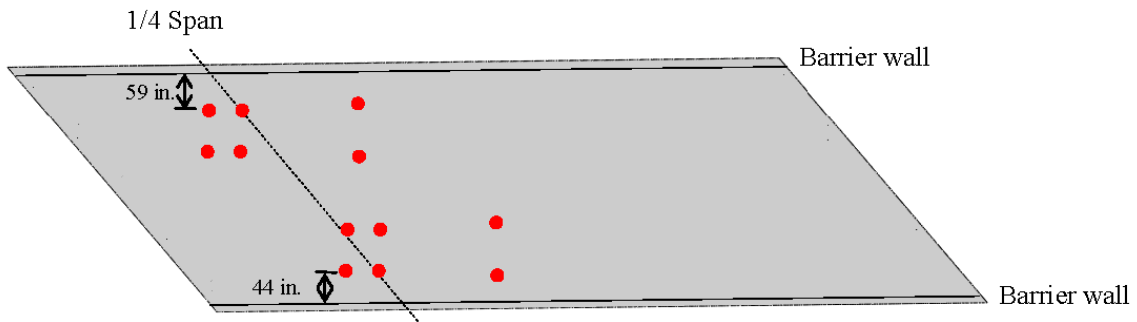


Figure 4-2: Truck positions during LT1 (1 in. = 2.54 cm)

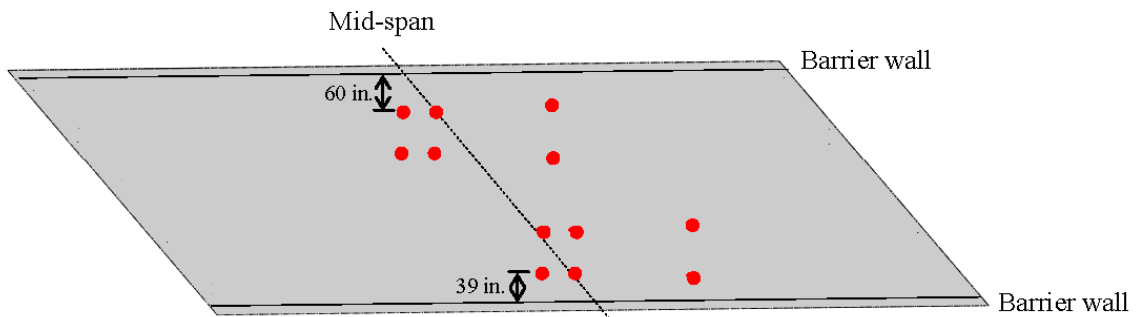


Figure 4-3: Truck positions during LT2 (1 in. = 2.54 cm)

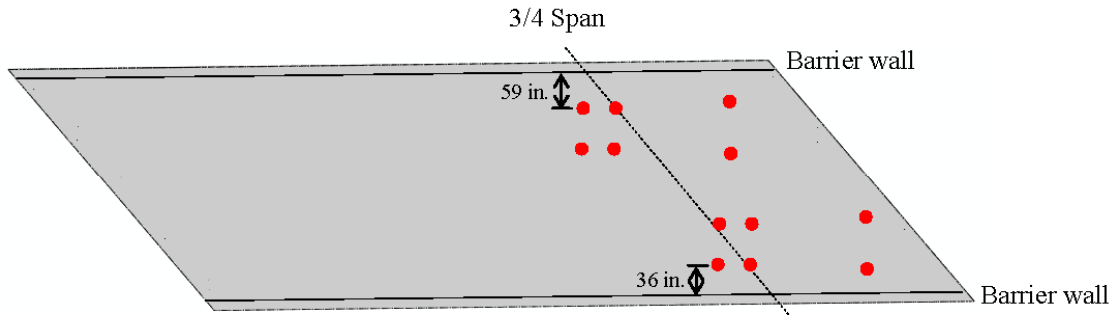
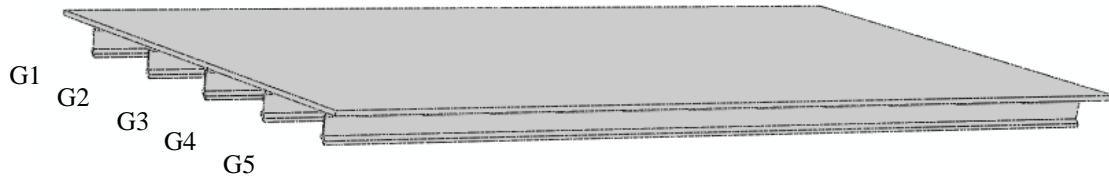


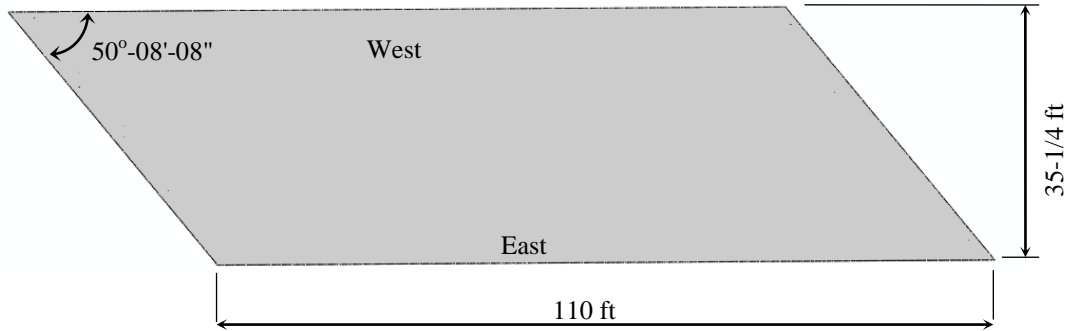
Figure 4-4: Truck positions during LT3 (1in. = 2.54 cm)

## 4.2 Finite Element Model Description

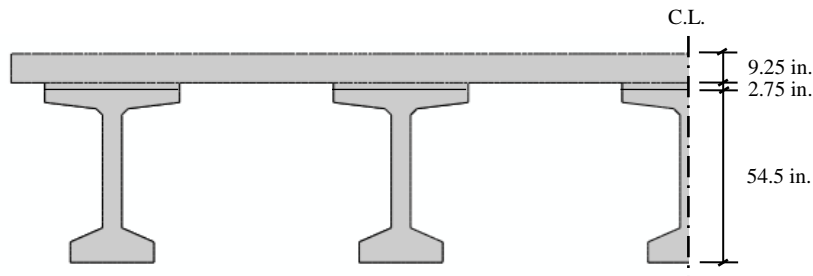
The numerical, finite element analysis was performed using ABAQUS. The geometries and dimensions of the bridge model used are illustrated in Figure 4-5. The model of the BT-54 girders accounted for a 0.5-inch depth added to the bottom flange of each girder, which resulted in a total depth of 54.5 inches (138.43cm) as shown in Figure 4-5 (c). The increased depth of the bottom flange was used to match the as built dimensions of the girders. In addition, the depth of the haunch between the top of the girder and the bottom of the deck along the length of the girder was determined to be an average of 2.75 in. (7.0 cm), which includes the height of the constructed haunch and half of the height of the fluted metal decking used to form the deck. This dimension actually varied by girder and along the length of the bridge. The thickness of the deck modeled includes the 7.75 in. (19.7 cm) constructed deck and half of the fluted metal decking height.



(a) 3D view of the bridge model



(b) Top plane view (bridge deck) of the bridge model (1ft = 30.48cm)



(c) Cross-section of the bridge model

Figure 4-5: (a) Isometric, (b) plan, and (c) cross-sectional views of FEM (1 in. = 2.54 cm)

#### 4.2.1 Mesh Description

Three-dimensional (3D) solid elements were used to model the bridge girders and the skewed bridge deck. Figure 4-6 shows the 3D finite element model of the bridge girders and deck. The five AASHTO BT-54 girders, 106 feet and 8-7/8 inches (32.53m) long between the centers of the bearing supports, were modeled with 3D 8-node linear elements, C3D8. The

bridge deck was idealized using 3D 6-node linear triangular prism and 8-node linear brick elements, C3D6 and C3D8, respectively. The element size was approximately 2 inches, which resulted in a total of 1,077,452 elements and 1,303,845 nodes. The contribution of prestressed bars and steel reinforcements to the behavior of the bridge were assumed to be negligible, since the loading did not induce cracking of the structure. Intermediate diaphragms constructed between the girders at approximately mid-span were not included in this model. A 3D finite element analysis modeling the intermediate diaphragms with axial rigid elements showed no influence on the vertical deformations of the bridge.

The concrete material properties used in this analysis were assumed to be linear elastic. Based on the concrete compressive strength obtained from cylinder tests (Chapters 2, 3), the modulus of elasticity of the concrete used in the bridge deck and girder was calculated to be 3,995ksi (27.5GPa) and 4,096 ksi (28.2GPa), respectively, at the time of load testing.

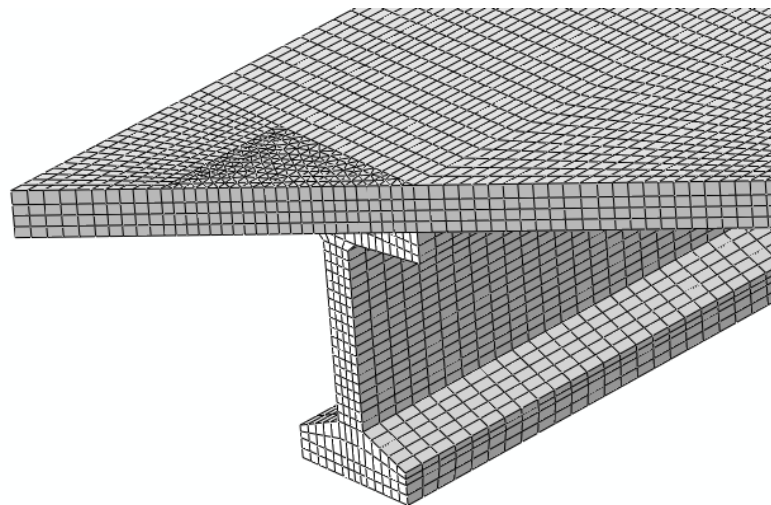


Figure 4-6: Finite element mesh of the bridge structure

#### 4.2.2 Support Boundary Conditions

The prestressed concrete BT-54 girders were supported by elastomeric bearing pads. In the middle of the pads, the elastomeric bearing pads have a dowel bar that provides lateral resistance to the girder. At the opposite end of the girder, the beam is slotted for free longitudinal movement of the girder.

The bearing pad support conditions provided under each girder were simulated by vertical restraints over the area of the bearing pads at both ends. The lateral and longitudinal restraints provided by the dowel bars, located in the middle of the bearing pads at the both ends, were defined as shown in Figure 4-7. The arrows shown in Figure 4-7 represent the restrained directions due to the bearing pads and the dowel bars. As shown in Figure 4-7 (b), the slotted hole at the opposite end of the girder provides only lateral restraints to the girder.

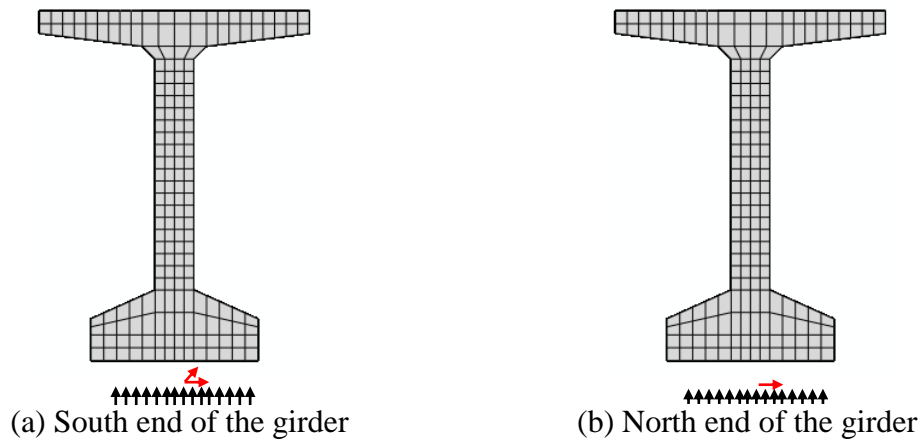


Figure 4-7: Support boundary conditions

## 4.3 Comparison of Results

### 4.3.1 Mid-Span Deflections

Table 4-1 summarizes the predicted and measured deflections at mid-span of each girder. The contour plots of the vertical deformation obtained from the finite element analysis for the three truck load tests are shown in Figures 4-8, 4-9, and 4-10. The vertical deformations obtained from the finite element analysis ranged from 0.16 to 0.19 in. (0.41 to 0.48 cm) in LT1, 0.21 to 0.26 in. (0.53 to 0.66 cm) in LT 2, and 0.12 to 0.16 in. (0.30 to 0.41 cm) in LT 3. The measured deflections were performed using a total station, and have a maximum accuracy of 0.03 in. (0.8 mm).

The measured deformations differed from the predicted values by a maximum of 0.09 in. (0.23 cm), 0.07 in. (0.18 cm), and 0.04 in. (0.10 cm) in LT 1, 2, and 3, respectively. The predicted deflections were consistently larger, with the exception of G1 and G2 in LT3. The difference in observed stiffnesses between the FEA and experimental results may be due to variances in the as-constructed dimensions of the deck, as well as variances in the haunch height between the top of the girder and the bottom of the deck. Additionally, variances in the elastic modulus of the deck concrete in different batches could slightly alter the results.

Table 4-1: Vertical deformations at mid-span of the bridge girders

Girder	Deflections, in. (cm)					
	LT1		LT2		LT3	
	FEA	Exp	FEA	Exp	FEA	Exp
G1	0.16 (0.40)	0.11 (0.29)	0.21 (0.54)	0.16 (0.41)	0.12 (0.31)	0.13 (0.33)
G2	0.17 (0.42)	0.12 (0.29)	0.23 (0.58)	0.19 (0.47)	0.13 (0.34)	0.14 (0.36)
G3	0.17 (0.44)	0.08 (0.20)	0.24 (0.60)	0.19 (0.47)	0.14 (0.36)	0.13 (0.32)
G4	0.18 (0.46)	0.14 (0.36)	0.25 (0.63)	0.21 (0.52)	0.15 (0.37)	0.11 (0.27)
G5	0.19 (0.47)	0.12 (0.30)	0.26 (0.66)	0.19 (0.48)	0.16 (0.40)	0.14 (0.36)

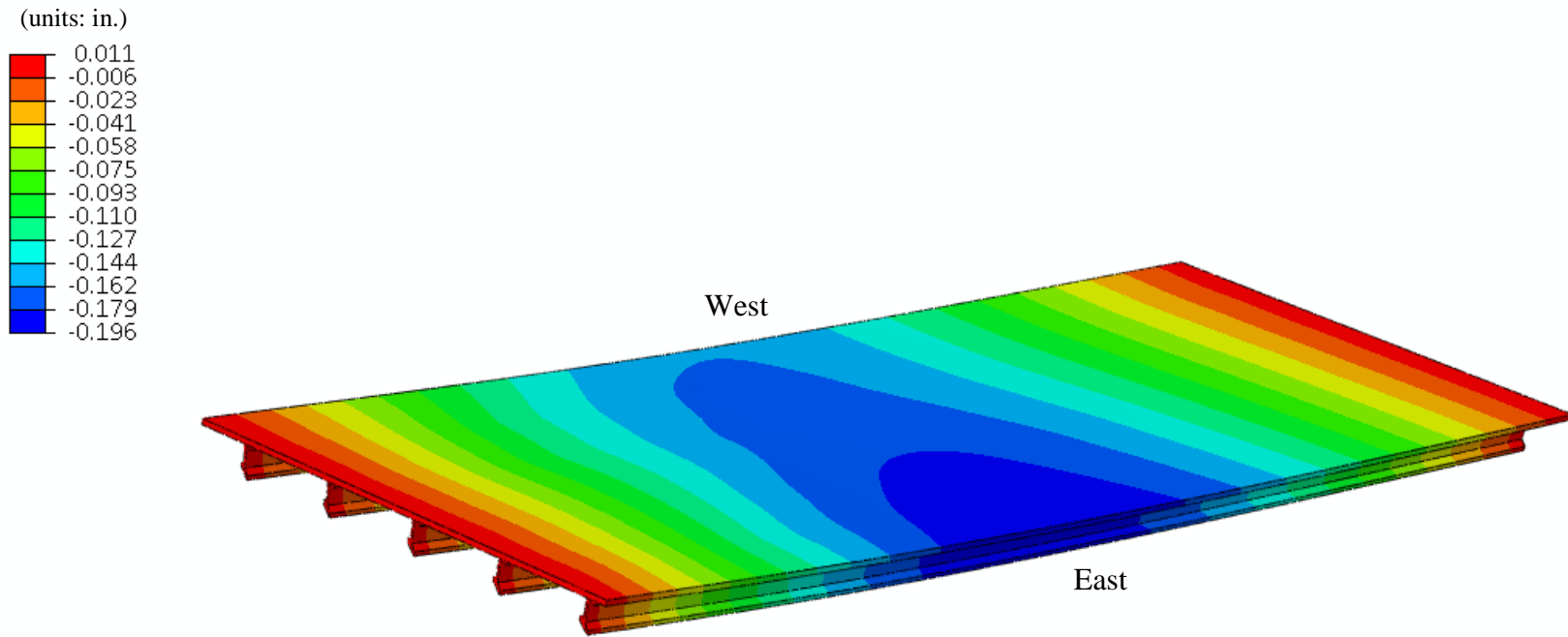


Figure 4-8: Vertical deformation contour from LT1 (1 in. = 2.54 cm)

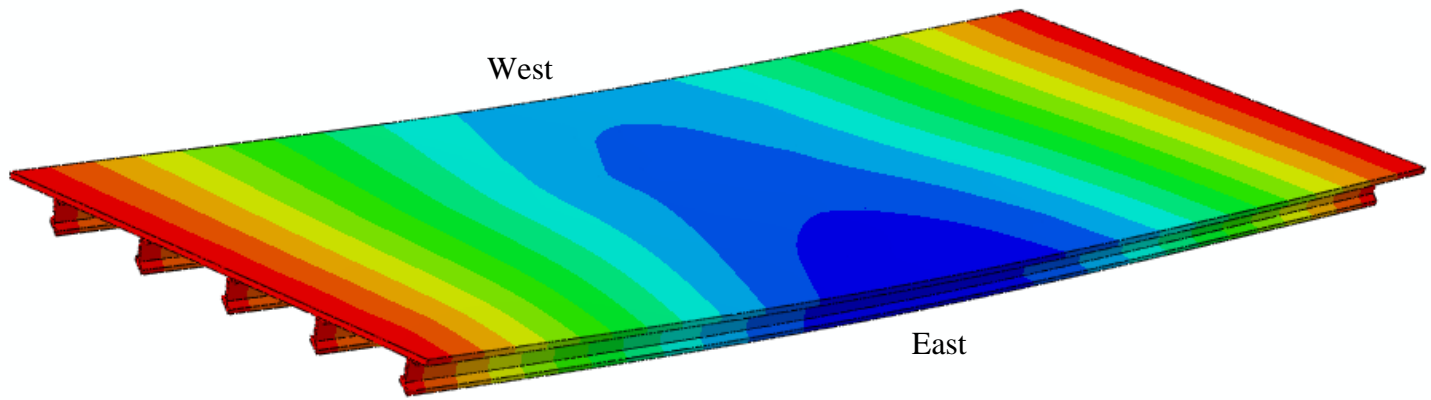
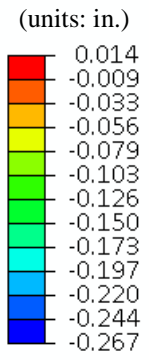


Figure 4-9: Vertical deformation contour from LT2 (1 in. = 2.54 cm)

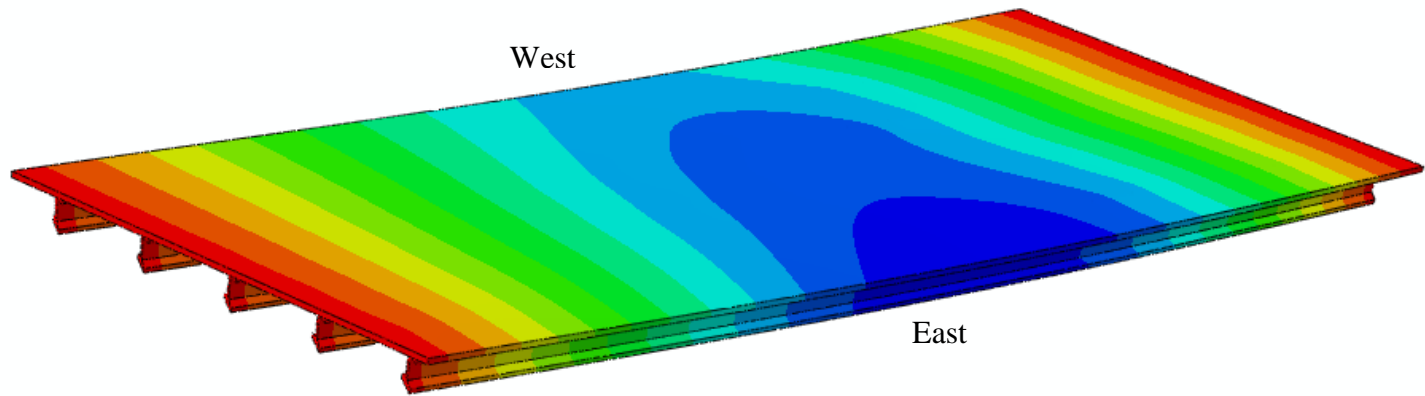
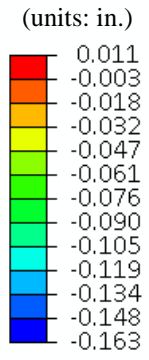


Figure 4-10: Vertical deformation contour from LT3 (1 in. = 2.54 cm)

### 4.3.2 Mid-Span Strain Profiles

The strain profiles were measured experimentally at mid-span using the imbedded VWSG's and compared with the predicted strains from the FEM. The strain profiles for each girder for all load cases are shown in Figures 4-11 through 4-15, where the experimental data are shown in a dashed blue line and the predicted in a solid red line. The strain values from the experimental and FEM analysis for LT1, 2, and 3 are given in Appendix A.

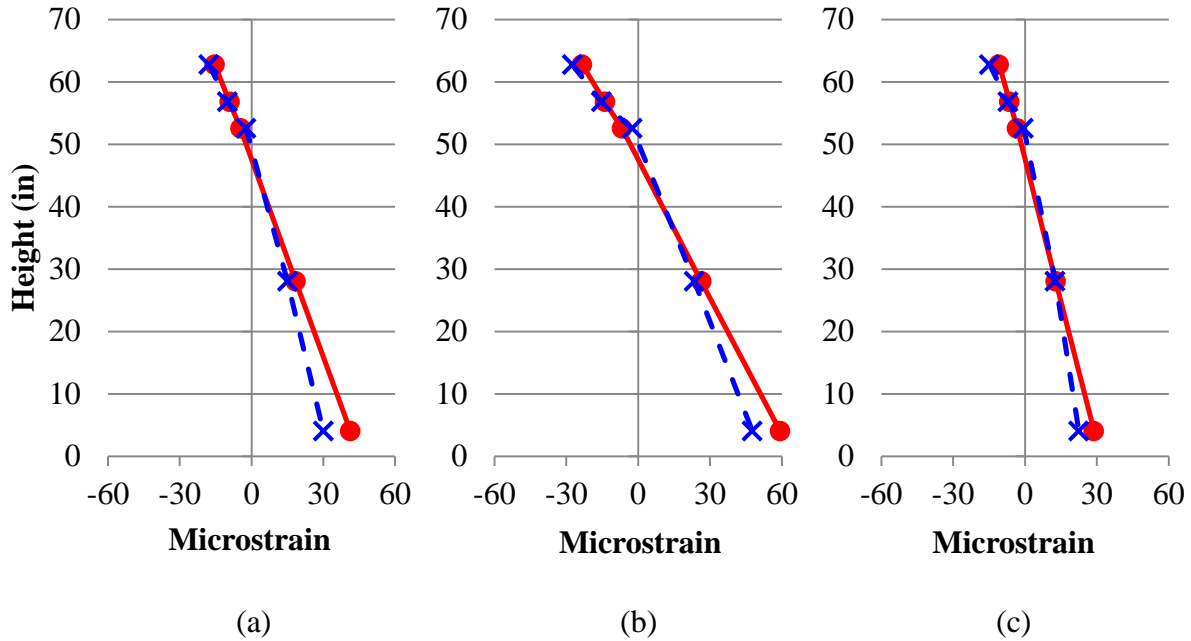


Figure 4-11: Strain profiles of girder 1 due to (a) LT1, (b) LT2, and (c) LT3 (1 in. = 2.54 cm)

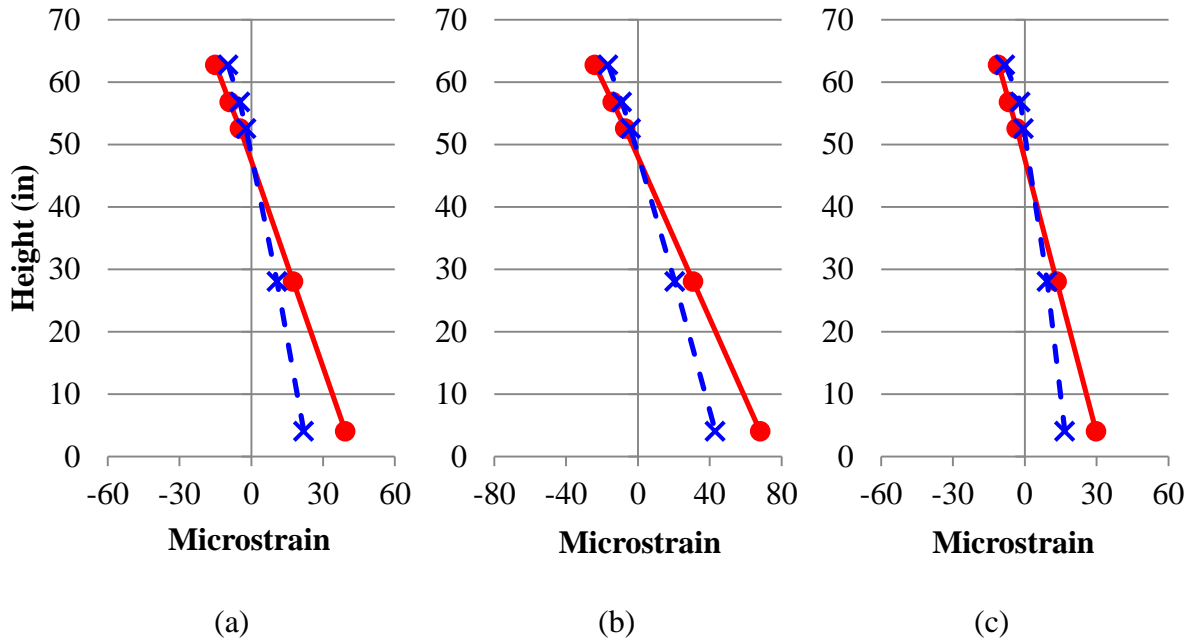


Figure 4-12: Strain profiles of girder 2 due to (a) LT1, (b) LT2, and (c) LT3 (1 in. = 2.54 cm)

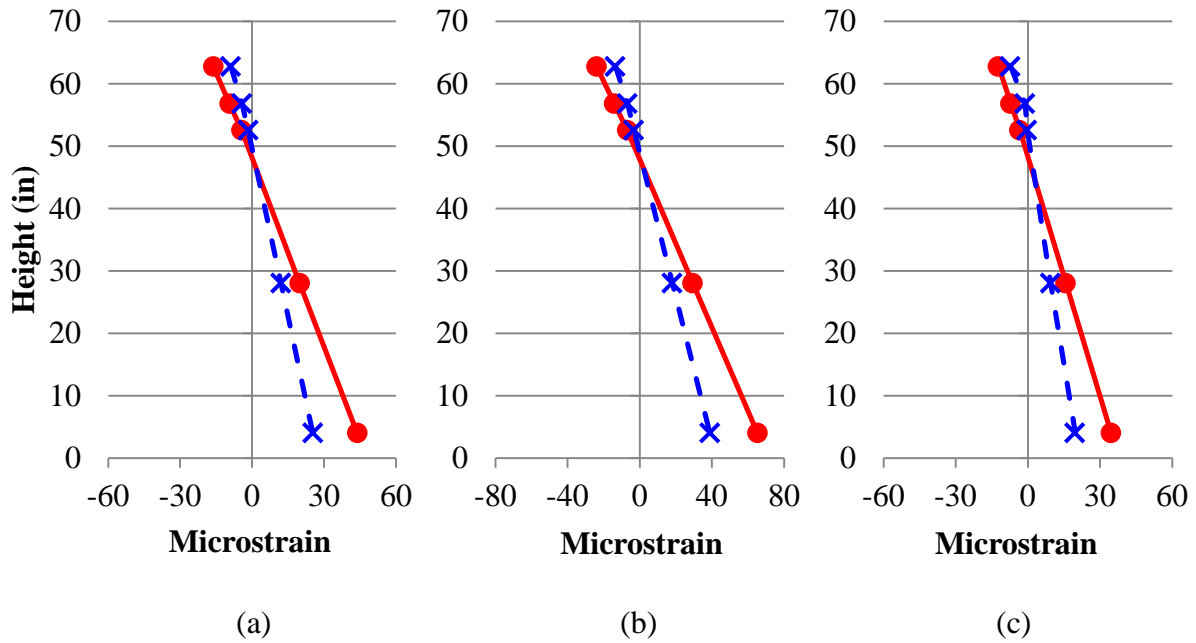


Figure 4-13: Strain profiles of girder 3 due to (a) LT1, (b) LT2, and (c) LT3 (1 in. = 2.54 cm)

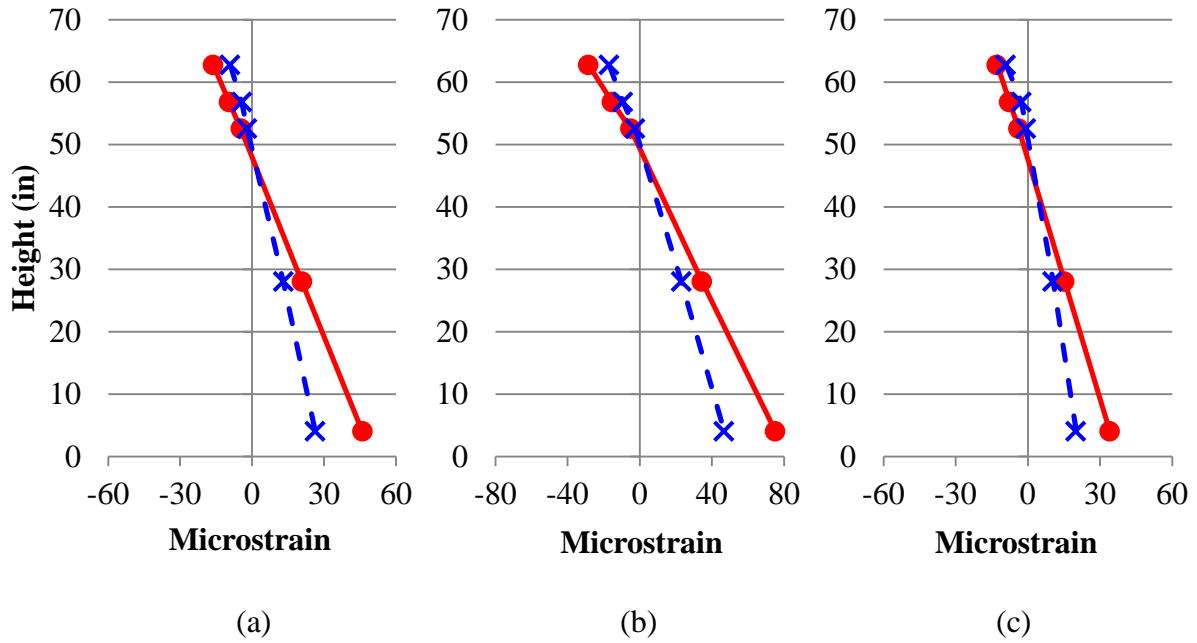


Figure 4-14: Strain profiles of girder 4 due to (a) LT1, (b) LT2, and (c) LT3 (1 in. = 2.54 cm)

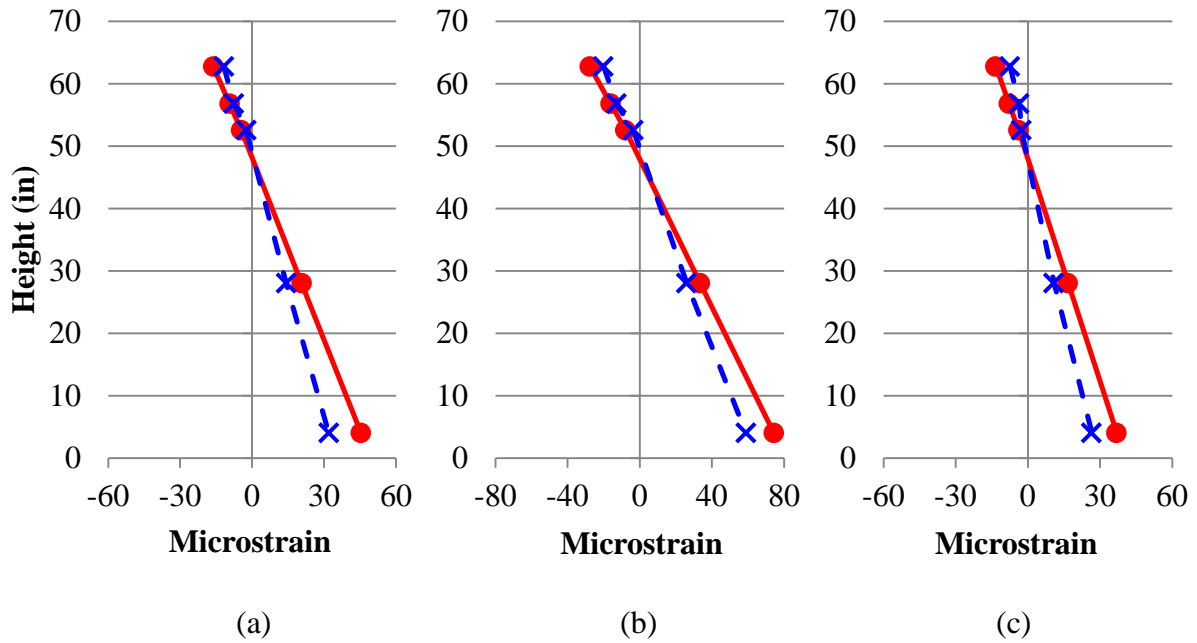


Figure 4-15: Strain profiles of girder 5 due to (a) LT1, (b) LT2, and (c) LT3 (1 in. = 2.54 cm)

The strain profiles exhibit the same trend of the deflection data: the as-built structure was stiffer than the FEM. Additionally, the neutral axis in the experimental data occurs higher in the section than the predicted, which suggests that the additional stiffness is occurring due to variations in the deck properties.

The curvatures, slope of the strain diagram, for each girder were calculated from the experimental and FEM results, and they are given in Table 4-2. The deflections were estimated from the curvatures by using an approximate moment diagram for a beam with the truck loads and scaling the mid-span curvature to the measured curvature from Table 4-2. Then, the deflection was calculated using direct integration of the curvature diagram and boundary conditions present at the bridge site. Table 4-3 presents the calculated deflections from the curvatures. Table 4-4 shows the calculated deflections from the curvatures and the experimentally measured deflections, which had a maximum difference of 0.05 in. (0.14 cm). The maximum calculated difference between FEA and experimental deflections from curvature was 0.11 in. (0.28 cm), which is larger than the 0.09 in. (0.23 cm) difference observed in the FEA predicted versus measured deflection (Table 4-1).

Table 4-2: Calculated curvatures during load tests

Girder	Curvatures, 1/in. x10 <sup>6</sup> (1/cm x10 <sup>6</sup> )					
	LT1		LT2		LT3	
	FEA	Exp	FEA	Exp	FEA	Exp
G1	0.95 (0.37)	0.67 (0.26)	1.36 (0.54)	1.03 (0.41)	0.66 (0.26)	0.47 (0.19)
G2	0.91 (0.36)	0.50 (0.20)	1.55 (0.61)	0.97 (0.38)	0.68 (0.27)	0.35 (0.14)
G3	0.99 (0.39)	0.56 (0.22)	1.49 (0.59)	0.87 (0.34)	0.78 (0.31)	0.41 (0.16)
G4	1.05 (0.41)	0.59 (0.23)	1.66 (0.65)	1.02 (0.40)	0.78 (0.31)	0.43 (0.17)
G5	1.03 (0.40)	0.71 (0.28)	1.69 (0.67)	1.29 (0.51)	0.84 (0.33)	0.60 (0.24)

Table 4-3: Calculated deflections from curvature profiles during load tests

Girder	Deflections, in. (cm)					
	LT1		LT2		LT3	
	FEA	Exp	FEA	Exp	FEA	Exp
G1	0.17 (0.43)	0.12 (0.30)	0.24 (0.61)	0.18 (0.46)	0.16 (0.41)	0.12 (0.29)
G2	0.16 (0.41)	0.09 (0.22)	0.27 (0.70)	0.17 (0.44)	0.17 (0.42)	0.09 (0.22)
G3	0.18 (0.45)	0.10 (0.25)	0.26 (0.67)	0.15 (0.39)	0.19 (0.49)	0.10 (0.26)
G4	0.19 (0.47)	0.10 (0.27)	0.29 (0.74)	0.18 (0.46)	0.19 (0.48)	0.10 (0.27)
G5	0.18 (0.47)	0.13 (0.32)	0.30 (0.76)	0.23 (0.58)	0.21 (0.52)	0.15 (0.37)

Table 4-4: Comparison of curvature calculated and measured deflections

Girder	Deflections, in. (cm)					
	LT1		LT2		LT3	
	Curvature	Exp	Curvature	Exp	Curvature	Exp
G1	0.12 (0.30)	0.11 (0.29)	0.18 (0.46)	0.16 (0.41)	0.12 (0.29)	0.13 (0.33)
G2	0.09 (0.22)	0.12 (0.29)	0.17 (0.44)	0.19 (0.47)	0.09 (0.22)	0.14 (0.36)
G3	0.10 (0.25)	0.08 (0.20)	0.15 (0.39)	0.19 (0.47)	0.10 (0.26)	0.13 (0.32)
G4	0.10 (0.27)	0.14 (0.36)	0.18 (0.46)	0.21 (0.52)	0.10 (0.27)	0.11 (0.27)
G5	0.13 (0.32)	0.12 (0.30)	0.23 (0.58)	0.19 (0.48)	0.15 (0.37)	0.14 (0.36)

#### 4.4 Simplified Line Load Model

A simplified analytical analysis of the bridge was performed by treating the truck wheel loads of each load case as a line load across the width of the bridge. A single simply supported girder with composite deck was analyzed for the load conditions at each location. The predicted deflections from the line load analysis (LLA) are compared with the observed deflections and FEA results in Table 4-4.

The simply supported line load case resulted in larger deflections than the finite element model and actual bridge structure. The maximum difference between the LLA and experimental

results was 0.15 in. (.38 cm), and the maximum difference between LLA and FEA was 0.07 in. (.18 cm). It is concluded that the FEA was a much better predictor of actual bridge behavior.

Table 4-4: Deflections from simplified analysis and FEA compared with experimental values

Girder	Deflections, in.								
	LT1			LT2			LT3		
	FEA	LLA	Exp	FEA	LLA	Exp	FEA	LLA	Exp
G1	0.16	0.19	0.11	0.21	0.25	0.16	0.12	0.16	0.13
G2	0.17	0.23	0.12	0.23	0.29	0.19	0.13	0.18	0.14
G3	0.17	0.23	0.08	0.24	0.29	0.19	0.14	0.18	0.13
G4	0.18	0.23	0.14	0.25	0.29	0.21	0.15	0.18	0.11
G5	0.19	0.19	0.12	0.26	0.25	0.19	0.16	0.16	0.14

#### 4.5 Summary of Composite Load Test

The bridge load test verified that the use of HSLW in prestressed precast girders can be successfully predicted and modeled using analytical techniques. The results suggested that the as-built structure was stiffer than what was predicted. The higher stiffness was most likely due to variances in the dimensions of the deck haunch and deck thickness.

## 5. Prestress Losses

In prestressed, precast bridge girders, the loss of prestressing occurs due to four primary mechanisms: elastic shortening, shrinkage of concrete, creep of concrete, and relaxation of the prestressing steel. Creep and shrinkage losses have been shown to vary with the service environment, curing conditions, and mix design parameters (PCI, 1975).

Strain measurements from the HSLW girders using the VWSG's provided data for actual prestress loss computations. 878 days of experimental data were collected, that included the transfer of prestressing, storage and placement of girders, deck placement, and over one year of service. Section 5.1 presents the experimental data and section 5.2 compares currently used prediction techniques with the experimental data.

### 5.1 Observed Losses

The measured prestress losses from the HSLW girders are shown in Figure 5-1. After the first 100 days, the rate of losses decreased significantly. This is in agreement with the results of the creep and shrinkage study performed on HSLW. Additionally, a noticeable trend of variation in measured losses occurred due to seasonal temperature variations. On June 6<sup>th</sup>, 2010, an average loss of 46.1 ksi was measured on a morning where the ambient temperature was 80.4°F (26.9 °C). However, on December 14<sup>th</sup>, 2010 the measured average loss was 52.8 ksi (364MPa) with an ambient air temperature of 20.1 °F (-6.6 °C). The variation of measured losses shows higher losses during the winter and lower losses during the summer, which is to be expected due to expansion and contraction of the girders due to temperature changes in the beams.

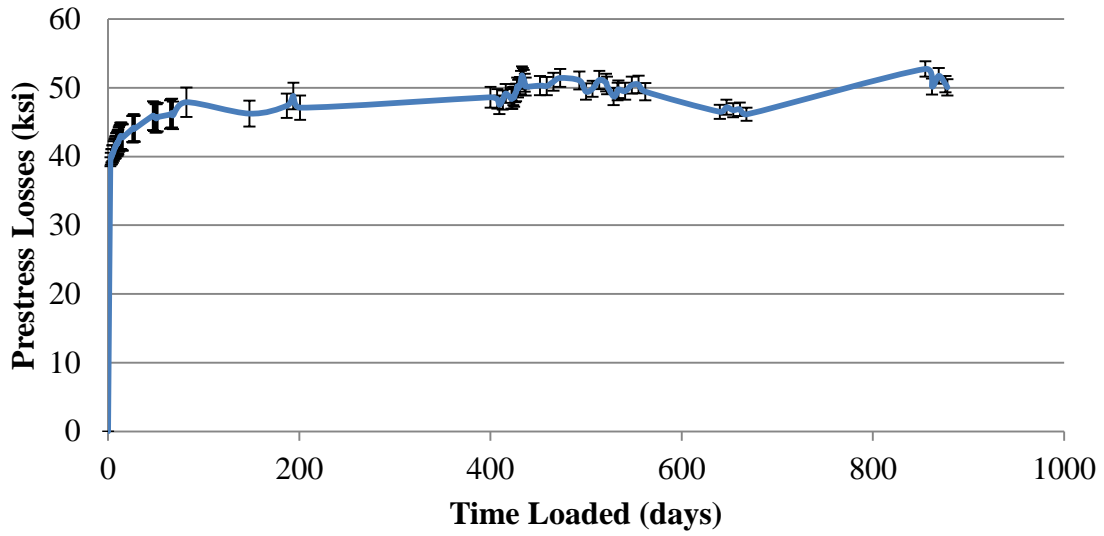


Figure 5-1: Measured prestress losses from HSLW girders (relaxation not included)  
(1 ksi = 6.9MPa)

A regression analysis of the data using a natural logarithmic relationship with time is shown in Figure 5-2. The analysis yielded good agreement with the data, and was utilized to extrapolate the measured loss data to 40 years of age. At 40 years, a total loss of 56.1 ksi (387 MPa) was predicted to occur (relaxation losses not included).

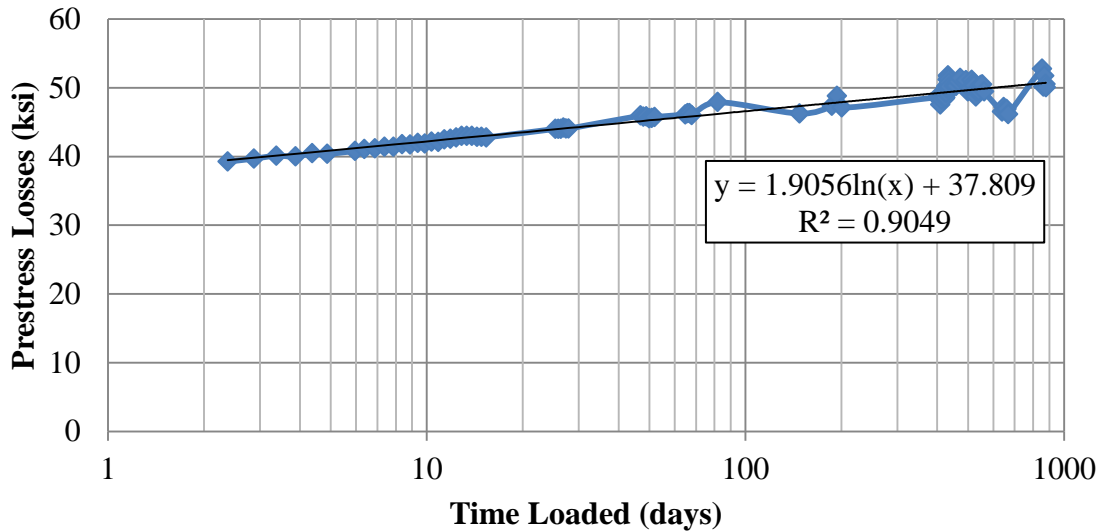


Figure 5-2: Lognormal regression of loss data (1 ksi = 6.9 MPa)

## 5.2 Comparison of Prestress Loss Predictions

Several methods for predicting the prestress losses have been developed. Six methods were investigated for comparison with experimental results. These methods were selected to encompass currently used design methods, as well as, methods specifically developed for HPC and HSLW concrete. The PCI Design Handbook (2004), ACI 209 (1992), and AASHTO LRFD (2007) lump sum and refined methods are commonly used in design of prestressed elements. The Tadros' method (Tadros, et. al., 2003) was developed for use with HPC, and the Shams' (2000) method was adapted for use specifically with HSLW by Lopez (2005).

Table 5-1 compares the experimental and estimated prestress losses after 40 years, where the experimental loss is based off the lognormal regression analysis. Additionally, the steel relaxation in the experimental data was determined with the AASHTO LRFD refined method, since the relaxation loss was not measured with the strain gages.

Table 5-1: Comparison between experimental and estimated prestress losses

Losses, ksi (Mpa)	AASHTO Lump Sum	AASHTO Refined	Shams Method	Tadros Method	ACI-209	PCI Method	Experimental
Elastic Shortening	27.9 (192.4)	27.9 (192.4)	27.9 (192.4)	28.6 (197.2)	27.9 (192.4)	30.2 (208.2)	27.6 (190.3)
Shrinkage of Concrete	N/A	11.6 (79.9)	4.5 (31.0)	11 (75.9)	10.3 (71.0)	5.7 (39.3)	N/A
Creep of Concrete	N/A	19.5 (134.5)	30.7 (211.7)	25.6 (176.5)	38.9 (268.2)	30.9 (213.1)	N/A
Creep + Shrinkage	N/A	31.1 (214.4)	35.2 (242.7)	36.5 (251.7)	49.2 (339.2)	36.7 (253.1)	28.6 (197.2)
Steel Relaxation	N/A	2.4 (16.6)	0.5 (3.5)	2.4 (16.6)	3.1 (21.4)	1.3 (8.9)	2.4 (16.6)
Total Time-Dependant Losses	21.8 (150.3)	33.5 (231.0)	35.8 (246.8)	38.9 (268.2)	52.3 (360.6)	38 (262.0)	31 (213.8)
<b>Total Losses</b>	49.7 (342.7)	61.4 (423.4)	63.7 (439.2)	67.5 (465.4)	80.2 (553.0)	68.2 (470.2)	58.5 (403.4)

Figure 5-3 shows the comparison of estimated and experimental losses by type of loss. The total experimental losses contains the AASHTO LRFD Refined (2007) estimate of relaxation losses. Creep and shrinkage of experimental data were measured as a single value, therefore, only the sum of the two effects can be compared with estimation methods. The ratio of predicted to measured values of elastic shortening, creep and shrinkage, and total losses is given in Figure 5-4.

The elastic shortening estimates were within 4% of the measured loss using all methods, with the exception of the PCI Design Handbook method which overestimated by 9.6%. For shrinkage and creep, a wide range of values were estimated between the prediction methods. For the combined shrinkage and creep effects, all methods over-estimated the measured values. The AASHTO LRFD Refined (2007) method predicted creep and shrinkage to within 9%.

The range of predicted total losses varied from 49.7 ksi (343GPa) to 80.2 ksi (553GPa). The AASHTO Lump Sum underestimated losses by 8.8 ksi (60.7GPa). The AASHTO LRFD

Refined method over-estimated the losses by 5%, and it provided the best estimate of total losses.

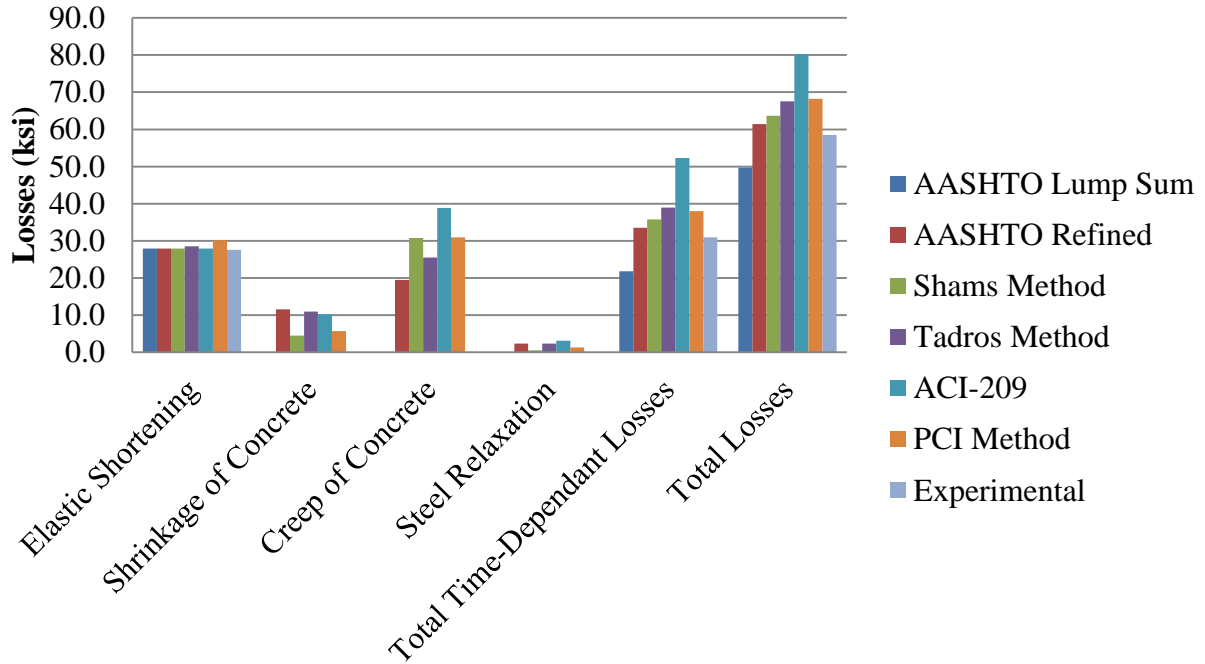


Figure 5-3: Comparison between estimation methods and measured values for losses by type (1ksi = 6.895MPa)

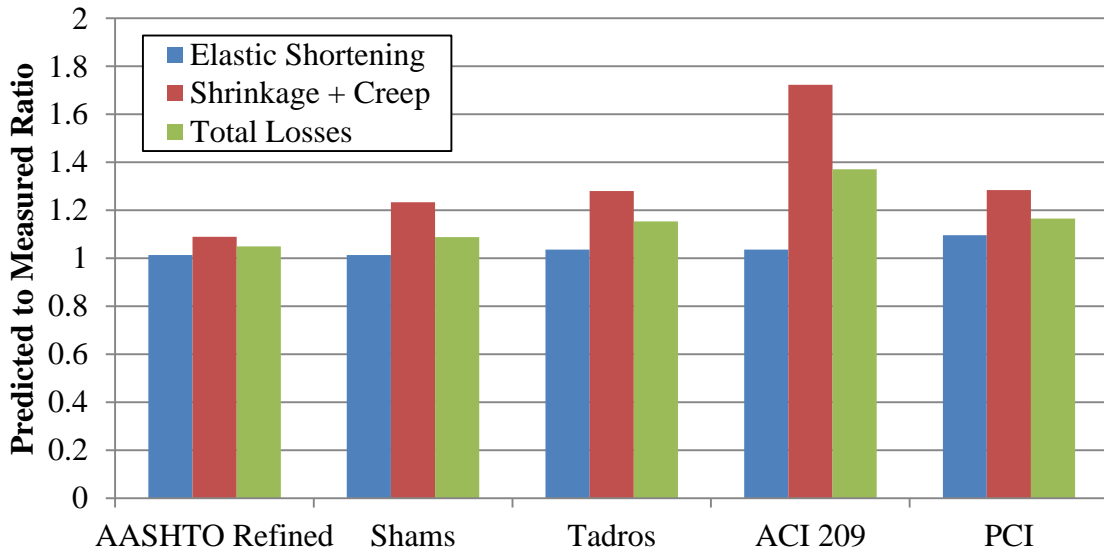


Figure 5-4: Comparison of predicted to measured ratios for loss types

### **5.3 Summary of Prestress Losses**

Current estimation methods were able to predict the observed prestress losses of HSLW girders to within 5%. All methods presented, except for the AASHTO LRFD Lump Sum method, over-estimated losses. The AASHTO LRFD Refined method provided the best estimate of the observed losses,

## 6. Camber in HSLW Girders

The prestressing force released into the girders causes an upward deflection, or camber. The camber of beams varies with the loss of prestressing, as well as with the addition of new loads during the life span of the structure. Predicting the camber is important for accurate profiling of bridge structures for a smooth riding surface. The observed camber behavior of the HSLW girders is presented in section 6.1 and a comparison with common estimation techniques in section 6.2. Modeling efforts of long-term camber effects are presented in section 6.3

### 6.1 Observed Camber Behavior

The camber of each girder was monitored using a taut wire system before deck placement. All of the readings were taken while the girders were being stored at the precast plant. The average camber readings before deck placement are shown in Figure 6-1. All readings were taken in the morning at dawn to ensure that a temperature gradient from solar heating would not affect the reading. An average camber of 4.25 in. (10.8 cm) was observed at 56 days of age. The data show an increase of camber with time, which is expected due to creep and shrinkage of the girder (Rosa, et. al., 2007).

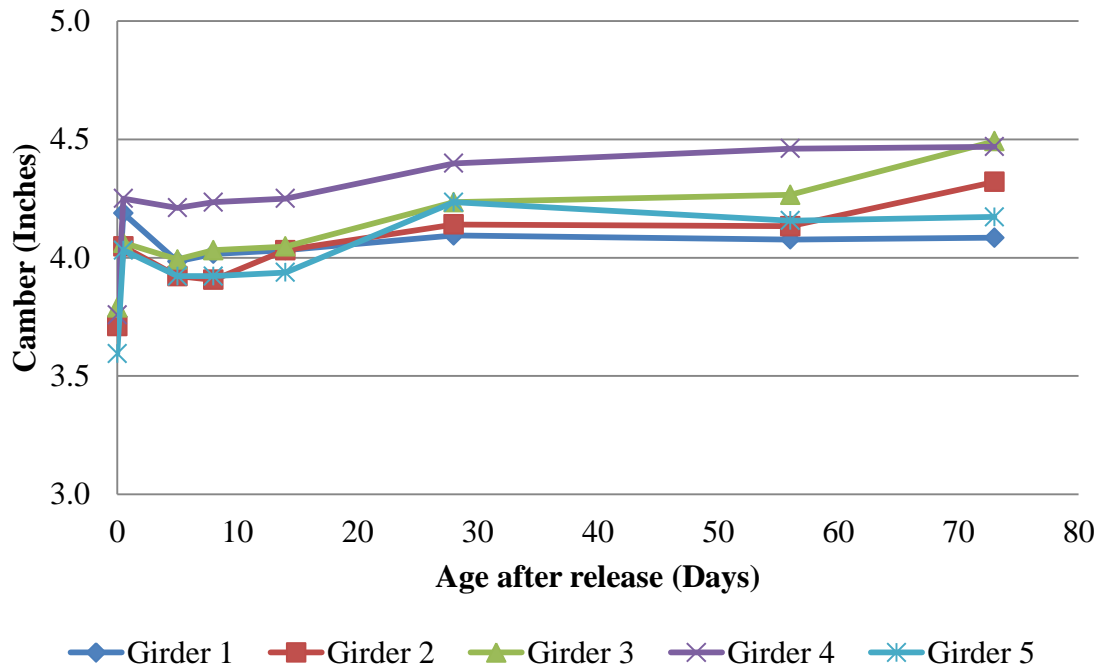


Figure 6-1: Observed camber before deck placement (1in = 2.54cm)

The camber of the girders was monitored using a total station after placement at the bridge site. Figure 6-2 shows the measured camber of each girder after deck placement. The loss of camber at 500 days was due to the placement of the barrier walls on the bridge. Additionally, the influence of seasonal temperature variations is seen by the increased camber between 550 and 650 days of age which corresponds to summer.

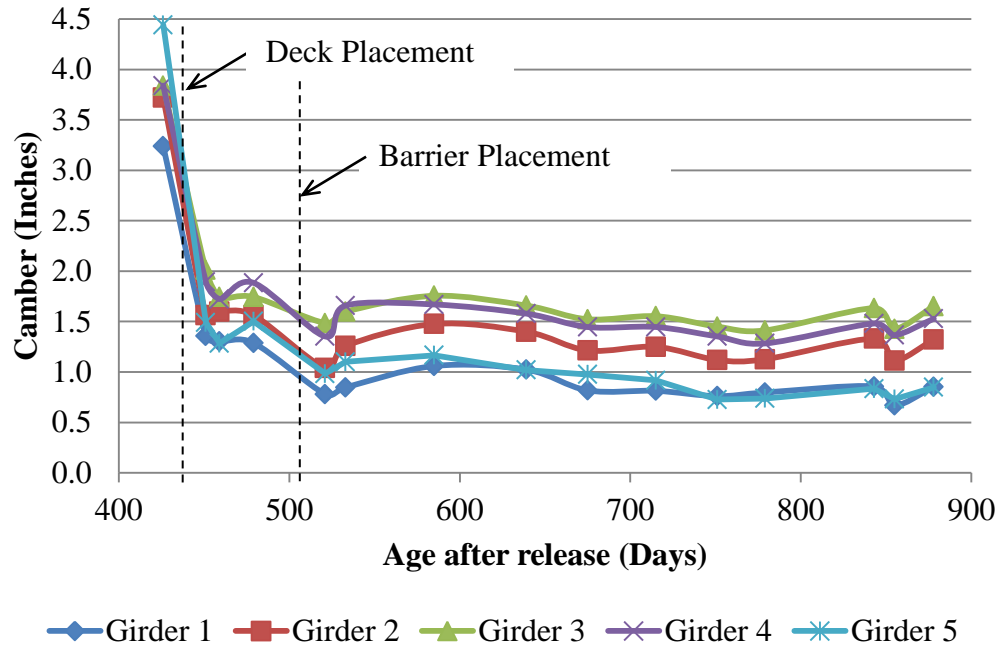


Figure 6-2: Observed camber after deck placement (1 in = 2.54cm)

## 6.2 Prediction Methods

Camber prediction methods have been developed for both initial and long-term camber behavior of precast prestressed concrete structures. The Washington State Department of Transportation (Rosa, et. al., 2007) developed a method for predicting initial camber of beams using a basic mechanics approach. The PCI Design Handbook (2004) provides a method to estimate the long term camber behavior.

### 6.2.1 Washington State Department of Transportation (WSDOT) Method

Washington State Department of Transportation (WSDOT) has developed a method for determining total camber of a beam after release. Equations 6-1 through 6-5 are from the WSDOT (Rosa, et. al., 2007) report.

$$\Delta = \Delta_{ps} - \Delta_{sw} \quad (\text{Eq. 6-1})$$

Where,

- $\Delta$  = Camber, in.  
 $\Delta_{ps}$  = Camber due to prestressing, in.  
 $\Delta_{sw}$  = Deflection due to self weight of girder, in.

$$\Delta_{ps} = \frac{PL^3}{8E_c I_g} \left[ e_{mid} + (e_{end} - e_{mid}) \frac{4a^2}{3L^2} \right] \quad (\text{Eq. 6-2})$$

Where,

- $P$  = Total prestressing force, lbs  
 $L$  = Length of beam, in.  
 $E_c$  = Experimental modulus of elasticity at 56 days, psi  
 $I_g$  = Measured moment of inertia, in.<sup>4</sup>  
 $e_{mid}$  = Eccentricity of strands at midspan, in.  
 $e_{end}$  = Eccentricity of strands at end, in.  
 $a$  = Distance from the end of the girder to the harping point, in.

$$\Delta_{sw} = \Delta_{overhang} + \Delta_{midspan} \quad (\text{Eq. 6-3})$$

Where,

- $\Delta_{overhang}$  = Deflection of overhang relative to the support, in.  
 $\Delta_{midspan}$  = Deflection at midspan relative to the support, in.

$$\Delta_{\text{overhang}} = \frac{\omega_{sw} L_c}{24 E_c I_g} [3 L_c^2 (L_c + 2 L_n) - L_n^3] \quad (\text{Eq. 6-4})$$

Where,

$\omega_{sw}$  = Weight per linear foot of girder, lb/ft

$L_c$  = Overhanging length, in.

$L_n$  = Distance between supports, in.

$$\Delta_{\text{midspan}} = \frac{\omega_{sw} L_n^2}{384 E_c I_g} (5 L_n^2 - 24 L_c^2) \quad (\text{Eq. 6-5})$$

Using these equations the expected camber for each girder was calculated. Table 6-1 compares the actual camber values at 56 days to the camber predicted by the WSDOT equations.

Table 6-1: Predicted camber and actual camber after release

	Camber, in (cm)		
	Actual	Predicted	Difference
1	4.19 (10.64)	4.06 (10.31)	3.04%
2	4.05 (10.28)	4.26 (10.82)	-5.27%
3	4.06 (10.32)	4.45 (11.29)	-9.44%
4	4.25 (10.80)	4.12 (10.45)	3.18%
5	4.03 (10.24)	4.10 (10.42)	-1.80%
<b>Average</b>	4.12 (10.45)	4.20 (10.66)	-2.06%

### 6.2.1 PCI Design Handbook Method

The PCI Design Handbook (2004) suggests the use of multiplier factors to account for long-term behavior of girders to various load types. Table 6-2 gives the multiplier factors to be applied to the elastic deflections for various loading types.

Table 6-2: Long-term deflection multipliers (PCI, 2004)

<b>Time Estimated</b>	<b>Load Type</b>	<b>Multiplier</b>
Erection	Self-weight	1.85
	Camber	1.8
Final	Self-weight	2.4
	Camber	2.2
	Slab	2.3

Figure 6-3 shows a comparison of the predicted cambers at erection and for final camber versus the observed values. The PCI method over-predicted the camber by over 3 in (7.62cm). at deck placement, and by approximately 2 in. (5.08cm) for the final predicted camber. The increased initial camber of HSLW due to the lower elastic modulus may cause the multiplier to over-estimate the long term effect of the camber.

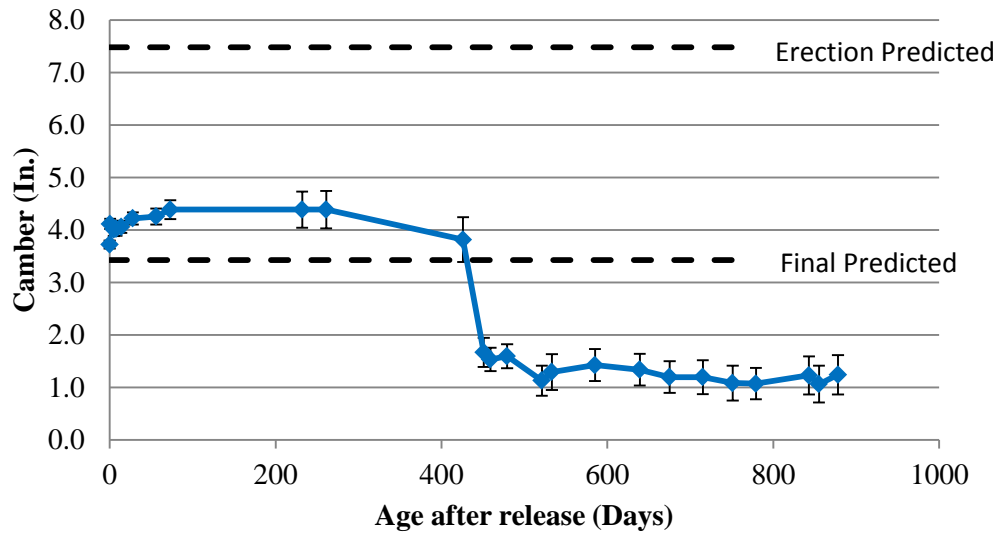


Figure 6-3: Comparison of predicted and measured camber (1 in. = 2.54 cm)

### 6.3 Modeling Camber Changes Caused by Deck Shrinkage

The decrease in camber after deck placement is due to shrinkage of the deck concrete. The results of section 3.4 were used to estimate the decrease in camber due to shrinkage of the normal-weight deck. A finite element model of the bridge (Chapter 4) was used to analyze the camber change by applying an equivalent thermal gradient, which in an unrestrained structure would cause the observed shrinkage strains. The application of the thermal gradients to the deck allowed for the calculation of camber changes due to the restraint provided by the connection of the deck to the girder.

Two cases were analyzed, which corresponded to the results of the prism specimens (section 3.4.1) and to slab shrinkage specimens (section 3.4.2). The two cases resulted in a uniform and linear shrinkage gradient, respectively, as shown in Figure 6-4.

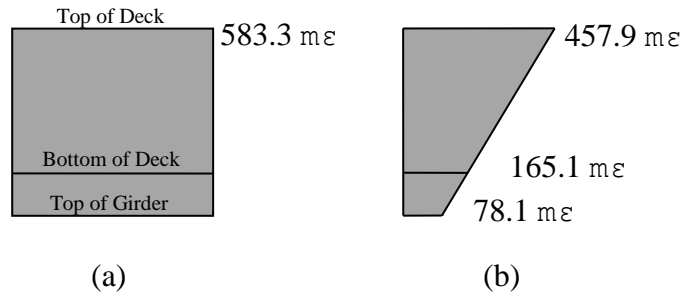


Figure 6-4: Shrinkage gradients for (a) uniform, and (b) linear gradient

The analysis of the uniform and gradient cases caused deflections of 1.99 in. (5.05 cm) and 1.05 in. (2.68 cm), respectively. These are larger than the measured change deflection of 0.42 in. (1.07 cm) found between the camber reading after deck placement and the reading 427 day later. The reading after deck placement was taken two weeks after the pour, therefore some shrinkage may have already occurred and caused deflection due to shrinkage that was not captured in the measured, experimental data.

## 7. Conclusions and Recommendations

The I-85 Ramp “B” Bridge over SR-34, Bullsboro Drive, in Coweta County, Georgia was the first use of HSLW for precast, prestressed bridge girders in Georgia. The performance of the girders demonstrated that HSLW can successfully be used to decrease the weight of girders during transport while still allowing for the increased spans by use of high strength concrete. Load testing of the bridge demonstrated that HSLW girders with a normal weight concrete (NWC) deck acts compositely as would be predicted using standard analysis procedures.

The following recommendations are supported by the findings of this investigation for future design and use of HSLW for precast, prestressed bridge girders:

1. Use the Meyer (2002) equation for prediction of the elastic modulus of high strength lightweight concrete made with expanded slate aggregate.
2. Estimate prestress losses of HSLW using the AASHTO LRFD Refined method (2007).
3. Use the WSDOT (Rosa, et. al., 2007) method for predicting initial camber.

## References

*AASHTO LRFD Bridge Design Specifications*, 4<sup>th</sup> ed. (2007), American Association of Highway and Transportation Officials, Washington D.C.

ACI Committee 209R-92, (1992). "Prediction of Creep, Shrinkage, and Temperature Effects in Concrete Structures," American Concrete Institute, Farmington Hills, Michigan.

ACI Committee 318 (2008). "Building Code Requirements for Structural Concrete (ACI 318-08) and Commentary," American Concrete Institute. Farmington Hills, Michigan.

ACI Committee 363R-92 (1997). "Report on High-Strength Concrete," American Concrete Institute. Farmington Hills, Michigan.

ASTM C 39 (2005), *Standard Test Method for Compressive Strength of Cylindrical Concrete Specimens*, American Society for Testing and Materials, West Conshohocken, PA, 7pp.

ASTM C 157 (2006), *Standard Test Method for Length Change of Hardened Hydraulic-Cement Mortar and Concrete*, American Society for Testing and Materials, West Conshohocken, PA, 7pp.

ASTM C 469 (2002), *Standard Test Method for Static Modulus of Elasticity and Poisson's Ratio of Concrete in Compression*, American Society for Testing and Materials, West Conshohocken, PA, 5pp.

ASTM C 512 (2002), *Standard Test Method for Creep of Concrete in Compression*, American Society for Testing and Materials, West Conshohocken, PA, 4pp.

Buchberg, Brandon S. (2002), "Investigation of Mix Design and Properties of High-Strength/High-Performance Lightweight Concrete," Masters Thesis, Georgia Institute of Technology, 453pp.

Cook, J. and Meyer, K.F. (2006), "Modulus of Elasticity," *ACI 213 Communication*.

CRD C 39 (1981), "Method of Test for Coefficient of Linear Thermal Expansion of Concrete," Handbook Concrete and Cement, U.S. Army Engineer Waterways Experiment Station, Vicksburg, MS, 2pp.

Lopez, Mauricio (2005), "Creep and Shrinkage of High Performance Lightweight Concrete: A Multi-scale Investigation," Doctoral Thesis, Georgia Institute of Technology, 530pp.

Meyer, Karl F. (2002), "Transfer Length and Development of 0.6-inch Diameter Prestressing Strand in High Strength Lightweight Concrete," Doctoral Thesis, Georgia Institute of Technology, 616pp.

Meyer, Karl F., and Lawrence F. Kahn (2002), "Lightweight Concrete Reduces Weight and Increases Span Length of Pretensioned Concrete Bridge Girders," *PCI JOURNAL* V. 47, No.1, January-February, pp. 68-75.

*National Cooperative Highway Research Program (2007), Report 595: Application of the LRFD Bridge Design Specifications to High-Strength Structural Concrete: Flexure and Compression Provisions*, Transportation Research Board, Washington D.C.

Neville, A.M. (1997), *Properties of Concrete*, 4 ed., John Wiley and Sons, New York, NY, pp. 844.

Ozyildirim, Celik (2009), "Evaluation of Lightweight High Performance Concrete in Bulb-T Beams and Decks in Two Bridges on Route 33 in Virginia," Virginia Transportation Research Council, Final Report VTRC 09-R22.

PCI Committee on Prestress Losses (1975), "Recommendations for Estimating Prestress Losses," *PCI Journal*, V. 28, July-August, pp. 43-75.

*PCI Design Handbook: Precast and Prestressed Concrete* (2004), Sixth Edition, Precast/Prestressed Concrete Institute, Chicago, Illinois.

Rosa, Michael A, et. al. (2007), "Improving Predictions for Camber in Precast, Prestressed Concrete Bridge Girders", Research Report Task 68, Washington State Department of Transportation, 323pp.

Shams, M. K. (2000), "Time-Dependent Behavior of High-Performance Concrete," Doctoral Thesis, Georgia Institute of Technology, 611pp.

Standard Concrete Products (2006), "Coweta Co., Georgia, I-85 over SR 34," Construction Documents, Job # 07663A-1.

Tadros, M.K., et. al. (2003), "NCHRP Report 496: Prestress Losses in Pretensioned High-Strength Concrete Bridge Girders," Transportation Research Board, Washington D.C., 73 pp.

## Appendix A: Bridge Load Test Data

### A.1 Experimental and FEM Strain Data

The experimental and FEM predicted strains due to LT1, LT2, and LT3 for girders 1-5 are shown below in Tables A-1 through A-5. The height given is the distance from the bottom of the girder to the gage location (as shown in Figure 1-4).

Table A-1: Girder 1 strains from bridge load tests

		Strains ( $\mu\epsilon$ )					
		LT1		LT2		LT3	
Gage Location	Height	FEA	Exp	FEA	Exp	FEA	Exp
D2	62.73	-15.4	-17.8	-23.4	-27.4	-10.8	-14.7
D1	56.75	-9.2	-10.1	-13.8	-15.3	-6.4	-7.0
Top Flange	52.5	-4.6	-2.3	-6.7	-2.4	-3.2	-0.5
Web	28	18.5	15.0	26.4	23.5	12.9	12.7
Bottom Flange	4	41.3	30.0	59.3	47.7	28.9	22.5

Table A-2: Girder 2 strains from bridge load tests

		Strains ( $\mu\epsilon$ )					
		LT1		LT2		LT3	
Gage Location	Height	FEA	Exp	FEA	Exp	FEA	Exp
D2	62.73	-14.9	-9.7	-23.9	-16.5	-10.9	-8.1
D1	56.75	-9.0	-4.7	-14.0	-8.9	-6.5	-1.8
Top Flange	52.5	-4.7	-2.2	-6.9	-4.0	-3.3	-0.4
Web	28	17.5	10.8	30.8	20.6	13.5	9.4
Bottom Flange	4	39.3	21.9	68.1	43.1	29.8	16.8

Table A-3: Girder 3 strains from bridge load tests

		Strains ( $\mu\epsilon$ )					
		LT1		LT2		LT3	
Gage Location	Height	FEA	Exp	FEA	Exp	FEA	Exp
D2	62.73	-16.1	-8.9	-23.9	-13.5	-12.2	-7.2
D1	56.75	-9.3	-4.2	-14.0	-6.7	-7.1	-1.1
Top Flange	52.5	-4.3	-1.6	-6.8	-3.2	-3.3	-0.2
Web	28	19.9	12.1	29.4	18.1	15.8	9.5
Bottom Flange	4	43.9	25.3	65.4	38.9	34.6	19.7

Table A-4: Girder 4 strains from bridge load tests

		Strains ( $\mu\epsilon$ )					
		LT1		LT2		LT3	
Gage Location	Height	FEA	Exp	FEA	Exp	FEA	Exp
D2	62.73	-16.3	-9.1	-28.3	-17.0	-12.7	-9.0
D1	56.75	-9.6	-4.3	-15.2	-9.2	-7.6	-2.6
Top Flange	52.5	-4.7	-2.1	-5.1	-2.6	-3.8	-0.7
Web	28	20.8	13.1	34.5	23.1	15.3	10.5
Bottom Flange	4	46.0	26.4	75.2	46.8	34.1	20.1

Table A-5: Girder 5 strains from bridge load tests

		Strains ( $\mu\epsilon$ )					
		LT1		LT2		LT3	
Gage Location	Height	FEA	Exp	FEA	Exp	FEA	Exp
D2	62.73	-16.2	-11.8	-27.6	-20.0	-13.3	-7.4
D1	56.75	-9.4	-7.6	-16.1	-12.9	-7.8	-3.5
Top Flange	52.5	-4.5	-2.4	-7.8	-3.4	-3.8	-2.6
Web	28	20.7	14.3	33.5	26.1	16.8	10.9
Bottom Flange	4	45.4	32.0	74.4	59.0	37.0	26.6

## A.2 Comparison of actual deflections and curvature based predictions

Tables A-6 through A-8 compare the measured deflections from the load test experiments and FEM model with the estimates calculated using the curvatures measured using internal instrumentation.

Table A-6: Deflection estimation comparison for LT1

Girder	Deflections, in.					
	FEA			Experimental		
	Actual	Curvature	% Difference	Actual	Curvature	% Difference
G1	0.159	0.169	-6.0%	0.113	0.119	-4.9%
G2	0.166	0.162	2.6%	0.115	0.088	23.1%
G3	0.174	0.177	-1.8%	0.078	0.099	-26.7%
G4	0.182	0.186	-2.2%	0.140	0.104	25.4%
G5	0.187	0.183	2.0%	0.118	0.126	-7.1%

Table A-7: Deflection estimation comparison for LT2

Girder	Deflections, in.					
	FEA			Experimental		
	Actual	Curvature	% Difference	Actual	Curvature	% Difference
G1	0.211	0.241	-14.4%	0.162	0.183	-13.0%
G2	0.228	0.274	-20.3%	0.186	0.172	7.5%
G3	0.235	0.264	-12.0%	0.185	0.154	16.9%
G4	0.248	0.293	-18.0%	0.205	0.181	11.9%
G5	0.259	0.300	-15.8%	0.189	0.228	-20.6%

Table A-8: Deflection estimation comparison for LT3

Girder	Deflections, in.					
	FEA			Experimental		
	Actual	Curvature	% Difference	Actual	Curvature	% Difference
G1	0.123	0.162	-31.8%	0.130	0.116	10.8%
G2	0.134	0.167	-24.4%	0.142	0.087	39.0%
G3	0.142	0.191	-34.6%	0.127	0.100	20.9%
G4	0.147	0.191	-30.1%	0.108	0.105	3.1%
G5	0.156	0.205	-31.9%	0.142	0.147	-3.5%

## Appendix B: Prestress Loss Data

The calculations of prestress losses are presented in sections B.1 through B.6. The experimental measurements of prestress losses are given in section B.7.

### B.1 AASHTO LRFD Approximate Method Calculations

#### B.1.1 Notation

The following notation was used in computing prestress losses according to the AASHTO LRFD Approximate Method (2007):

$A_g$	=	gross cross-sectional area, in. <sup>2</sup>
$A_{ps}$	=	total area of prestressing steel, in. <sup>2</sup>
$A_{strand}$	=	area of single prestressing strand, in. <sup>2</sup>
$e$	=	eccentricity of prestressing strands, in.
$E_p$	=	elastic modulus of prestressing steel, ksi
$E_{ct}$	=	elastic modulus of concrete at time of transfer, ksi
$f_{c56}'$	=	56-day concrete compressive strength, ksi
$f_{cgp}$	=	stress at center gravity of prestressing due to prestress forces and self-weight, ksi
$f_{ci}'$	=	concrete compressive strength at time of transfer, ksi
$f_{pe}$	=	prestressing stress after transfer in steel, ksi
$f_{pi}$	=	initial prestressing stress in steel, ksi
$H$	=	average annual relative humidity, %
$I_g$	=	gross cross-sectional moment of inertia, in. <sup>4</sup>
$L$	=	span length, ft
$M_g$	=	moment due to self-weight, kip-ft
$n_{strand}$	=	number of prestressing strands
$P_{ES}$	=	prestressing force after elastic shortening, kip
$P_i$	=	prestressing force before losses, kip
$\Delta f_{pES}$	=	loss of prestress due to elastic shortening, ksi
$\Delta f_{pLT}$	=	long-term prestress losses, ksi
$\Delta f_{pR}$	=	loss of prestress due to relaxation of prestressing steel, ksi
$\Delta f_{ps\_instant}$	=	instantaneous loss of prestressing, ksi
$\Delta f_{ps\_time}$	=	total time-dependent loss of prestressing, ksi
$\Delta f_{ps\_total}$	=	total loss of prestressing, ksi
$\gamma_c$	=	unit weight of concrete, pcf
$\gamma_h$	=	correction factor for relative humidity
$\gamma_{st}$	=	correction factor for concrete strength at time of transfer

## B.1.2 Calculation of Losses

### Section and Material Properties:

$$\begin{aligned} A_g &:= 659 \text{ in}^2 & e &:= -22.604 \text{ in} & n_{\text{strand}} &:= 38 & f_{c56} &:= 10.137 \text{ ksi} \\ I_g &:= 268051 \text{ in}^4 & E_p &:= 28500 \text{ ksi} & f_{pi} &:= 178.8 \text{ ksi} & f_{ci} &:= 7.849 \text{ ksi} \\ \gamma_c &:= 122 \text{pcf} & E_{ct} &:= 3529 \text{ ksi} & A_{\text{strand}} &:= .217 \text{ in}^2 \\ L &:= 106.76042 \text{ ft} \end{aligned}$$

### Determine Loading Properties:

$$\begin{aligned} A_{ps} &:= n_{\text{strand}} \cdot A_{\text{strand}} & A_{ps} &= 8.246 \text{ in}^2 \\ P_i &:= A_{ps} \cdot f_{pi} & P_i &= 1.474 \times 10^3 \text{ kip} \\ M_g &:= \frac{\gamma_c \cdot A_g \cdot L^2}{8} & M_g &= 795.451 \text{ kip-ft} \end{aligned}$$

### Elastic Shortening Losses:

$$P_{ES0} := 1244.3 \text{ kip} \quad (\text{Iterate on } P_{ES0} \text{ until equal to } P_{ES})$$

$$f_{cgp} := -\frac{P_{ES0}}{A_g} - \frac{P_{ES0} \cdot e^2}{I_g} - \frac{M_g \cdot e}{I_g} \quad f_{cgp} = -3.455 \text{ ksi}$$

$$\Delta f_{pES} := -\frac{E_p}{E_{ct}} \cdot f_{cgp} \quad (\text{Eq. 5.9.5.2.3a-1})$$

$$\boxed{\Delta f_{pES} = 27.903 \text{ ksi}}$$

$$f_{pt} := f_{pi} - \Delta f_{pES}$$

$$f_{pt} = 150.897 \cdot \text{ksi}$$

$$P_{ES} := f_{pt} \cdot A_{ps}$$

$$P_{ES} = 1.244 \times 10^3 \cdot \text{kip}$$

$$f_{cgp} := -\frac{P_{ES}}{A_g} - \frac{P_{ES} \cdot e^2}{I_g} - \frac{M_g \cdot e}{I_g}$$

$$f_{cgp} = -3.455 \cdot \text{ksi}$$

$$\Delta f_{pES1} := -\frac{E_p}{E_{ct}} \cdot f_{cgp}$$

$$\Delta f_{pES1} = 27.903 \cdot \text{ksi}$$

### Estimate of Long Term Losses:

$$H := 70$$

$$\gamma_h := 1.7 - 0.01H \quad (\text{Eq. 5.9.5.3-2})$$

$$\gamma_h = 1$$

$$\gamma_{st} := \frac{5}{\left(1 + \frac{f_{ci}}{\text{ksi}}\right)} \quad (\text{Eq. 5.9.5.3-3})$$

$$\gamma_{st} = 0.565$$

$$\Delta f_{pR} := 2.4 \cdot \text{ksi}$$

$$\Delta f_{pLT} := 10.0 \cdot \frac{f_{pi} \cdot A_{ps}}{A_g} \cdot \gamma_h \cdot \gamma_{st} + 12.0 \cdot \text{ksi} \cdot \gamma_h \cdot \gamma_{st} + \Delta f_{pR} \quad (\text{Eq. 5.9.5.3-1})$$

$$\Delta f_{pLT} = 21.822 \cdot \text{ksi}$$

### Total Losses:

$$\Delta f_{ps\_instant} := \Delta f_{pES}$$

$$\Delta f_{ps\_instant} = 27.903 \cdot \text{ksi}$$

$$\Delta f_{ps\_time} := \Delta f_{pLT}$$

$$\Delta f_{ps\_time} = 21.822 \cdot \text{ksi}$$

$$\Delta f_{ps\_total} := \Delta f_{ps\_instant} + \Delta f_{ps\_time}$$

$$\Delta f_{ps\_total} = 49.725 \cdot \text{ksi}$$

## B.2 AASHTO LRFD Refined Method Calculations

### B.2.1 Notation

The following notation was used in computing prestress losses according to the AASHTO LRFD Refined Method (2007):

$A_c$	=	transformed composite cross-sectional area, in. <sup>2</sup>
$A_g$	=	gross cross-sectional area, in. <sup>2</sup>
$A_{strand}$	=	area of single prestressing strand, in. <sup>2</sup>
$A_{ps}$	=	total area of prestressing steel, in. <sup>2</sup>
$b_d$	=	effective width of deck over girder, ft
$e_d$	=	eccentricity of deck from centroid of composite section, in.
$e_{pc}$	=	eccentricity of prestressing strands in composite section, in.
$e_{pg}$	=	eccentricity of prestressing strands, in.
$E_{cd}$	=	elastic modulus of deck concrete, ksi
$E_{ci}$	=	elastic modulus of concrete at initial time, ksi
$E_{ct}$	=	elastic modulus of concrete at time of transfer, ksi
$E_p$	=	elastic modulus of prestressing steel, ksi
$f_{c56}'$	=	56-day concrete compressive strength, ksi
$f_{cd}'$	=	56-day concrete compressive strength of deck concrete, ksi
$f_{cgp}$	=	stress at center gravity of prestressing due to prestress forces and self-weight, ksi
$f_{ci}'$	=	concrete compressive strength at time of transfer, ksi
$f_{pd}$	=	prestressing stress in steel at time of deck placement, ksi
$f_{pi}$	=	initial prestressing stress in steel, ksi
$f_{pt}$	=	prestressing stress after transfer in steel, ksi
$f_{pu}$	=	ultimate strength of prestressing steel, ksi
$f_{py}$	=	yield strength of prestressing steel, ksi
$H$	=	average annual relative humidity, %
$I_c$	=	transformed composite cross-sectional moment of inertia, in. <sup>4</sup>
$I_g$	=	gross cross-sectional moment of inertia, in. <sup>4</sup>
$K_{id}, K_{df}$	=	transformed section coefficient
$K_L$	=	factor for type of prestressing strand used, 30 for low relaxation
$k_f$	=	factor for effect of concrete strength
$k_{hc}$	=	humidity factor for creep
$k_{hs}$	=	humidity factor for shrinkage
$k_s$	=	factor for effect of the volume-to-surface ratio of the component
$k_{td}$	=	time development factor
$L$	=	span length, ft
$M_d$	=	moment due to deck placement, kip-ft
$M_g$	=	moment due to self-weight, kip-ft
$n_d$	=	modular ratio of deck to girder
$n_{strand}$	=	number of prestressing strands
$P_i$	=	prestressing force before losses, kip

$P_{id}$	=	prestressing force at time of deck placement, kip
$P_{ES}$	=	prestressing force after elastic shortening, kip
$S$	=	surface area exposed to drying, ft <sup>2</sup>
$t_d$	=	age at time of deck placement, days
$t_f$	=	age at end time (40 years), days
$t_i$	=	age at transfer of prestressing, days
$t_s$	=	thickness of slab, in.
$V$	=	volume, ft <sup>3</sup>
$y_b$	=	depth from centroid of beam to bottom face, in.
$y_{bt}$	=	depth from centroid of transformed composite section to bottom face of girder, in.
$\gamma_c$	=	unit weight of concrete, pcf
$\gamma_{cd}$	=	unit weight of deck concrete, pcf
$\Delta f_{cd}$	=	change in stress at center gravity of prestressing steel due to deck placement, ksi
$\Delta f_{cdf}$	=	change in stress at center gravity of prestressing steel due to deck shrinkage, ksi
$\Delta f_{pCD}$	=	loss of prestress due to creep of girder after deck placement, ksi
$\Delta f_{pCR}$	=	loss of prestress due to creep of girder prior to deck placement, ksi
$\Delta f_{pES}$	=	loss of prestress due to elastic shortening, ksi
$\Delta f_{pR1}$	=	loss of prestress due to relaxation of prestressing steel prior to deck placement, ksi
$\Delta f_{pR2}$	=	loss of prestress due to relaxation of prestressing steel after deck placement, ksi
$\Delta f_{pSD}$	=	loss of prestress due to shrinkage of girder after deck placement, ksi
$\Delta f_{pSR}$	=	loss of prestress due to shrinkage of girder prior to deck placement, ksi
$\Delta f_{pSS}$	=	prestress gain due to shrinkage of deck concrete, ksi
$\Delta f_{ps\_df}$	=	total loss of prestressing after deck placement, ksi
$\Delta f_{ps\_id}$	=	total time dependent loss of prestressing at time of deck placement, ksi
$\Delta f_{ps\_instant}$	=	instantaneous loss of prestressing, ksi
$\Delta f_{ps\_total}$	=	total loss of prestressing, ksi
$\epsilon$	=	shrinkage strain
$\psi$	=	creep coefficient

## B.2.2 Calculation of Losses

### Section and Material Properties:

$A_g := 659 \text{ in}^2$	$e_{pg} := 22.604 \text{ in}$	$f_{py} := 256.2 \text{ ksi}$	$f_{c56} := 10.238 \text{ ksi}$
$I_g := 268051 \text{ in}^4$	$E_p := 28500 \text{ ksi}$	$n_{strand} := 38$	$f_{ci} := 7.849 \text{ ksi}$
$\gamma_c := 122 \text{ pcf}$	$E_{ct} := 3529 \text{ ksi}$	$f_{pi} := 178.8 \text{ ksi}$	$t_i := 5 \text{ days}$
$L := 106.76042 \text{ ft}$	$E_{ci} := 3682 \text{ ksi}$	$A_{strand} := .217 \text{ in}^2$	$t_f := 14600 \text{ days}$
$y_b := 27.63 \text{ in}$	$f_{pu} := 270 \text{ ksi}$	$t := t_f \text{ days}$	$t_d := 422 \text{ days}$
	$E_c := 3729 \text{ ksi}$		

### Determine Loading Properties:

$A_{ps} := n_{strand} \cdot A_{strand}$	$A_{ps} = 8.246 \text{ in}^2$
$P_i := A_{ps} \cdot f_{pi}$	$P_i = 1.474 \times 10^3 \cdot \text{kip}$
$M_g := \frac{\gamma_c \cdot A_g \cdot L^2}{8}$	$M_g = 795.451 \cdot \text{kip} \cdot \text{ft}$

### Elastic Shortening Losses:

$$P_{ES0} := 1244.3 \text{ kip} \quad (\text{Iterate on } P_{ES0} \text{ until equal to } P_{ES})$$

$$f_{cgp} := -\frac{P_{ES0}}{A_g} - \frac{P_{ES0} \cdot e_{pg}^2}{I_g} - \frac{M_g \cdot (-e_{pg})}{I_g} \quad f_{cgp} = -3.455 \text{ ksi}$$

$$\Delta f_{pES} := -\frac{E_p}{E_{ct}} \cdot f_{cgp} \quad (\text{Eq. 5.9.5.2.3a-1}) \quad \boxed{\Delta f_{pES} = 27.903 \text{ ksi}}$$

$$f_{pt} := f_{pi} - \Delta f_{pES} \quad f_{pt} = 150.897 \text{ ksi}$$

$$P_{ES} := f_{pt} \cdot A_{ps} \quad P_{ES} = 1.244 \times 10^3 \cdot \text{kip}$$

$$f_{cgp} := -\frac{P_{ES}}{A_g} - \frac{P_{ES} \cdot e_{pg}^2}{I_g} - \frac{M_g \cdot (-e_{pg})}{I_g} \quad f_{cgp} = -3.455 \text{ ksi}$$

$$\Delta f_{pES1} := -\frac{E_p}{E_{ct}} \cdot f_{cgp} \quad (\text{Eq. 5.9.5.2.3a-1}) \quad \boxed{\Delta f_{pES1} = 27.903 \text{ ksi}}$$

**Shrinkage Losses (before deck):**

$$H := 70 \quad (\text{From Figure 5.4.2.3.3-1})$$

$$V := A_g \cdot L$$

$$V = 488.577 \cdot \text{ft}^3$$

$$S := 218.838 \text{in} \cdot L$$

$$S = 1.947 \times 10^3 \cdot \text{ft}^2$$

$$k_s := 1.45 - 0.13 \cdot \left( \frac{V}{S \cdot \text{in}} \right) \quad (\text{Eq. 5.4.2.3.2-2})$$

$$k_s = 1.059$$

$$k_f := \frac{5}{1 + \frac{f_{ci}}{\text{ksi}}} \quad (\text{Eq. 5.4.2.3.2-4})$$

$$k_f = 0.565$$

$$k_{td} := \left( \frac{t_f}{61 - 4 \cdot \frac{f_{ci}}{\text{ksi}} + t_f} \right) \quad (\text{Eq. 5.4.2.3.2-5})$$

$$k_{td} = 0.998$$

$$k_{hs} := (2 - 0.014H) \quad (\text{Eq. 5.4.2.3.3-2})$$

$$k_{hs} = 1.02$$

$$k_{hc} := (1.56 - 0.008H) \quad (\text{Eq. 5.4.2.3.2-3})$$

$$k_{hc} = 1$$

$$\epsilon_{bid} := k_s \cdot k_{hs} \cdot k_f \cdot k_{td} \cdot 0.48 \times 10^{-3} \quad (\text{Eq. 5.4.2.3.3-1})$$

$$\epsilon_{bid} = 2.922 \times 10^{-4}$$

$$\Psi_b := 1.9 \cdot k_s \cdot k_{hc} \cdot k_f \cdot k_{td} \cdot t_i^{-.118} \quad (\text{Eq. 5.4.2.3.2-1})$$

$$\Psi_b = 0.938$$

$$K_{id} := \frac{1}{1 + \frac{E_p}{E_{ci}} \cdot \frac{A_{ps}}{A_g} \cdot \left( 1 + \frac{A_g \cdot e_{pg}^2}{I_g} \right)} \cdot (1 + 0.7 \cdot \Psi_b)$$

$$(\text{Eq. 5.9.5.4.2a-2})$$

$$K_{id} = 0.734$$

$$\Delta f_{pSR} := \epsilon_{bid} \cdot E_p \cdot K_{id} \quad (\text{Eq. 5.9.5.4.2a-1})$$

$$\Delta f_{pSR} = 6.115 \cdot \text{ksi}$$

**Creep Losses (before deck):**

$$k_{td} := \left[ \frac{(t_d - t_i)}{61 - 4 \cdot \frac{f_{ci}}{\text{ksi}} + (t_d - t_i)} \right] \quad (\text{Eq. 5.4.2.3.2-5})$$

$$\Psi_{bc} := 1.9 \cdot k_s \cdot k_{hc} \cdot k_f \cdot k_{td} \cdot t_i^{-.118} \quad (\text{Eq. 5.4.2.3.2-1})$$

$$\Psi_b = 0.938$$

$$\Delta f_{pCR} := -\frac{E_p}{E_{ci}} \cdot f_{cgp} \cdot \Psi_{bc} \cdot K_{id} \quad (\text{Eq. 5.9.5.4.2b-1})$$

$$\Delta f_{pCR} = 17.231 \cdot \text{ksi}$$

**Relaxation Losses (before deck):**

$$f_{pt} := \max(f_{pi} - \Delta f_{pES}, 0.55f_{pu})$$

$$f_{pt} = 150.897 \cdot \text{ksi}$$

$$K_L := 30 \quad (\text{For low relaxation strands})$$

$$\Delta f_{pR1} := \max\left[\frac{f_{pt}}{K_L} \cdot \left(\frac{f_{pt}}{f_{py}} - 0.55\right), 1.2 \text{ksi}\right] \quad (\text{Eq. 5.9.5.4.2c-1})$$

$$\Delta f_{pR1} = 1.2 \cdot \text{ksi}$$

**Deck Properties:**

$$t_s := 9.25 \text{in} \quad \gamma_{cd} := 145 \text{pcf} \quad f_{cd} := 5.626 \text{ksi}$$

$$b_d := 7.5 \text{ft} \quad E_{cd} := 3811 \text{ksi}$$

**Transformed Composite Section Properties:**

$$n_d := \frac{E_{cd}}{E_{ct}}$$

$$n_d = 1.08$$

$$A_c := A_g + n_d \cdot t_s \cdot b_d$$

$$A_c = 1.558 \times 10^3 \cdot \text{in}^2$$

$$y_{bt} := \frac{A_g \cdot y_b + n_d \cdot t_s \cdot b_d \cdot \left(54 \text{in} + \frac{t_s}{2}\right)}{A_c}$$

$$y_{bt} = 45.515 \cdot \text{in}$$

$$I_c := I_g + A_g \cdot (y_b - y_{bt})^2 + n_d \cdot \frac{b_d \cdot t_s^3}{12} + n_d \cdot t_s \cdot b_d \cdot \left(54 \text{in} + \frac{t_s}{2} - y_{bt}\right)^2$$

$$I_c = 6.398 \times 10^5 \cdot \text{in}^4$$

$$e_{pc} := e_{pg} + (y_{bt} - y_b)$$

$$e_{pc} = 40.489 \cdot \text{in}$$

**Determine Girder Shrinkage Losses (post deck):**

$$k_{td\_d} := \left[ \frac{(t - t_d)}{61 - 4 \cdot \frac{f_{ci}}{\text{ksi}} + (t - t_d)} \right] \quad (\text{Eq. 5.4.2.3.2-5})$$

$$k_{td\_d} = 0.998$$

$$\epsilon_{bdf} := k_s \cdot k_{hs} \cdot k_f \cdot k_{td\_d} \cdot 0.48 \times 10^{-3} \quad (\text{Eq. 5.4.2.3.3-1})$$

$$\epsilon_{bdf} = 2.922 \times 10^{-4}$$

$$K_{df} := \frac{1}{1 + \frac{E_p}{E_{ci}} \cdot \frac{A_{ps}}{A_c} \left( 1 + \frac{A_c \cdot e_{pc}^2}{I_c} \right)} \cdot (1 + 0.7 \Psi_b) \quad (\text{Eq. 5.9.5.4.3a-2}) \quad K_{df} = 0.747$$

$$\Delta f_{pSD} := \varepsilon_{bdf} \cdot E_p \cdot K_{df} \quad (\text{Eq. 5.9.5.4.3a-1})$$

$$\Delta f_{pSD} = 6.221 \cdot \text{ksi}$$

Determine Creep Losses (post deck):

$$M_d := \frac{t_s \cdot b_d \cdot \gamma_{cd} \cdot L^2}{8}$$

$$M_d = 1.194 \times 10^3 \cdot \text{kip} \cdot \text{ft}$$

$$\Delta f_{p\_id} := \Delta f_{pES} + \Delta f_{pSR} + \Delta f_{pCR} + \Delta f_{pR1}$$

$$\Delta f_{p\_id} = 52.449 \cdot \text{ksi}$$

$$f_{pd} := f_{pi} - \Delta f_{p\_id}$$

$$f_{pd} = 126.351 \cdot \text{ksi}$$

$$P_{id} := f_{pd} \cdot A_{ps}$$

$$P_{id} = 1.042 \times 10^3 \cdot \text{kip}$$

$$\Delta f_{cd} := \frac{P_{id}}{A_g} - \frac{P_{id} \cdot e_{pg}^2}{I_g} - \frac{M_d \cdot (-e_{pg})}{I_g} - f_{cgp}$$

$$\Delta f_{cd} = 1.097 \cdot \text{ksi}$$

$$k_{tdfi} := \left[ \frac{(t_f - t_i)}{61 - 4 \cdot \frac{f_{ci}}{\text{ksi}} + (t_f - t_i)} \right] \quad (\text{Eq. 5.4.2.3.2-5})$$

$$k_{tdfi} = 0.998$$

$$\Psi_{fi} := 1.9 \cdot k_s \cdot k_{hc} \cdot k_f \cdot k_{tdfi} \cdot t_i^{-.118} \quad (\text{Eq. 5.4.2.3.2-1})$$

$$\Psi_{fi} = 0.938$$

$$k_{tddi} := \left[ \frac{(t_d - t_i)}{61 - 4 \cdot \frac{f_{ci}}{\text{ksi}} + (t_d - t_i)} \right] \quad (\text{Eq. 5.4.2.3.2-5})$$

$$k_{tddi} = 0.934$$

$$\Psi_{di} := 1.9 \cdot k_s \cdot k_{hc} \cdot k_f \cdot k_{tddi} \cdot t_i^{-.118} \quad (\text{Eq. 5.4.2.3.2-1})$$

$$\Psi_{di} = 0.878$$

$$k_{tdfd} := \left[ \frac{(t_f - t_d)}{61 - 4 \cdot \frac{f_{ci}}{\text{ksi}} + (t_f - t_d)} \right] \quad (\text{Eq. 5.4.2.3.2-5})$$

$$k_{tdfd} = 0.998$$

$$\Psi_{fd} := 1.9 \cdot k_s \cdot k_{hc} \cdot k_f \cdot k_{tdfd} \cdot t_d^{-.118} \quad (\text{Eq. 5.4.2.3.2-1})$$

$$\Psi_{fd} = 0.556$$

$$\Delta f_{pCD} := \frac{E_p}{E_{ci}} \cdot f_{cgp} \cdot (\Psi_{fi} - \Psi_{di}) \cdot K_{df} + \frac{E_p}{E_c} \cdot \Delta f_{cd} \cdot \Psi_{fd} \cdot K_{df} \quad (\text{Eq. 5.9.5.4.3b-1})$$

$$\Delta f_{pCD} = 2.272 \cdot \text{ksi}$$

**Determine Relaxation Losses (post deck):**

$$\Delta f_{pR2} := \Delta f_{pR1} \quad (\text{Eq. 5.9.5.4.3c-1})$$

$$\Delta f_{pR2} = 1.2 \cdot \text{ksi}$$

**Determine Shrinkage of Deck Losses:**

$$V := t_s \cdot b_d \cdot L$$

$$V = 617.209 \cdot \text{ft}^3$$

$$S := (2 \cdot b_d - 42 \text{in}) \cdot L$$

$$S = 1.228 \times 10^3 \cdot \text{ft}^2$$

$$k_s := 1.45 - 0.13 \cdot \left( \frac{V}{S \cdot \text{in}} \right) \quad (\text{Eq. 5.4.2.3.2-2})$$

$$k_s = 0.666$$

$$k_f := \frac{5}{1 + \frac{f_{cd}}{\text{ksi}}} \quad (\text{Eq. 5.4.2.3.2-4})$$

$$k_f = 0.755$$

$$k_{td} := \left[ \frac{(t_f - t_d)}{61 - 4 \cdot \frac{f_{cd}}{\text{ksi}} + (t_f - t_d)} \right] \quad (\text{Eq. 5.4.2.3.2-5})$$

$$k_{td} = 0.997$$

$$\epsilon_{ddf} := k_s \cdot k_{hs} \cdot k_f \cdot k_{td} \cdot 0.48 \times 10^{-3} \quad (\text{Eq. 5.4.2.3.3-1})$$

$$\epsilon_{ddf} = 2.453 \times 10^{-4}$$

$$\Psi_d := 1.9 \cdot k_s \cdot k_{hc} \cdot k_f \cdot k_{td} \cdot t_i^{-.118} \quad (\text{Eq. 5.4.2.3.2-1})$$

$$\Psi_d = 0.787$$

$$e_d := 54 \text{in} - y_{bt} + \frac{t_s}{2}$$

$$e_d = 13.11 \cdot \text{in}$$

$$\Delta f_{cdf} := -\frac{\epsilon_{ddf} \cdot t_s \cdot b_d \cdot E_{cd}}{(1 + 0.7 \Psi_d)} \cdot \left( \frac{1}{A_c} - \frac{e_{pc} \cdot e_d}{I_c} \right)$$

$$\Delta f_{cdf} = 0.094 \cdot \text{ksi}$$

$$\Psi_b(t) := 1.9 \cdot k_s \cdot k_{hc} \cdot k_f \cdot k_{td} \cdot t_i^{-.118}$$

$$\Psi_b(t_f) = 0.787$$

$$\Delta f_{pSS} := \frac{E_p}{E_c} \cdot \Delta f_{cdf} \cdot K_{df} \cdot (1 + 0.7 \Psi_{fd}) \quad (\text{Eq. 5.9.5.4.3d-1})$$

$$\Delta f_{pSS} = 0.747 \cdot \text{ksi}$$

**Total Losses:**

$$\Delta f_{ps\_instant} := \Delta f_{pES}$$

$$\Delta f_{ps\_instant} = 27.903 \cdot \text{ksi}$$

$$\Delta f_{ps\_id} := \Delta f_{pSR} + \Delta f_{pCR} + \Delta f_{pR1}$$

$$\Delta f_{ps\_id} = 24.546 \cdot \text{ksi}$$

$$\Delta f_{ps\_df} := \Delta f_{pSD} + \Delta f_{pCD} + \Delta f_{pR2} - \Delta f_{pSS}$$

$$\Delta f_{ps\_df} = 8.946 \cdot \text{ksi}$$

$$\Delta f_{ps\_total} := \Delta f_{ps\_instant} + \Delta f_{ps\_id} + \Delta f_{ps\_df}$$

$$\Delta f_{ps\_total} = 61.394 \cdot \text{ksi}$$

## B.3 ACI 209 Method Calculations

### B.3.1 Notation

The following notation was used in computing prestress losses according to the ACI 209

Method (1992):

$A_g$	=	gross cross-sectional area, in. <sup>2</sup>
$A_{g1}$	=	gross cross-sectional area of deck, in. <sup>2</sup>
$A_{strand}$	=	area of single prestressing strand, in. <sup>2</sup>
$A_{ps}$	=	total area of prestressing steel, in. <sup>2</sup>
CR1	=	loss of prestress due to creep of girder prior to deck placement, ksi
CR2	=	loss of prestress due to creep of girder after deck placement, ksi
CR3	=	loss of prestress due to creep of girder due to deck placement, ksi
$e_{pg}$	=	eccentricity of prestressing strands, in.
$E_{c1}$	=	elastic modulus of deck concrete, ksi
$E_{c56}$	=	elastic modulus of concrete at initial time, ksi
$E_{ct}$	=	elastic modulus of concrete at time of transfer, ksi
$E_p$	=	elastic modulus of prestressing steel, ksi
ES	=	loss of prestress due to elastic shortening, ksi
$f_{c56}'$	=	56-day concrete compressive strength, ksi
$f_c$	=	stress at center gravity of prestressing due to prestress forces and self-weight, ksi
$f_{ci}'$	=	concrete compressive strength at time of transfer, ksi
$f_{cs}$	=	change in stress at center gravity of prestressing steel due to deck placement, ksi
$f_{pi}$	=	initial prestressing stress in steel, ksi
$f_{pt}$	=	prestressing stress after transfer in steel, ksi
$f_{pu}$	=	ultimate strength of prestressing steel, ksi
$f_{py}$	=	yield strength of prestressing steel, ksi
$f_{si}$	=	prestressing stress after transfer losses, ksi
$f_{sr}$	=	prestressing loss at any time due to relaxation, ksi
$F_o, F_s, F_t$	=	factors for effective prestressing at various ages
$I_c$	=	transformed composite cross-sectional moment of inertia, in. <sup>4</sup>
$I_g$	=	gross cross-sectional moment of inertia, in. <sup>4</sup>
L	=	span length, ft
$M_g$	=	moment due to self-weight, kip-ft
m	=	modular ratio of prestressing steel to girder
$n_{strand}$	=	number of prestressing strands
$P_i$	=	prestressing force before losses, kip
$P_{ES}$	=	prestressing force after elastic shortening, kip
RE	=	loss of prestress due to relaxation of prestressing steel, ksi
S	=	surface area exposed to drying, ft <sup>2</sup>
SR	=	loss of prestress due to shrinkage of girder prior to deck placement, ksi

$t_f$	=	age at end time (40 years), days
$t_i$	=	age at transfer of prestressing, days
$t_s$	=	age at time of deck placement, days
$V$	=	volume, ft <sup>3</sup>
$\gamma_c$	=	unit weight of concrete, pcf
$\gamma_{sh}$	=	factor for effect of relative humidity on shrinkage
$\gamma_{vs}$	=	factor for effect of the volume-to-surface ratio of the component
$\gamma_\lambda$	=	factor for relative humidity
$\Delta f_{ps\_instant}$	=	instantaneous loss of prestressing, ksi
$\Delta f_{ps\_time}$	=	total time dependent loss of prestressing, ksi
$\Delta f_{ps\_total}$	=	total loss of prestressing, ksi
$\epsilon$	=	shrinkage strain
$\lambda$	=	average annual relative humidity, %
$\xi_s$	=	factor for interaction of prestressing steel
$\rho$	=	prestressed reinforcement ratio
$\nu$	=	creep coefficient

### B.3.2 Calculation of Losses

#### Section and Material Properties:

$A_g := 659\text{in}^2$	$e_{pg} := 22.604\text{in}$	$f_{py} := 256.2\text{ksi}$	$f_{c56} := 10.238\text{ksi}$
$I_g := 268051\text{in}^4$	$E_p := 28500\text{ksi}$	$n_{strand} := 38$	$f_{ci} := 7.849\text{ksi}$
$\gamma_c := 122\text{pcf}$	$E_{ct} := 3529\text{ksi}$	$f_{pi} := 178.8\text{ksi}$	$t_i := 5\text{ days}$
$L := 106.76042\text{ft}$	$f_{pu} := 270\text{ksi}$	$A_{strand} := .217\text{in}^2$	$t_f := 14600\text{ days}$
$n := \frac{E_p}{E_{ct}}$	$I_c := 639800\text{in}^4$	$t := t_f\text{ days}$	$t_s := 422\text{ days}$
$I_2 := I_g$	$E_{c56} := 4192\text{ksi}$	$E_{c1} := 3995\text{ksi}$	
	$A_{g1} := 7.5\text{ft} \cdot 9.25\text{in}$		

#### Determine Loading Properties:

$A_{ps} := n_{strand} \cdot A_{strand}$	$A_{ps} = 8.25 \cdot \text{in}^2$
$P_i := A_{ps} \cdot f_{pi}$	$P_i = 1.47 \times 10^3 \cdot \text{kip}$
$M_g := \frac{\gamma_c \cdot A_g \cdot L^2}{8}$	$M_g = 795.45 \cdot \text{kip} \cdot \text{ft}$

#### Elastic Shortening Losses:

$P_{ES0} := 1244.3\text{kip}$ (Iterate on $P_{ES0}$ until equal to $P_{ES}$ )	
$f_c := \frac{P_{ES0}}{A_g} + \frac{P_{ES0} \cdot e_{pg}^2}{I_g} - \frac{M_g \cdot e_{pg}}{I_g}$	$f_c = 3.46\text{-ksi}$
$ES := n \cdot f_c$ (Eq. 4-19 Term 1)	$ES = 27.9\text{-ksi}$
$f_{pt} := f_{pi} - ES$	$f_{pt} = 150.9\text{-ksi}$
$P_{ES} := f_{pt} \cdot A_{ps}$	$P_{ES} = 1.24 \times 10^3 \cdot \text{kip}$
$f_c := -\frac{P_{ES}}{A_g} - \frac{P_{ES} \cdot e_{pg}^2}{I_g} - \frac{M_g \cdot (-e_{pg})}{I_g}$	$f_c = -3.46\text{-ksi}$
$ES1 := -n \cdot f_c$ (Eq. 5.9.5.2.3a-1)	$ES1 = 27.9\text{-ksi}$

**Girder Creep Losses (Before Deck Casting):**

$$\lambda := 70 \quad (\text{Average Annual Relative Humidity})$$

$$\gamma_\lambda := 1.27 - .0067 \cdot \lambda$$

$$\gamma_\lambda = 0.8$$

$$\gamma_{vs} := 0.81 \quad (\text{Table 2.5.5.2})$$

$$v_u := 2.35 \cdot \gamma_\lambda \cdot \gamma_{vs}$$

$$v_u = 1.52$$

$$v_t(t) := \frac{t^{0.6}}{10 + t^{0.6}} \cdot v_u$$

$$v_t(t_s) = 1.2$$

$$F_s := .16 \quad (\text{From Table 4.4.1.2})$$

$$F_o := 1$$

$$CR1 := (-n \cdot f_c) \cdot v_t(t_s) \cdot \left(1 - \frac{F_s}{2 \cdot F_o}\right) \quad (\text{Eq. 4-19 Term 2})$$

$$CR1 = 30.92 \cdot \text{ksi}$$

**Girder Creep Losses (After Deck Casting):**

$$F_t := 0.05 \quad (\text{From Table 4.4.1.2})$$

$$CR2 := (-n \cdot f_c) \cdot (v_t(t) - v_t(t_s)) \cdot \left(1 - \frac{F_s + F_t}{2 \cdot F_o}\right) \cdot \left(\frac{I_2}{I_c}\right) \quad (\text{Eq. 4-19 Term 3})$$

$$CR2 = 2.86 \cdot \text{ksi}$$

**Shrinkage Losses (Before Deck Placement):**

$$\gamma_{sh} := 1.40 - 0.01 \cdot \lambda \quad (\text{Eq. 2-14})$$

$$\gamma_{sh} = 0.7$$

$$V := A_g \cdot L$$

$$V = 488.58 \cdot \text{ft}^3$$

$$S := 218.838 \text{in} \cdot L$$

$$S = 1.95 \times 10^3 \cdot \text{ft}^2$$

$$\frac{V}{S} = 3.01 \cdot \text{in}$$

$$\gamma_{vs} := .84 \quad (\text{Table 2.5.5.2})$$

$$\epsilon_{sh\_u} := 780 \cdot \gamma_{sh} \cdot \gamma_{vs} \cdot 10^{-6}$$

$$\epsilon_{sh\_u} = 4.59 \times 10^{-4}$$

$$\epsilon_{sh\_t}(t) := \frac{t}{55 + t} \cdot \epsilon_{sh\_u} \quad (\text{Eq. 2-10})$$

$$\epsilon_{sh\_t}(t) = 4.57 \times 10^{-4}$$

$$\rho := \frac{A_{ps}}{A_g}$$

$$\rho = 0.01$$

$$\xi_s := 2.6$$

$$SR := \frac{\varepsilon_{sh\_t(t)} \cdot E_p}{1 + n \cdot \rho \cdot \xi_s}$$

(Eq. 4-19 Term 4)

$$SR = 10.31 \text{ ksi}$$

#### Relaxation Losses:

$$f_{si} := f_{pi} - ES$$

$$f_{sr}(t) := 0.005 \cdot f_{si} \cdot \log(t)$$

(From Table 4.4.1.3)

$$f_{sr}(t) = 3.14 \text{ ksi}$$

$$RE := f_{sr}(t)$$

(Eq. 4-19 Term 5)

$$RE = 3.14 \text{ ksi}$$

#### Creep from Slab Load:

$$\gamma_{vs} := 0.81 \quad (\text{Table 2.5.5.2})$$

$$v_u := 2.35 \cdot \gamma_\lambda \cdot \gamma_{vs}$$

$$v_u = 1.52$$

$$v_{t1}(t) := \frac{t^{0.6}}{10 + t^{0.6}} \cdot v_u$$

$$v_t(t_s) = 1.2$$

$$f_{cs} := 1.208 \text{ ksi}$$

$$m := \frac{E_p}{E_{c56}}$$

$$m = 6.8$$

$$CR3 := (m \cdot f_{cs}) \cdot v_{t1}(t_f) \cdot \frac{I_2}{I_c}$$

(Eq. 4-19 Term 7)

$$CR3 = 5.08 \text{ ksi}$$

#### Total Losses:

$$\Delta f_{ps\_instant} := ES$$

$$\Delta f_{ps\_instant} = 27.9 \text{ ksi}$$

$$\Delta f_{ps\_time} := SR + CR1 + CR2 + CR3 + RE$$

$$\Delta f_{ps\_time} = 52.32 \text{ ksi}$$

$$\Delta f_{ps\_total} := \Delta f_{ps\_instant} + \Delta f_{ps\_time}$$

$$\Delta f_{ps\_total} = 80.22 \text{ ksi}$$

## B.4 PCI Design Handbook Method Calculations

### B.4.1 Notation

The following notation was used in computing prestress losses according to the PCI

Design Handbook Method (2004):

$A_g$	=	gross cross-sectional area, in. <sup>2</sup>
$A_{strand}$	=	area of single prestressing strand, in. <sup>2</sup>
$A_{ps}$	=	total area of prestressing steel, in. <sup>2</sup>
$C$	=	factor for effect of stress level on relaxation, ksi
$CR$	=	loss of prestress due to creep of girder, ksi
$e$	=	eccentricity of prestressing strands, in.
$E_c$	=	elastic modulus of concrete at initial time, ksi
$E_{ci}$	=	elastic modulus of concrete at time of transfer, ksi
$E_{ps}$	=	elastic modulus of prestressing steel, ksi
$ES$	=	loss of prestress due to elastic shortening, ksi
$f_{cir}$	=	stress at center gravity of prestressing due to prestress forces and self-weight, ksi
$f_{cds}$	=	change in stress at center gravity of prestressing steel due to deck placement, ksi
$f_{pi}$	=	initial prestressing stress in steel, ksi
$f_{pu}$	=	ultimate strength of prestressing steel, ksi
$I_g$	=	gross cross-sectional moment of inertia, in. <sup>4</sup>
$J$	=	factor for type of prestressing steel utilized
$K_{es}$	=	1.0 for pretensioned member
$K_{cir}$	=	0.9 for pretensioned member
$K_{cr}$	=	1.6 for sand-lightweight concrete
$K_{re}$	=	factor for type of prestressing steel utilized
$K_{sh}$	=	1.0 for pretensioned member
$L$	=	span length, ft
$M_g$	=	moment due to self-weight, kip-ft
$n_{strand}$	=	number of prestressing strands
$P_i$	=	prestressing force before losses, kip
$P_{ES}$	=	prestressing force after elastic shortening, kip
$RE$	=	loss of prestress due to relaxation of prestressing steel, ksi
$RH$	=	average annual relative humidity, %
$S$	=	surface area exposed to drying, ft <sup>2</sup>
$SH$	=	loss of prestress due to shrinkage of girder, ksi
$V$	=	volume, ft <sup>3</sup>
$\gamma_c$	=	unit weight of concrete, pcf
$\Delta f_{ps\_instant}$	=	instantaneous loss of prestressing, ksi
$\Delta f_{ps\_time}$	=	total time dependent loss of prestressing, ksi
$\Delta f_{ps\_total}$	=	total loss of prestressing, ksi

## B.4.2 Calculation of Losses

### Section and Material Properties:

$$\begin{array}{lll}
 A_g := 659 \text{ in}^2 & f_{pu} := 270 \text{ ksi} & n_{strand} := 38 \\
 I_g := 268051 \text{ in}^4 & e := 22.604 \text{ in} & f_{pi} := 178.8 \text{ ksi} \\
 \gamma_c := 122 \text{ pcf} & E_{ps} := 28500 \text{ ksi} & A_{strand} := .217 \text{ in}^2 \\
 L := 106.76042 \text{ ft} & E_{ci} := 3529 \text{ ksi} & \\
 & E_c := 3729 \text{ ksi} & 
 \end{array}$$

### Determine Loading Properties:

$$\begin{array}{ll}
 A_{ps} := n_{strand} \cdot A_{strand} & A_{ps} = 8.246 \text{ in}^2 \\
 P_i := A_{ps} \cdot f_{pi} & P_i = 1.474 \times 10^3 \text{ kip} \\
 M_g := \frac{\gamma_c \cdot A_g \cdot L^2}{8} & M_g = 795.451 \text{ kip-ft}
 \end{array}$$

### Elastic Shortening Losses:

$$\begin{array}{ll}
 K_{es} := 1.0 & \\
 K_{cir} := 0.9 & \\
 P_{ES} := f_{pi} \cdot n_{strand} \cdot A_{strand} & P_{ES} = 1.474 \times 10^3 \text{ kip} \\
 f_{cir} := K_{cir} \cdot \left( \frac{P_{ES}}{A_g} + \frac{P_{ES} \cdot e^2}{I_g} \right) - \frac{M_g \cdot e}{I_g} \quad (\text{Eq. 4.7.3.3}) & f_{cir} = 3.738 \text{ ksi} \\
 ES := K_{es} \cdot E_{ps} \cdot \frac{f_{cir}}{E_{ci}} \quad (\text{Eq. 4.7.3.2}) & \boxed{ES = 30.188 \text{ ksi}}
 \end{array}$$

### Creep Losses:

$$\begin{array}{ll}
 K_{cr} := 1.6 \quad (\text{For sand-lightweight concrete}) & \\
 f_{c ds} := 1.208 \text{ ksi} \quad (\text{Stress due to superimposed dead loads}) & \\
 CR := K_{cr} \cdot \left( \frac{E_{ps}}{E_c} \right) \cdot (f_{cir} - f_{c ds}) \quad (\text{Eq. 4.7.3.4}) & \boxed{CR = 30.938 \text{ ksi}}
 \end{array}$$

### Shrinkage Losses:

$$K_{sh} := 1.0 \quad (\text{For pretensioned members})$$

$$V := A_g \cdot L$$

$$V = 488.577 \cdot \text{ft}^3$$

$$S := 218.838 \text{in} \cdot L$$

$$S = 1.947 \times 10^3 \cdot \text{ft}^2$$

$$\frac{V}{S} = 3.011 \cdot \text{in}$$

$$RH := 70 \quad (\text{From Figure 3.12.2})$$

$$SH := \left(8.2 \times 10^{-6}\right) \cdot K_{sh} \cdot E_{ps} \cdot \left(1 - .06 \frac{V}{S \cdot \text{in}}\right) \cdot (100 - RH) \quad (\text{Eq. 4.7.3.6}) \quad \boxed{SH = 5.744 \cdot \text{ksi}}$$

### Relaxation Losses:

$$K_{re} := 5000 \text{psi}$$

(From Table 4.7.3.1)

$$J := .04$$

$$\frac{f_{pi}}{f_{pu}} = 0.662$$

$$C := .57 \quad (\text{From Table 4.7.3.2})$$

$$RE := \left[K_{re} - J \cdot (SH + CR + ES)\right] \cdot C \quad (\text{Eq. 4.7.3.7}) \quad \boxed{RE = 1.325 \cdot \text{ksi}}$$

### Total Losses:

$$\Delta f_{ps\_instant} := ES$$

$$\Delta f_{ps\_instant} = 30.188 \cdot \text{ksi}$$

$$\Delta f_{ps\_time} := SH + CR + RE$$

$$\Delta f_{ps\_time} = 38.007 \cdot \text{ksi}$$

$$\Delta f_{ps\_total} := \Delta f_{ps\_instant} + \Delta f_{ps\_time}$$

$$\Delta f_{ps\_total} = 68.195 \cdot \text{ksi}$$

## B.5 Sham's Method Calculations

### B.5.1 Notation

The following notation was used in computing prestress losses according to the Sham's

Method (2000):

$A_g$	=	gross cross-sectional area, in. <sup>2</sup>
$A_{ps}$	=	total area of prestressing steel, in. <sup>2</sup>
$A_{strand}$	=	area of single prestressing strand, in. <sup>2</sup>
$e$	=	eccentricity of prestressing strands, in.
$E_p$	=	elastic modulus of prestressing steel, ksi
$E_c$	=	elastic modulus of concrete at 56-days of age, ksi
$E_{ci}$	=	elastic modulus of concrete at time of transfer, ksi
$f_{c56}$	=	56-day concrete compressive strength, ksi
$f_{cgp}$	=	stress at center gravity of prestressing due to prestress forces and self-weight, ksi
$f_{ci}$	=	concrete compressive strength at time of transfer, ksi
$f_{pt}$	=	prestressing stress after transfer in steel, ksi
$f_{pi}$	=	initial prestressing stress in steel, ksi
$H$	=	average annual relative humidity, %
$I_g$	=	gross cross-sectional moment of inertia, in. <sup>4</sup>
$k_1, k_2$	=	factor for effect of compressive strength on creep
$L$	=	span length, ft
$M_g$	=	moment due to self-weight, kip-ft
$n_{strand}$	=	number of prestressing strands
$P_{ES}$	=	prestressing force after elastic shortening, kip
$P_i$	=	prestressing force before losses, kip
$\Delta f_{cdp}$	=	change in stress at level of prestressing steel due to superimposed dead loads, ksi
$\Delta f_{pCR}$	=	loss of prestress due to creep, ksi
$\Delta f_{pES}$	=	loss of prestress due to elastic shortening, ksi
$\Delta f_{pR2}$	=	loss of prestress due to relaxation of prestressing steel, ksi
$\Delta f_{pSR}$	=	loss of prestress due to shrinkage, ksi
$\Delta f_{ps\_instant}$	=	instantaneous loss of prestressing, ksi
$\Delta f_{ps\_time}$	=	total time-dependent loss of prestressing, ksi
$\Delta f_{ps\_total}$	=	total loss of prestressing, ksi
$\gamma_c$	=	unit weight of concrete, pcf

## B.5.2 Calculation of Losses

### Section and Material Properties:

$$\begin{array}{llll}
 A_g := 659 \text{ in}^2 & e := -22.604 \text{ in} & n_{\text{strand}} := 38 & f_{c56} := 10.238 \text{ ksi} \\
 I_g := 268051 \text{ in}^4 & E_p := 28500 \text{ ksi} & f_{pi} := 178.8 \text{ ksi} & f_{ci} := 7.849 \text{ ksi} \\
 \gamma_c := 122 \text{pcf} & E_{ci} := 3529 \text{ ksi} & A_{\text{strand}} := .217 \text{ in}^2 & \\
 L := 106.76042 \text{ ft} & E_c := 3729 \text{ ksi} & & 
 \end{array}$$

### Determine Loading Properties:

$$\begin{array}{ll}
 A_{ps} := n_{\text{strand}} \cdot A_{\text{strand}} & A_{ps} = 8.246 \text{ in}^2 \\
 P_i := A_{ps} \cdot f_{pi} & P_i = 1.474 \times 10^3 \cdot \text{kip} \\
 M_g := \frac{\gamma_c \cdot A_g \cdot L^2}{8} & M_g = 795.451 \cdot \text{kip} \cdot \text{ft}
 \end{array}$$

### Elastic Shortening Losses:

$$P_{ES0} := 1244.3 \text{ kip} \quad (\text{Iterate on } P_{ES0} \text{ until equal to } P_{ES})$$

$$f_{cgp} := -\frac{P_{ES0}}{A_g} - \frac{P_{ES0} \cdot e^2}{I_g} - \frac{M_g \cdot e}{I_g} \quad f_{cgp} = -3.455 \text{ ksi}$$

$$\Delta f_{pES} := -\frac{E_p}{E_{ci}} \cdot f_{cgp} \quad (\text{Eq. 3.26}) \quad \boxed{\Delta f_{pES} = 27.903 \text{ ksi}}$$

$$f_{pt} := f_{pi} - \Delta f_{pES} \quad f_{pt} = 150.897 \text{ ksi}$$

$$P_{ES} := f_{pt} \cdot A_{ps} \quad P_{ES} = 1.244 \times 10^3 \cdot \text{kip}$$

$$f_{cgp} := -\frac{P_{ES}}{A_g} - \frac{P_{ES} \cdot e^2}{I_g} - \frac{M_g \cdot e}{I_g} \quad f_{cgp} = -3.455 \text{ ksi}$$

$$\Delta f_{pES1} := -\frac{E_p}{E_{ci}} \cdot f_{cgp} \quad (\text{Eq. 3.26}) \quad \boxed{\Delta f_{pES1} = 27.903 \text{ ksi}}$$

### Creep Losses:

$$\Delta f_{cdp} := 1.208 \text{ksi} \quad (\text{Change in stress due to superimposed dead loads})$$

$$k_1 := \frac{E_p}{E_{ci}} \cdot \left( 1.4 - \frac{f_{ci}}{14.75 \text{ksi}} \right) \quad k_1 = 7.009$$

$$k_2 := \frac{E_p}{E_c} \cdot \left( 1.4 - \frac{f_{c56}}{14.75 \text{ksi}} \right) \quad k_2 = 5.395$$

$$\Delta f_{pCR} := -(k_1 \cdot f_{cgp} - k_2 \cdot \Delta f_{cdp}) \quad (\text{Eq. 5.13}) \quad \Delta f_{pCR} = 30.733 \text{ksi}$$

### Shrinkage Losses:

$$H := 70$$

$$\Delta f_{pSR} := \begin{cases} (17.0 - .15 \cdot H) \cdot \text{ksi} & \text{if } f_{c56} < 10 \text{ksi} \\ [(15.0 - .15 \cdot H) \cdot \text{ksi}] & \text{if } f_{c56} \geq 10 \text{ksi} \end{cases} \quad (\text{Eq. 5.12}) \quad \Delta f_{pSR} = 4.5 \text{ksi}$$

### Relaxation Losses:

$$\Delta f_{pR2} := .3 \cdot [20.0 \text{ksi} - 0.4 \cdot \Delta f_{pES} - 0.2 \cdot (\Delta f_{pSR} + \Delta f_{pCR})] \quad (\text{Eq. 3.29}) \quad \Delta f_{pR2} = 0.538 \text{ksi}$$

- Note: 30% of equation value used due to use of low-relaxation strands

### Total Losses:

$$\Delta f_{ps\_instant} := \Delta f_{pES} \quad \Delta f_{ps\_instant} = 27.903 \text{ksi}$$

$$\Delta f_{ps\_time} := \Delta f_{pSR} + \Delta f_{pCR} + \Delta f_{pR2} \quad \Delta f_{ps\_time} = 35.771 \text{ksi}$$

$$\Delta f_{ps\_total} := \Delta f_{ps\_instant} + \Delta f_{ps\_time} \quad \Delta f_{ps\_total} = 63.673 \text{ksi}$$

## B.6 Tadro's Method Calculations

### B.6.1 Notation

The following notation was used in computing prestress losses according to the Tadro's

Method (2007):

$A_d$	=	gross cross-sectional area of deck, in. <sup>2</sup>
$A_g$	=	gross cross-sectional area, in. <sup>2</sup>
$A_{gc}$	=	gross cross-sectional of transformed composite section area, in. <sup>2</sup>
$A_{ti}$	=	transformed cross-sectional area, in. <sup>2</sup>
$A_{strand}$	=	area of single prestressing strand, in. <sup>2</sup>
$A_{ps}$	=	total area of prestressing steel, in. <sup>2</sup>
$b_d$	=	effective width of deck over girder, ft
$e_{dc}$	=	eccentricity of deck from centroid of composite section, in.
$e_{pc}$	=	eccentricity of prestressing strands in composite section, in.
$e_{pg}$	=	eccentricity of prestressing strands, in.
$e_{pti}$	=	eccentricity of prestressing strands in transformed section, in.
$E_{cd}$	=	elastic modulus of deck concrete, ksi
$E_{ct}$	=	elastic modulus of concrete at time of transfer, ksi
$E_p$	=	elastic modulus of prestressing steel, ksi
$f_{c56}'$	=	56-day concrete compressive strength, ksi
$f_{cd}'$	=	56-day concrete compressive strength of deck concrete, ksi
$f_{cgp}$	=	stress at center gravity of prestressing due to prestress forces and self-weight, ksi
$f_{ci}'$	=	concrete compressive strength at time of transfer, ksi
$f_{pd}$	=	prestressing stress in steel at time of deck placement, ksi
$f_{pi}$	=	initial prestressing stress in steel, ksi
$f_{pt}$	=	prestressing stress after transfer in steel, ksi
$f_{pu}$	=	ultimate strength of prestressing steel, ksi
$f_{py}$	=	yield strength of prestressing steel, ksi
$H$	=	average annual relative humidity, %
$I_{gc}$	=	gross cross-sectional moment of inertia for transformed composite section, in. <sup>4</sup>
$I_g$	=	gross cross-sectional moment of inertia, in. <sup>4</sup>
$I_{ti}$	=	transformed cross-sectional moment of inertia, in. <sup>4</sup>
$K_{id}, K_{df}$	=	transformed section coefficient
$K_L$	=	factor for type of prestressing strand used, 30 for low relaxation
$k_f$	=	factor for effect of concrete strength
$k_{hc}$	=	humidity factor for creep
$k_{hs}$	=	humidity factor for shrinkage
$k_s$	=	factor for effect of the volume-to-surface ratio of the component
$k_{td}$	=	time development factor
$L$	=	span length, ft
$M_g$	=	moment due to self-weight, kip-ft

$n$	=	modular ratio of prestressing steel to girder
$n_d$	=	modular ratio of deck to girder
$n_{strand}$	=	number of prestressing strands
$P_i$	=	prestressing force before losses, kip
$S$	=	surface area exposed to drying, $ft^2$
$t_d$	=	age at time of deck placement, days
$t_f$	=	age at end time (40 years), days
$t_i$	=	age at transfer of prestressing, days
$t_s$	=	thickness of slab, in.
$V$	=	volume, $ft^3$
$y_b$	=	depth from centroid of beam to bottom face, in.
$y_{b_t}$	=	depth from centroid of transformed beam to bottom face, in.
$y_{bt}$	=	depth from centroid of transformed composite section to bottom face of girder, in.
$\alpha_n$	=	factor for initial net section properties
$\gamma_c$	=	unit weight of concrete, pcf
$\gamma_{cd}$	=	unit weight of deck concrete, pcf
$\gamma_{cr}$	=	adjustment factor for creep
$\gamma_{sh}$	=	adjustment factor for shrinkage
$\Delta f_{cdp}$	=	change in stress at center gravity of prestressing steel due to deck placement, ksi
$\Delta f_{cdf}$	=	change in stress at center gravity of prestressing steel due to deck shrinkage, ksi
$\Delta f_{pCD1}$	=	loss of prestress due to creep of girder after deck placement, ksi
$\Delta f_{pCD2}$	=	loss of prestress due to creep of girder due to deck placement, ksi
$\Delta f_{pCR}$	=	loss of prestress due to creep of girder prior to deck placement, ksi
$\Delta f_{pES}$	=	loss of prestress due to elastic shortening, ksi
$\Delta f_{pR}$	=	loss of prestress due to relaxation of prestressing steel, ksi
$\Delta f_{pSD}$	=	loss of prestress due to shrinkage of girder after deck placement, ksi
$\Delta f_{pSR}$	=	loss of prestress due to shrinkage of girder prior to deck placement, ksi
$\Delta f_{pSS}$	=	prestress gain due to shrinkage of deck concrete, ksi
$\Delta f_{ps\_df}$	=	total loss of prestressing after deck placement, ksi
$\Delta f_{ps\_id}$	=	total time dependent loss of prestressing at time of deck placement, ksi
$\Delta f_{ps\_instant}$	=	instantaneous loss of prestressing, ksi
$\Delta f_{ps\_total}$	=	total loss of prestressing, ksi
$\Delta y_{bt}$	=	change in depth from centroid of beam to bottom face when considering transformed section, in.
$\epsilon$	=	shrinkage strain
$\rho_n$	=	tensile reinforcement ratio for initial net section
$\Psi$	=	creep coefficient
$\chi$	=	aging coefficient

## B.6.2 Calculation of Losses

### Section and Material Properties:

$$\begin{array}{llll}
 A_g := 659 \text{ in}^2 & e_{pg} := 22.604 \text{ in} & f_{py} := 256.2 \text{ ksi} & f_{c56} := 10.238 \text{ ksi} \\
 I_g := 268051 \text{ in}^4 & E_p := 28500 \text{ ksi} & n_{strand} := 38 & f_{ci} := 7.849 \text{ ksi} \\
 \gamma_c := 122 \text{ pcf} & E_{ct} := 3529 \text{ ksi} & f_{pi} := 178.8 \text{ ksi} & t_1 := 5 \text{ days} \\
 L := 106.76042 \text{ ft} & f_{pu} := 270 \text{ ksi} & A_{strand} := .217 \text{ in}^2 & t_f := 14600 \text{ days} \\
 n := \frac{E_p}{E_{ct}} & & t := t_f \text{ days} & t_d := 422 \text{ days} \\
 y_b := 27.63 \text{ in} & & & 
 \end{array}$$

### Determine Loading Properties:

$$\begin{array}{ll}
 A_{ps} := n_{strand} \cdot A_{strand} & A_{ps} = 8.25 \cdot \text{in}^2 \\
 P_i := A_{ps} \cdot f_{pi} & P_i = 1.47 \times 10^3 \cdot \text{kip} \\
 M_g := \frac{\gamma_c \cdot A_g \cdot L^2}{8} & M_g = 795.45 \cdot \text{kip} \cdot \text{ft}
 \end{array}$$

### Determine Transformed Section Properties:

$$\begin{array}{ll}
 A_{ti} := A_g + (n - 1) \cdot A_{ps} & A_{ti} = 717.35 \cdot \text{in}^2 \\
 \Delta y_{bt} := \frac{(n - 1) A_{ps} \cdot e_{pg}}{A_g + (n - 1) \cdot A_{ps}} & \Delta y_{bt} = 1.84 \cdot \text{in} \\
 y_{b\_t} := y_b - \Delta y_{bt} & y_{b\_t} = 25.79 \cdot \text{in} \\
 e_{pti} := e_{pg} - \Delta y_{bt} & e_{pti} = 20.77 \cdot \text{in} \\
 I_{ti} := I_g + A_g \cdot \Delta y_{bt}^2 + (n - 1) \cdot A_{ps} \cdot e_{pti}^2 & I_{ti} = 2.95 \times 10^5 \cdot \text{in}^4
 \end{array}$$

### Elastic Shortening Losses:

$$f_{cgp} := P_i \cdot \left( \frac{1}{A_{ti}} + \frac{e_{pti}^2}{I_{ti}} \right) - \frac{M_g \cdot e_{pti}}{I_{ti}} \quad f_{cgp} = 3.54 \cdot \text{ksi}$$

$$\Delta f_{pES} := n \cdot f_{cgp}$$

$$\Delta f_{pES} = 28.56 \cdot \text{ksi}$$

**Shrinkage Losses (Before Deck Placement):**

$H := 70$  (Average Annual Relative Humidity)

$V := A_g \cdot L$

$V = 488.58 \cdot \text{ft}^3$

$S := 218.838 \text{in} \cdot L$

$S = 1.95 \times 10^3 \cdot \text{ft}^2$

$\frac{V}{S} = 3.01 \cdot \text{in}$

$k_{td} := \frac{t_f}{61 - \frac{4 \cdot f_{ci}}{\text{ksi}} + t_f}$

$k_{td} = 1$

$k_{hs} := 2.00 - 0.0143H$

$k_{hs} = 1$

$k_s := \frac{1064 - \frac{94 \cdot V}{S \cdot \text{in}}}{735}$

$k_s = 1.06$

$k_f := \frac{5}{1 + \frac{f_{ci}}{\text{ksi}}}$

$k_f = 0.57$

$\gamma_{sh} := k_{td} \cdot k_s \cdot k_{hs} \cdot k_f$

$\gamma_{sh} = 0.6$

$\epsilon_{bid} := 480 \cdot 10^{-6} \cdot \gamma_{sh}$

$\epsilon_{bid} = 2.87 \times 10^{-4}$

$\alpha_n := \left( 1 + \frac{A_g \cdot e_{pg}^2}{I_g} \right)$

$\alpha_n = 2.26$

$\rho_n := \frac{A_{ps}}{A_g}$

$\rho_n = 0.01$

$\chi := 0.7$

$k_{la} := t_i^{-.118}$

$k_{la} = 0.83$

$k_{hc} := 1.56 - 0.008H$

$k_{hc} = 1$

$\gamma_{cr} := k_{td} \cdot k_{la} \cdot k_s \cdot k_{hc} \cdot k_f$

$\gamma_{cr} = 0.5$

$\Psi_{bif} := 1.9 \cdot \gamma_{cr}$

$\Psi_{bif} = 0.94$

$$K_{id} := \frac{1}{1 + n \cdot \rho_n \cdot \alpha_n \cdot (1 + \chi \cdot \Psi_{bid})}$$

$$\Delta f_{pSR} := \epsilon_{bid} \cdot E_p \cdot K_{id}$$

$$\Delta f_{pSR} = 5.94 \text{ ksi}$$

Creep Losses (Before Deck Casting):

$$k_{td} := \frac{(t_d - t_i)}{61 - \frac{4 \cdot f_{ci}}{\text{ksi}} + (t_d - t_i)}$$

$$k_{td} = 0.93$$

$$\gamma_{cr} := k_{td} \cdot k_{la} \cdot k_s \cdot k_{hc} \cdot k_f$$

$$\gamma_{cr} = 0.46$$

$$\Psi_{bid} := 1.9 \cdot \gamma_{cr}$$

$$\Psi_{bid} = 0.88$$

$$\Delta f_{pCR} := n \cdot f_{cgp} \cdot \Psi_{bid} \cdot K_{id}$$

$$\Delta f_{pCR} = 18.25 \text{ ksi}$$

Relaxation Losses:

$$\Delta f_{pR} := 2.4 \text{ ksi}$$

$$\Delta f_{pR} = 2.4 \text{ ksi}$$

Deck Properties:

$$t_s := 9.25 \text{ in}$$

$$\gamma_{cd} := 145 \text{ pcf}$$

$$f_{cd} := 5.626 \text{ ksi}$$

$$b_d := 7.5 \text{ ft}$$

$$E_{cd} := 3811 \text{ ksi}$$

$$A_d := t_s \cdot b_d = 832.5 \text{ in}^2$$

Transformed Composite Section Properties:

$$n_d := \frac{E_{cd}}{E_{ct}}$$

$$n_d = 1.08$$

$$A_{gc} := A_g + n_d \cdot t_s \cdot b_d$$

$$A_{gc} = 1.56 \times 10^3 \text{ in}^2$$

$$y_{bt} := \frac{A_g \cdot y_b + n_d \cdot t_s \cdot b_d \cdot \left(54 \text{ in} + \frac{t_s}{2}\right)}{A_{gc}}$$

$$y_{bt} = 45.51 \text{ in}$$

$$I_{gc} := I_g + A_g \cdot (y_b - y_{bt})^2 + n_d \cdot \frac{b_d \cdot t_s^3}{12} + n_d \cdot t_s \cdot b_d \cdot \left(54 \text{ in} + \frac{t_s}{2} - y_{bt}\right)^2$$

$$I_{gc} = 6.4 \times 10^5 \text{ in}^4$$

$$e_{pc} := e_{pg} + (y_{bt} - y_b)$$

$$e_{pc} = 40.49 \text{ in}$$

$$e_{dc} := y_{bt} - 54 \text{ in} - \frac{t_s}{2}$$

$$e_{dc} = -13.11 \text{ in}$$

#### Shrinkage of Concrete Girder in Composite Section:

$$k_{td} := \frac{(t_f - t_d)}{61 - \frac{4 \cdot f_{ci}}{\text{ksi}} + (t_f - t_d)}$$

$$k_{td} = 1$$

$$\gamma_{sh} := k_{td} \cdot k_s \cdot k_{hs} \cdot k_f$$

$$\gamma_{sh} = 0.6$$

$$\epsilon_{bdf} := 480 \cdot 10^{-6} \cdot \gamma_{sh}$$

$$\epsilon_{bid} = 2.87 \times 10^{-4}$$

$$\gamma_{cr} := k_{td} \cdot k_{la} \cdot k_s \cdot k_{hc} \cdot k_f$$

$$\gamma_{cr} = 0.5$$

$$\Psi_{bdf} := 1.9 \cdot \gamma_{cr}$$

$$\Psi_{bif} = 0.94$$

$$K_{df} := \frac{1}{1 + n \cdot \rho_n \cdot \alpha_n \cdot (1 + \chi \cdot \Psi_{bdf})}$$

$$\Delta f_{pSD} := \epsilon_{bdf} \cdot E_p \cdot K_{df}$$

$$\Delta f_{pSD} = 5.94 \text{ ksi}$$

#### Creep of Concrete Girder in Composite Section due to SW and Prestressing:

$$k_{td} := \frac{(t_f - t_i)}{61 - \frac{4 \cdot f_{ci}}{\text{ksi}} + (t_f - t_i)}$$

$$k_{td} = 1$$

$$\gamma_{cr} := k_{td} \cdot k_{la} \cdot k_s \cdot k_{hc} \cdot k_f$$

$$\gamma_{cr} = 0.5$$

$$\Psi_{bif} := 1.9 \cdot \gamma_{cr}$$

$$\Psi_{bid} = 0.88$$

$$\Delta f_{pCD1} := n \cdot f_{cgp} \cdot (\Psi_{bif} - \Psi_{bid}) \cdot K_{df}$$

$$\Delta f_{pCD1} = 1.26 \text{ ksi}$$

#### Creep of Concrete Girder in Composite Section due to Deck Weight:

$$\Delta f_{cdp} := 1.097 \text{ ksi}$$

$$\Delta f_{pCD2} := n \cdot \Delta f_{cdp} \cdot \Psi_{bdf} \cdot K_{df}$$

$$\Delta f_{pCD2} = 6.05 \text{ ksi}$$

**Shrinkage of Deck Concrete:**

$$k_{td} := \frac{(t_f - t_d)}{61 - \frac{4 \cdot f_{cd}}{\text{ksi}} + (t_f - t_d)} \quad k_{td} = 1$$

$$k_s := \frac{1064 - \frac{94 \cdot A_d \cdot L}{(b_d + b_d - 42\text{in}) \cdot \text{in} \cdot L}}{735} \quad k_s = 0.68$$

$$k_f := \frac{5}{1 + \frac{f_{cd}}{\text{ksi}}} \quad k_f = 0.75$$

$$\gamma_{sh} := k_{td} \cdot k_s \cdot k_{hs} \cdot k_f \quad \gamma_{sh} = 0.51$$

$$\epsilon_{ddf} := 480 \cdot 10^{-6} \cdot \gamma_{sh} \quad \epsilon_{ddf} = 2.44 \times 10^{-4}$$

$$\gamma_{cr} := k_{td} \cdot k_{la} \cdot k_s \cdot k_{hc} \cdot k_f \quad \gamma_{cr} = 0.42$$

$$\Psi_{ddf} := 1.9 \cdot \gamma_{cr} \quad \Psi_{bif} = 0.94$$

$$\Delta f_{cdf} := \left( \frac{\epsilon_{ddf} \cdot A_d \cdot E_{cd}}{1 + 0.7 \cdot \Psi_{ddf}} \right) \cdot \left( \frac{1}{A_{gc}} + \frac{e_{pc} \cdot e_{dc}}{I_{gc}} \right)$$

$$\Delta f_{pSS} := n \cdot \Delta f_{cdf} \cdot K_{df} \cdot (1 + \chi \cdot \Psi_{bdf}) \quad \Delta f_{pSS} = -0.91 \cdot \text{ksi}$$

**Total Losses:**

$$\Delta f_{ps\_instant} := \Delta f_{pES} \quad \Delta f_{ps\_instant} = 28.56 \cdot \text{ksi}$$

$$\Delta f_{ps\_id} := \Delta f_{pSR} + \Delta f_{pCR} + \frac{\Delta f_{pR}}{2} \quad \Delta f_{ps\_id} = 25.39 \cdot \text{ksi}$$

$$\Delta f_{ps\_df} := \left( \Delta f_{pSD} + \Delta f_{pCD1} + \Delta f_{pCD2} + \frac{\Delta f_{pR}}{2} \right) + \Delta f_{pSS} \quad \Delta f_{ps\_df} = 13.54 \cdot \text{ksi}$$

$$\Delta f_{ps\_total} := \Delta f_{ps\_instant} + \Delta f_{ps\_id} + \Delta f_{ps\_df} \quad \Delta f_{ps\_total} = 67.49 \cdot \text{ksi}$$

## B.7 Prestress Loss Experimental Data

Table B-1 shows the measured losses of the beams over time and the dates when measurements were made.

Table B-1: Prestress losses of HSLW girders

Age (days)	Date	Average (ksi)	Age (days)	Date	Average (ksi)	Age (days)	Date	Average (ksi)
0	8/11/08	0.00	47	9/27/08	45.94	435	10/20/09	51.25
2	8/12/08	39.24	48	9/28/08	45.79	436	10/21/09	50.73
3	8/13/08	39.69	49	9/29/08	45.81	437	10/22/09	50.18
3	8/14/08	40.10	50	9/30/08	45.56	452	11/6/09	50.32
4	8/15/08	39.98	51	10/1/08	45.57	459	11/13/09	50.26
4	8/16/08	40.46	52	10/2/08	45.75	466	11/19/09	50.89
5	8/16/08	40.37	65	10/14/08	46.10	473	11/27/09	51.42
6	8/17/08	40.81	66	10/15/08	46.28	493	12/17/09	51.06
6	8/17/08	41.06	67	10/17/08	46.31	500	12/24/09	49.44
7	8/18/08	41.15	68	10/18/08	45.99	507	12/30/09	49.87
7	8/18/08	41.40	82	11/1/08	47.90	514	1/7/10	51.13
8	8/19/08	41.40	148	1/6/09	46.24	521	1/14/10	50.76
8	8/19/08	41.78	187	2/14/09	47.38	522	1/15/10	50.32
9	8/20/08	41.71	194	2/21/09	48.81	529	1/22/10	48.73
9	8/20/08	41.95	201	2/28/09	47.11	533	1/26/10	49.47
10	8/21/08	41.87	400	9/15/09	48.62	534	1/27/10	49.78
10	8/21/08	42.15	407	9/22/09	48.37	541	2/3/10	49.51
11	8/22/08	42.11	409	9/24/09	47.53	548	2/10/10	50.39
11	8/22/08	42.48	413	9/28/09	48.24	555	2/17/10	50.47
12	8/23/08	42.58	416	10/1/09	49.17	562	2/24/10	49.44
12	8/23/08	42.76	422	10/6/08	48.37	640	5/13/10	46.51
13	8/24/08	42.96	423	10/7/09	48.49	647	5/20/10	47.16
13	8/24/08	42.97	424	10/8/09	48.80	654	5/27/10	46.75
14	8/25/08	43.01	425	10/9/09	48.58	661	6/3/10	46.87
14	8/25/08	42.83	426	10/10/09	49.22	668	6/9/10	46.13
15	8/26/08	42.83	427	10/11/09	49.32	855	12/14/10	52.74
15	8/26/08	42.77	428	10/12/09	50.21	862	12/21/10	50.16
25	9/4/08	44.02	429	10/13/09	49.89	869	12/27/10	51.75
26	9/5/08	44.02	430	10/14/09	50.20	876	1/4/11	50.53
26	9/5/08	44.02	431	10/15/09	50.32	878	1/6/211	50.06
27	9/7/08	44.21	432	10/17/09	51.17			
27	9/7/08	44.06	433	10/18/09	51.79			
28	9/8/08	44.05	434	10/19/09	51.61			

## Appendix C: Camber Data

Table C-1 presents the measured camber in the girders. After October 23, 2008, the girders were placed at the bridge site and had a bearing length of 106.74 ft. The deck was cast on October 6<sup>th</sup>, 2009. The barriers were placed on December 16<sup>th</sup>, 2009.

Table C-1: Measured cambers of HSLW girders

<b>Date</b>	<b>Time</b>	<b>Age (days)</b>	<b>Girder 1</b>	<b>Girder 2</b>	<b>Girder 3</b>	<b>Girder 4</b>	<b>Girder 5</b>	<b>Average</b>
8/11/08	After cut	0	3.75	3.71	3.79	3.76	3.59	3.72
8/11/08	7:00p	0.5	4.19	4.05	4.06	4.25	4.03	4.12
8/16/08	8:15a	5	3.98	3.92	3.99	4.21	3.92	4.01
8/19/08	8:05a	8	4.02	3.91	4.03	4.23	3.92	4.02
8/25/08	8:00a	14	4.03	4.03	4.05	4.25	3.94	4.06
9/8/08	8:00a	28	4.09	4.14	4.23	4.40	4.23	4.22
10/6/08	9:18a	56	4.08	4.13	4.27	4.46	4.16	4.26
10/23/08	8:30a	73	4.08	4.32	4.49	4.47	4.17	4.39
3/31/09	7:30	232	3.93	4.67	3.82	3.93	4.18	4.39
4/29/09	8:00	261	3.78	4.55	3.75	3.93	4.33	4.39
10/05/09	8:00	419	3.24	3.72	3.84	3.84	4.44	3.82
11/5/09	7:40	451	1.36	1.56	2.01	1.89	1.49	1.66
11/13/09	7:20	459	1.30	1.60	1.74	1.72	1.28	1.53
12/3/09	7:50	479	1.29	1.56	1.74	1.88	1.50	1.60
1/14/10	7:45	521	0.78	1.04	1.49	1.35	0.98	1.13
1/26/10	8:20	533	0.85	1.26	1.60	1.66	1.10	1.29
3/19/10	8:00	585	1.06	1.48	1.76	1.67	1.17	1.43
5/12/10	7:05	639	1.02	1.40	1.66	1.58	1.02	1.34
6/17/10	6:25	675	0.82	1.21	1.52	1.45	0.98	1.20
7/27/10	6:45	715	0.81	1.25	1.55	1.45	0.92	1.20
9/1/10	7:08	751	0.76	1.12	1.45	1.35	0.73	1.08
9/29/10	7:05	779	0.80	1.13	1.41	1.28	0.74	1.07
12/2/10	7:24	843	0.86	1.33	1.63	1.48	0.83	1.23
12/14/10	7:30	855	0.67	1.11	1.43	1.37	0.73	1.06
1/6/11	8:01	878	0.85	1.32	1.65	1.53	0.85	1.24

# Appendix D: Transfer Length

## D.1 Introduction

Transfer length of prestressed girders is discussed in this appendix. The definition of transfer length is discussed along with current code provisions required by both ACI and AASHTO. These standards are compared with the experimental transfer lengths values found for the HSLW girders.

## D.2 Definition

Transfer length is the distance required to transfer the fully effective prestressing force from the strand to the concrete. The transfer length is measured from the end of the girder to the point where the concrete around the strand is carrying the effective prestressing force. There is constant stress in the steel from the transfer point through the length of the beam to the transfer point at the opposite end. Figure D-1 shows an idealized view of transfer length as a function of steel stress across the length of the beam.

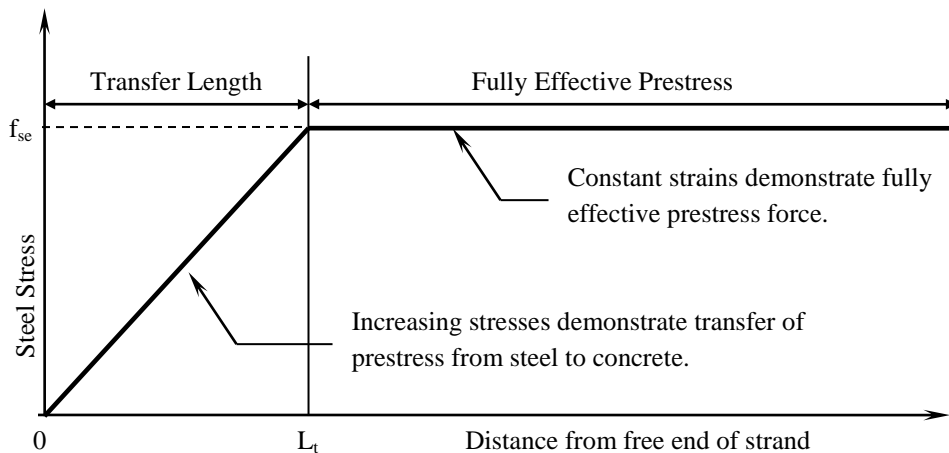


Figure D-1: Idealized stress in steel strand in a prestressed concrete member

### D.3 Current Code Provisions

Currently both ACI and AASHTO have recommended values for transfer length. ACI 318-08 uses the effective prestressing stress,  $f_{se}$ , and the diameter of the bar, or in this case strand,  $d_b$ , to calculate transfer length, shown in Eq. D-1.

$$l_t = \frac{f_{se} d_b}{3} \quad (\text{Eq. D-1})$$

AASHTO (2007) currently only used the strand diameter to define the transfer length, shown in Eq. D-2.

$$l_t = 60d_b \quad (\text{Eq. D-2})$$

Previous research (Meyer, 2002) has shown both of these equations to be conservative.

### D.4 Test Specimens

All five HSLW girders were instrumented to measure transfer length. DEMEC embedments were placed at the North and South ends of each girder, with North and South referring to final bridge positions. These embedments were placed over a 40 in. length on the same side of the girder along the bottom flange as pictured in Figure D-2.



Figure D-2: Grey boxes indicate location of embedments spaced at 2 inches over a 50 inch length.

All 5 girders used 0.6 inch diameter 7-wire low-relaxation strand. The strands were stressed to approximately the same prestressing force of 45 kips. Due to the early age of the girders, the initial stress of the strands was used for effective stress in calculations. The initial stress was found to be 137.2 ksi using load cell data of tension in the strand just before cut-down.

#### **D.5 Measurement of Transfer Length**

The concrete surface strain (CSS) method was used to calculate the transfer length. This method uses the assumption that as the prestressing strand develops a bond with the surrounding concrete, the concrete will move in the same way the strand does. Strains in the strand are then the same as the compressive strain in the concrete. Using this idea, the change in length can be measured at the surface and directly correlated to the strand inside the girder.

A DEMEC gage was used to take the CSS measurements monitoring the change in length of the girder, and thus the strain in the concrete. The DEMEC gage, shown in Figure D-3, required embedments in the concrete to take the readings. These embedments were spaced 2 inches apart from the end of the beam moving toward the center for 40 inches. The distance between these holes was then measured with the DEMEC gage, which reads to accuracy of 0.0001 inches. The DEMEC gage has two conical points spaced 8 inches apart, with one point on a spring, which can adjust. Figure D-4 shows a researcher taking DEMEC readings with a second researcher recording values.



Figure D-3: DEMEC gage used for this research.



Figure D-4: Researchers Jennifer Dunbeck and Brett Holland taking DEMEC readings.

Several steps were taken to ensure accurate usage of the DEMEC gage. First, the same DEMEC gage was used for all readings. Second, the DEMEC gage was zeroed before each use. A steel bar with conical holes spaced at 8 inches was provided by the manufacturer. This bar and the gage were allowed to reach ambient temperature before the tool was zeroed and then used to take readings. Third, the same researcher took all DEMEC readings, with another research present to record the data. Care was taken to hold the gage in the same manner each time. Finally, all readings were taken close to 8:00 a.m. before direct sunlight hit the girders. This prevented thermal affects from playing a factor in the results.

#### **D.6 Determination of Transfer Length**

The strains in the concrete were measured by finding the difference between the initial CSS reading, which was before cut-down, and the reading of a given day. These strains were already partly “smoothed out” due to the nature of taking the readings. The 8 inch gage length meant that each reading would cover 4 embedment points: one at each point of the DEMEC gage and 2 in the middle. This averaged any change in length over 8 inches rather than only over 2 inches. A second tool was used to further “smooth out” the data. Using an Excel spreadsheet, the strains for a given point were averaged using a 3 point floating average, shown in Eq. D-3.

$$\varepsilon_x = \frac{\varepsilon_{(x-1)} + \varepsilon_{(x)} + \varepsilon_{(x+1)}}{3} \quad (\text{Eq. D-3})$$

These smoothed out values were then plotted against their distance from the girder end. The “95% Average Maximum Strain” method was used to calculate the transfer length. This method uses a “strain plateau”, which ideally is the constant strain value across the middle of the girder once full transfer of effective prestress is reached. This plateau is used to determine the “Average Maximum Strain” of all values inside the plateau. 95% of this average is taken and

plotted against the data. The transfer length is then determined by the intersection of the 95% line with the “smoothed” strain profile.

This method is considered to be conservative when compared to the “idealized” transfer length. The idealized transfer length would be located at the intersection of the strain plateau and a trendline of the smoothed strains. This idealized transfer length is typically less than the measured transfer length. However, a different result was found for much of this data when using this method. Some graphs were similar to expectations, such as the graph shown in Figure D-5, but some were far from standard, such as Figure D-6. These atypical graphs resulted in a measured transfer length less than the idealized transfer length.

Another anomaly of the data was that several data sets showed negative strains at the end of the girder. This was probably the result of small cracks that occurred after the initial readings were taken on the bed. The negative values were not used in creating the trendlines.

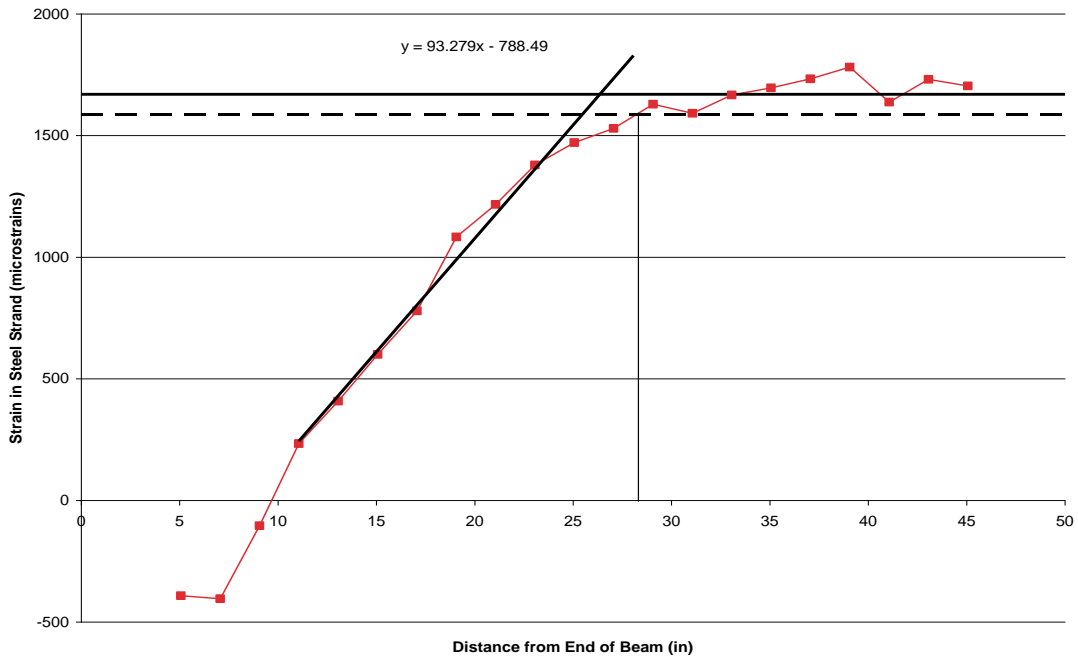


Figure D-5: Smoothed CSS readings for the South end of Girder 1 at day 8.

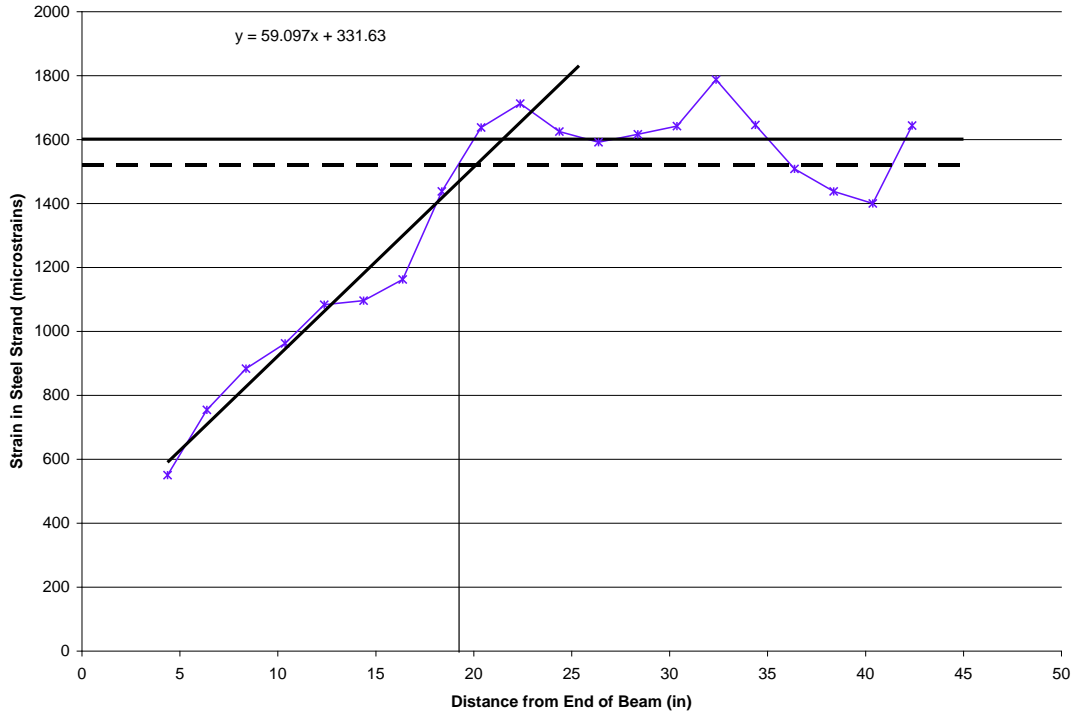


Figure D-6: Smoothed CSS readings for the South end of Girder 5 at day 80.

## D.7 Transfer Length Results

Table D-1 shows all values found, except for those of the North end of Girder 4. These data points had to be thrown out due to error readings obtained by the DEMEC gage. Tables D-2 through D-6 show the average measured and idealized transfer lengths for each reading day. Table D-7 summarizes these averages for comparison.

Table D-1: Measured and idealized transfer lengths for all girders.

Girder	Days after Cut-down	Measured Transfer Length (in)	Idealized Transfer Length (in)
1 South	5d	33.06	27.13
	8d	28.10	26.36
	14d	28.20	26.49
	28d	33.20	29.32
	80d	32.25	29.42
1 North	5d	27.00	31.40
	8d	27.56	31.82
	14d	27.50	34.44
	28d	30.40	31.22
	80d	21.50	24.52
2 South	5d	25.25	25.45
	8d	25.80	23.55
	14d	24.33	24.81
	28d	18.25	19.34
	80d	25.80	28.18
2 North	5d	16.80	19.93
	8d	25.00	27.89
	14d	25.40	28.68
	28d	24.75	26.16
	80d	24.60	28.75
3 South	5d	25.00	35.07
	8d	26.20	24.94
	14d	26.70	44.44
	28d	26.20	30.49
3 North	5d	34.50	39.57
	8d	30.20	30.89
	14d	30.40	35.42
	28d	29.60	29.47
	80d	33.80	33.55
4 South	5d	23.20	25.13
	8d	25.40	26.24
	14d	23.60	25.51
	28d	24.75	26.76
5 South	5d	18.00	14.59
	8d	25.20	23.33
	14d	18.50	19.34
	28d	19.30	20.35
	80d	19.20	21.48
5 North	5d	33.60	32.61
	8d	35.05	38.06
	14d	32.10	34.00
	28d	32.13	35.62
	80d	35.75	38.60

Table D-2: Average transfer lengths at 5 days.

Girder	Measured Transfer Length (in)	Idealized Transfer Length (in)
1 South	33.06	27.13
1 North	27.00	31.40
2 South	25.25	25.45
2 North	16.80	19.93
3 South	25.00	35.07
3 North	34.50	39.57
4 South	23.20	25.13
5 South	18.00	14.59
5 North	33.60	32.61
5 Day Average	26.27	27.87
Standard Deviation	6.50	7.72

Table D-3: Average transfer lengths at 8 days.

Girder	Measured Transfer Length (in)	Idealized Transfer Length (in)
1 South	28.10	26.36
1 North	27.56	31.82
2 South	25.80	23.55
2 North	25.00	27.89
3 South	26.20	24.94
3 North	30.20	30.89
4 South	25.40	26.24
5 South	25.20	23.33
5 North	35.05	38.06
8 Day Average	27.61	28.12
Standard Deviation	3.26	4.75

Table D-4: Average transfer lengths at 14 days.

Girder	Measured Transfer Length (in)	Idealized Transfer Length (in)
1 South	28.20	26.49
1 North	27.50	34.44
2 South	24.33	24.81
2 North	25.40	28.68
3 South	26.70	44.44
3 North	30.40	35.42
4 South	23.60	25.51
5 South	18.50	19.34
5 North	32.10	32.10
14 Day Average	26.30	30.14
Standard Deviation	4.01	7.39

Table D-5: Average transfer lengths at 28 days.

Girder	Measured Transfer Length (in)	Idealized Transfer Length (in)
1 South	33.20	29.32
1 North	30.40	31.22
2 South	18.25	19.34
2 North	24.75	26.16
3 South	26.20	30.49
3 North	29.60	29.47
4 South	24.75	26.76
5 South	19.30	20.35
5 North	32.13	35.62
28 Day Average	26.51	27.64
Standard Deviation	5.33	5.19

Table D-6: Average transfer lengths at 80 days.

Girder	Measured Transfer Length (in)	Idealized Transfer Length (in)
1 South	32.25	29.42
1 North	21.50	24.52
2 South	25.80	28.18
2 North	24.60	28.75
3 North	33.80	33.55
5 South	19.20	21.48
5 North	35.75	38.60
80 Day Average	27.56	29.22
Standard Deviation	6.41	5.63

Table D-7: Summary of average transfer lengths.

Averages	Measured Transfer Length (in)	Idealized Transfer Length(in)
5 Day	26.27	27.87
8 Day	27.61	28.12
14 Day	26.30	30.14
28 Day	26.51	27.64
80 Day	27.56	29.22

## D.8 Discussion of Results

The values from day 8 were selected to be used as the transfer lengths for this beam. The day 8 values had the lowest standard deviations, and therefore the best agreement between numbers. Also, when compared to the averages from other days in Table D-7 the measured transfer length from day 8 is the longest length. Using this value is conservative.

The transfer length of the HSLW girders was 27.61 inches. This number is slightly less than the value suggested by AASHTO, confirming that the equation is conservative. The ACI equation was extremely close to the actual transfer length. Table D-8 compares the three values.

Table D-8: HSLW transfer length compared to code requirements.

Source	Equation	Transfer Length (in)
HSLW Girders		27.61
ACI	$\frac{f_{se}d_b}{3}$	27.45
AASHTO	$60 d_b$	36.00

The variations in transfer length between girders ends were more than expected. Previous research (Meyer, 2002) has suggested that girders constructed at the free end, or dead end, of the bed have longer transfer lengths. Typically multiple beams are constructed on a bed starting at the live end and moving toward the dead end. There is often a space left at the dead end of the bed between the last beam and the abutment. From this research, Girder 3 was on the free end of pour 1 with 79 feet of free prestressing cable, and Girder 5 was on the free end of pour 2 with 190 feet of free prestressing cable. The average transfer length of the Girder 3 was 4.09 inches and of Girder 5 was 6.12 inches greater than the transfer length for all the girders. This would imply that the length of the free strand has the stated effect on the transfer length.